Effect of Electric Current on Ceramic Processing

Theo Graves Saunders

Submitted in partial fulfilment of the requirements

of the Degree of Doctor of Philosophy

School of Engineering and Materials Science,

Queen Mary, University of London,

London, UK

October 2016

Declaration

I, Theo Graves Saunders confirm that the research included within this thesis is my own work or that where it has been carried out in collaboration with, or supported by others, that this is duly acknowledged below and my contribution indicated. Previously published material is also acknowledged below.

I attest that I have exercised reasonable care to ensure that the work is original, and does not to the best of my knowledge break any UK law, infringe any third party's copyright or other Intellectual Property Right, or contain any confidential material.

I accept that the College has the right to use plagiarism detection software to check the electronic version of the thesis.

I confirm that this thesis has not been previously submitted for the award of a degree by this or any other university.

The copyright of this thesis rests with the author and no quotation from it or information derived from it may be published without the prior written consent of the author.

Signature: TSaunders

Date: October 2016

Abstract

This work was on the effect of electric current on the processing of ceramics. The focus was on electromigration/electrochemistry and plasma effects.

While there is no solid evidence that there is plasma in Spark Plasma Sintering, (SPS), newer techniques e.g. flash, use different conditions so there is an interest in understanding the conditions under which a plasma forms. The minimum arcing voltage was found from literature to be from 10-15V for materials of interest. This is above that found in SPS (10V). However, due to the many contact points in a powder compact much higher voltages (50V) were required in practical experiments. Optical spectroscopy was used to verify the formation of a plasma, and emission peaks from the powder compact material were visible implying they were vaporised and formed the plasma.

Electromigration was exploited to alter the oxidation of zirconium diboride, by passing current through the oxide layer (120µm zirconia base grown at 1200°C) oxygen could be pumped either away or toward the diboride bulk. Small cubes (3mm) of diboride had platinum foil electrodes applied on both sides and oxidation was performed at 1400°C for 5hr. Without a field the oxide grew to 360µm, by applying 10V and 100mA the oxide grew to 150µm under the +ve electrode but 1400µm under the -ve electrode. Electrochemical reduction was believed to have occurred due to the electrical properties of the material changing during oxidation and visible blackening of the oxide.

Combining the techniques from both earlier works, a contactless flash sintering

setup was developed. This used two plasma arcs as electrodes to heat and pass current through the sample. Various materials, currents and times were used, but the best result was with SiC:B_4C which was sintered in 3s with 6A, the microstructure showed sharp grains, no segregation and limited grain growth (initially 0.7μm SiC and 0.5μm B_4C, this grew to 1.1μm and 1.4μm). This was the first recorded case of contactless flash sintering and the technique has the potential to sinter ceramics in a continuous manner.

Acknowledgments

I would like to sincerely thank the following people for their help during my PhD. My supervisor Mike Reece for his support, guidance and always asking the most awkward questions. Salvatore Grasso for his unending optimism and perseverance in the face of seemingly unending setbacks. Peter Tatarko For the many hours of microscopy together. Andrew Davis from Anglia instruments for his patient help with optical spectroscopy. The Whole of the ceramics group at Nano force for the many stimulating discussions and help about the lab. My former flatmates for their tolerance of all my tools and foolhardy projects. My family for their support, encouragement and understanding for the duration. And of course the Funding bodies that made this work possible The European framework 7 ADMACOM (Advanced manufacturing routes for metal/Composite components for aerospace) (EC FP7 2007-2013) EPSRC Materials for Extreme Environments (EP/K008749/1, XMat).

Glossary

ac	Alternating Current
AES	Atomic Emission Spectroscopy
CCD	Charge-Coupled Device
CCV	Closed Circuit Voltage
CFS	Contactless Flash Sintering
CVD	Chemical Vapour Deposition
dc	Direct Current
DCE	Direct Contact Electrode
ECAS	Electric Current Assisted Sintering
ECE	Electric Current Effects
ECS	External Charge Source
EDM	Electro Discharge Machining
EDX	Energy Dispersive X-Ray
EM	Electro Magnetic
FFC	Process named after developers Farthing, Fray and Chen
FIB	Focused Ion Beam
FS	Flash Sintering
FSPS	Flash Spark Plasma Sintering
HF	High Frequency
HV	High Voltage
IC	Integrated Circuit

ICPS Inductively Couple Plasma Spectroscopy

NCE Non-Contact Electrode

NTC Negative Temperature Coefficient

OCV Open Circuit Voltage

PS Power Supply

PSU Power Supply Unit

PZT Lead Zirconate Titanate

RF Radio Frequency

rms Root Mean Square

SEM Scanning Electron Microscopy

SPS Spark Plasma Sintering

TIG Tungsten Inert Gas

UHT Ultra High Temperature

UHTC Ultra High Temperature Ceramic

XRD X-ray Diffraction

YSZ Yttria Stabilized zirconia

Table of Contents

Chapter 1. Contents

Table of Figures

Table of Tables

Chapter 1. Introduction

This work is focused on the effect of current on the behaviour of ceramic materials. This is distinct from the more traditional field of electroceramics, which studies piezoelectric materials and other such functional materials. Electroceramics are normally dielectrics, so while under ac conditions a current can flow from the electrodes no current actually flows through the dielectric, and very large fields (kV per mm) can be applied. For this reason, studying current effects in ceramics might appear to be a foolish endeavour as most ceramics are generally considered to be insulators. However, there are several that are conductors at room temperatures (diborides and carbides) or semiconductors (SiC, B_4C, and ZnO). Even those that are good insulators often become conductive at higher temperatures e.g. zirconia. Almost all ceramics and glasses are conductive in the liquid phase, so ceramics made by liquid phase sintering are likely to have some conductivity once their secondary phase melts or softens. Doping can also allow even good insulators to pass significant current at modest temperatures. Considering that most ceramic processing occurs at elevated temperature, the study of current effects is of some interest. Normally, ceramics are heated for processing using resistive heating elements to indirectly heat the materials as in conventional furnaces (radiative heating). As industries strive for greater efficiency there has been a shift to more direct methods to heat materials, either by thermal conduction heating, e.g. with hot dies or tooling, or Joule heating generating heat inside the material to be processed. A variety of modern materials processing techniques result in either some current flowing through the sample or the sample experiencing an applied voltage. Due to the way the current / field couple with the material it is possible

that the material can be processed differently or the final microstructure can be effected by the electric current. For the rest of this work these effects are describes as ECEs, which includes any way that the flow of current can alter the material as compared to non-electric processing).

Chapter 2. Review of Industrial Processes that are/ could be Affected by ECEs

2.1 Introduction

Before attempting to exploit ECEs for new processes it's important to know what electrical current assisted processes are already in use or development. This can best be achieved by a broad literature review. It is important to remain critical as while there are a great many papers reporting various proposed effects occurring during new electric current assisted processes, e.g. SPS and flash, it is important to look at all the possible processes that might have ECEs. For this reason some processes that are currently only used for metals but could be used with ceramics in the future are studied. Particular interest was paid to processes that are based around ECEs as the working principle of their operation. The various processes were split into groups according to how the current was applied to the material or the dominant mechanism. Once the various processes were identified, the possible mechanism behind them were investigated. Some simple calculations were found to allow the magnitude or likelihood of theses mechanisms to be evaluated for a given set of conditions.

2.2 Bulk Current Processes

2.2.1 Flash Sintering

In this setup a pre sintered, or green body sample is preheated in a conventional furnace and a relatively high voltage (100V 0.1-1A) is applied to the sample via platinum wire/foil[1] as depicted in Figure 2.1. Above a critical temperature the material becomes sufficiently electrically conductive to draw enough current to initiate thermal runaway. The main process variables are electric field, current limit and preheating temperature. The process can produce the densification of materials in seconds. Newer derivatives also use pressure to aid densification, making them very similar to as SPS[2]. Not all materials can be processed with this technique and new materials are currently being investigated[3-6]. Current understanding is that the material to be sintered should have a NTC of resistance profile as it encourages thermal runaway [7,8] . In flash sintering the all the current passes through the sample and densification normally takes 1-3s. There is much academic work ongoing to isolate the different mechanism that are at play and there have already been several reviews on the subject already[9-11]. Various ECEs have been associated with flash sintering. Plasma effects have been suggested to explain rapid sintering[12] and optical emissions have been seen at the electrodes especially in glasses[13] however alternate non plasma explanations for the emissions exist[14]. Electroplastic softening has also been suggested as a possible mechanism[12,13]. There is strong evidence of electrochemical reduction occurring at the electrodes[15,16], but it's not clear if it

contributes to flash sintering or is just a by-product.

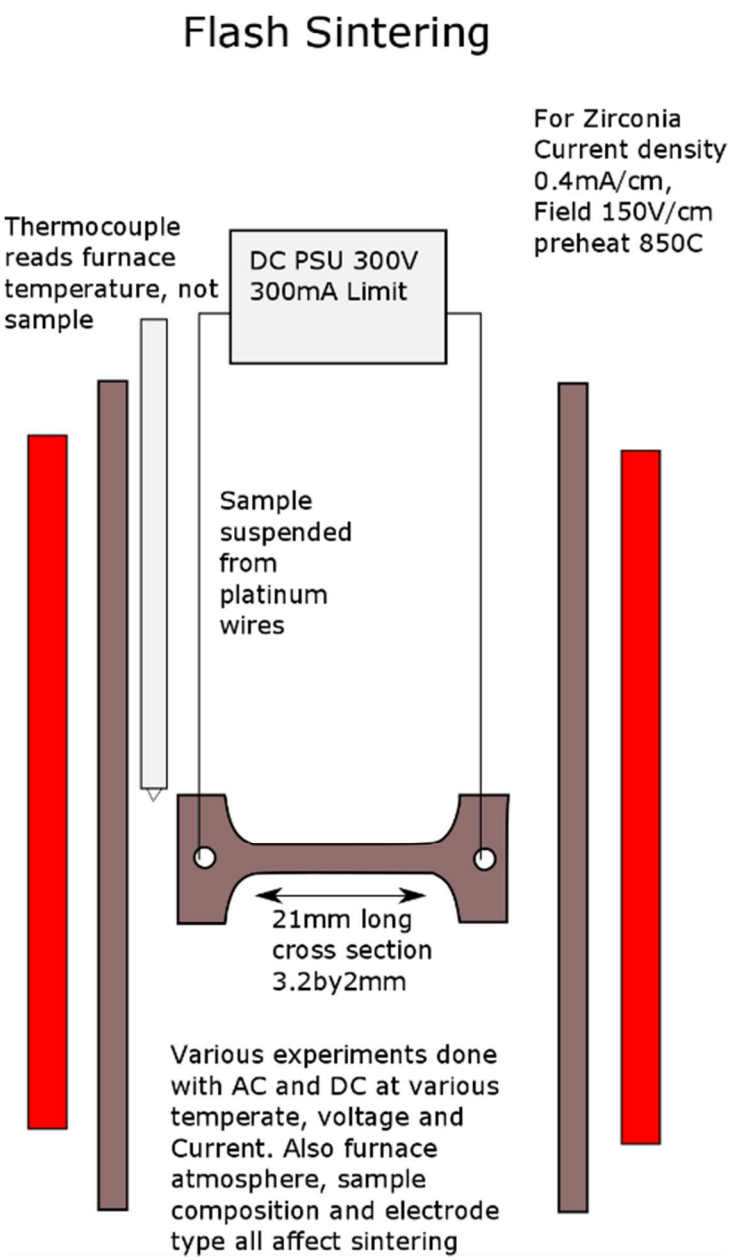

Figure 2.1 Schematic of Traditional Flash Sintering Setup

2.2.2 **Spark Plasma Sintering (SPS)**

SPS is a sintering technique where powders (ceramic or metal) are loaded into a

graphite die and punch set. They are then heated by application of a low voltage (typically below 10V at several kA) and the temperature is usually controlled by a pyrometer aimed at the punches or die. The process can sinter materials in minutes, typically used heating rates are ~100°C/min). Machines range from labs scale ones producing samples with dimensions of the order of 20mm to industrial ones that can achieve 400mm. The proportion of the current passing through the sample varies according to the ratio of conductivity of the sample relative to the carbon tooling[17]. This means that unless the sample is conductive (the situation in Figure 2.2 (b)), or becomes conductive above room temperature, very little current flows through the sample (Figure 2.2 (a)). Fast heating is achieved either through internal Joule heating, or due to the applied pressure ensuring good thermal contact between the powder and the hot graphite die [18]. This results in much shorter processing times, around 10-30mins, as opposed to many hours for hot pressing or pressureless sintering. SPS is normal attributed with various improvements in sintering speed and final density, over the years many different explanations/mechanism have been proposed to explain this. The process was actually named after the proposed mechanism, sparking and plasma were hypothesised to clean the particles surfaces, but the consensus now is that that this is not the case[19]. There is, however, much speculation on other possible mechanisms (e.g. thermal hot spots[20]). The majority of the improvement is usually attributed to the effect of rapid heating altering the thermodynamic kinetics of sintering[21], which is not a ECE. Recent advances with Flash SPS (FSPS) ensure all the current passes through the sample (Figure 2.2 (c)) increasing the probability of ECEs contributing to the sintering, due to the higher

current density and greater effective voltage.

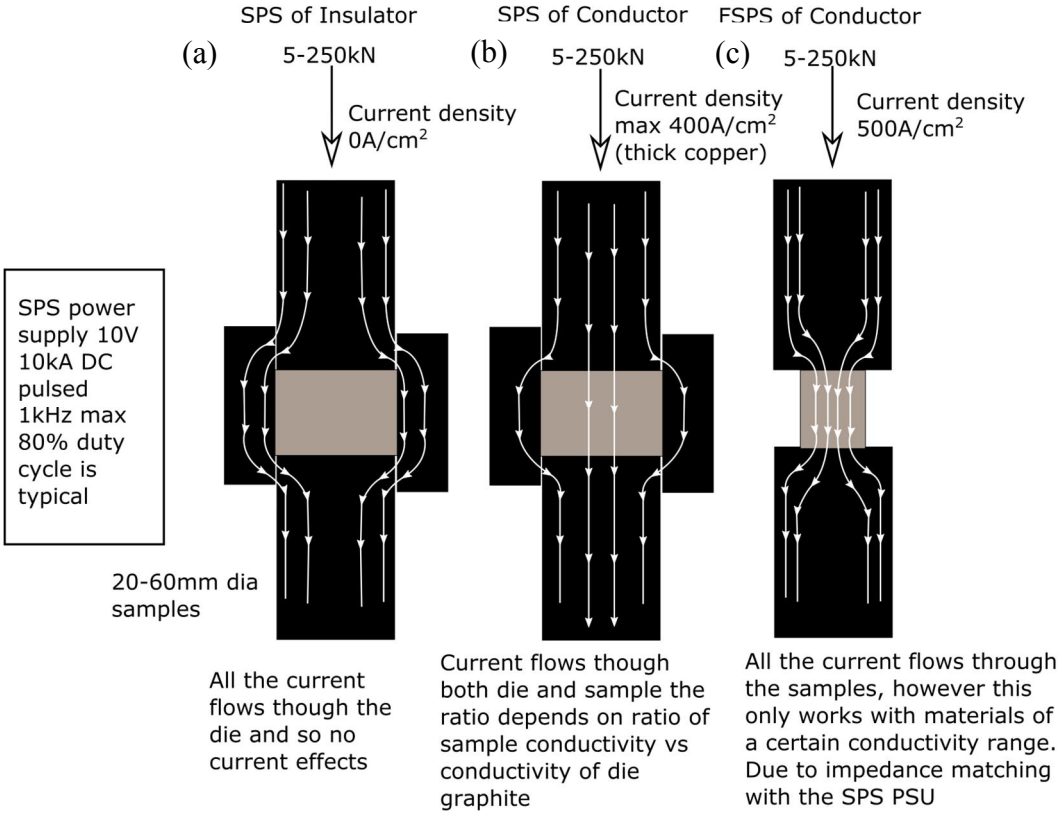

Figure 2.2 Current distribution in various SPS configurations; (a) insulating powder (b) conductive powder and (c) conductive powder in FSPS.

2.2.3 **Spot Welding**

In spot welding a transformer is used to reduce mains voltage to low voltages (~2 V) but very high current (several kA) in the form of a single pulse (0.1-1s). Spot welding is a very clear case of localized heating. In the most common configuration two metal plates are clamped between two copper electrodes. A clamping force (applied with the soft copper electrodes) is used to ensure good electrical connection between the top and bottom electrodes and their respective metal

surface's (Figure 2.3 (a)). However, at the interface between the two plates the contact pressure is much lower, resulting in a high interface/contact resistance. When current is applied this results in localized heating at the interface (Figure 2.3 (b)), which produces a weld nugget that propagates across the interface to produce the joint[22]. Some newer systems use capacitor discharge for spot welding. They are advantageous for precision work such as battery tabs and jewellery[23], as the total

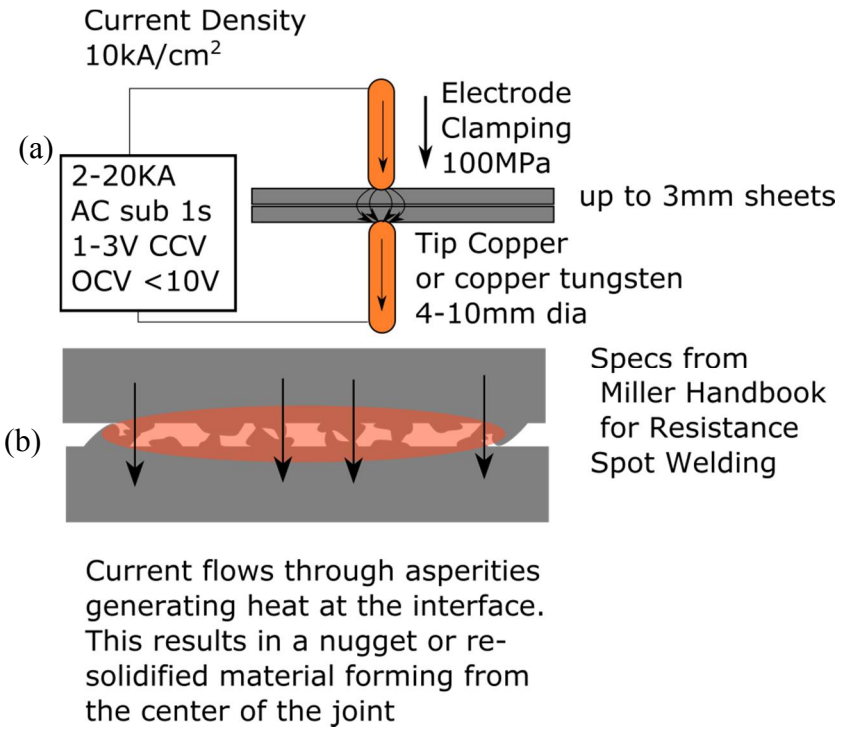

energy supplied can be more carefully controlled. Seam welding is a continuous spot weld produced by using rolling electrodes.

Figure 2.3 (a) Schematic of Spot welding of metals, (b) showing close-up of interface.

2.2.4 **Electrical Upset Forging**

In this technique solid rods of metal are gripped circumferential and pushed into an

anvil while applying a high current (several kAs at low voltage <10V). The material heats up and deforms, flattening as it's pushed into the anvil (Figure 2.4). By applying heat in this manner greater deformation can be achieved at a lower force as opposed to traditional upset forging[24] which can requiring several cycles of heating and deformation. Electroplastic effects are expected to help the process, due to the high current density and high pressure[25].

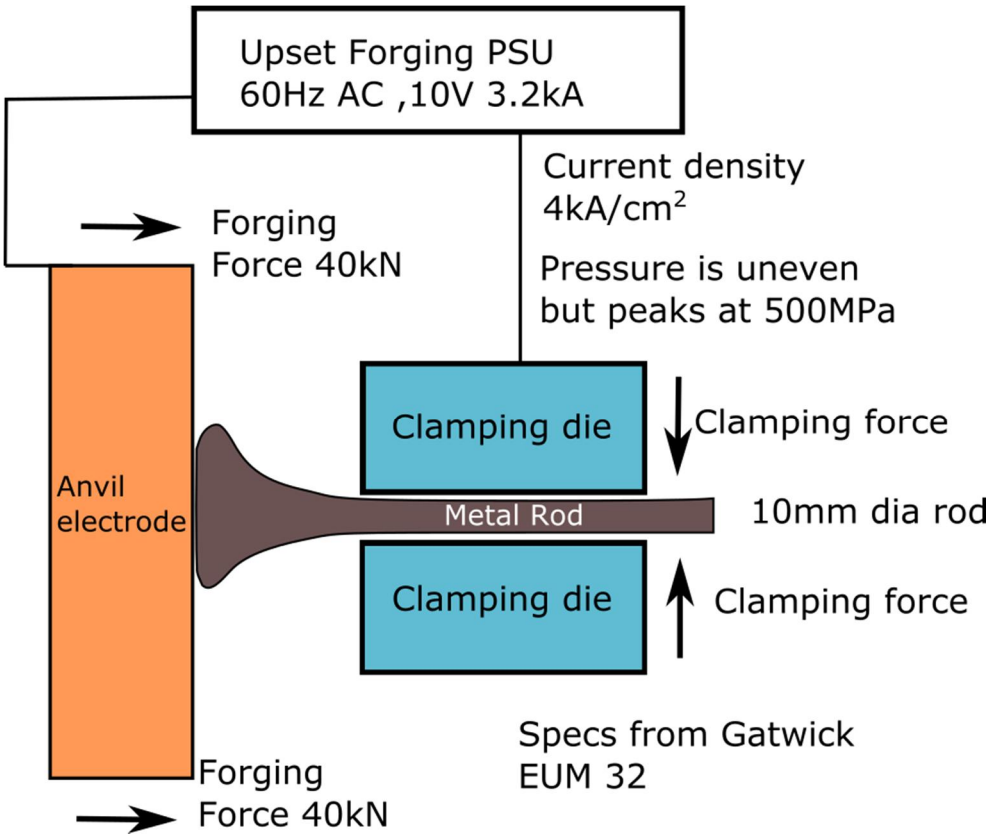

Figure 2.4 Schematic of Electrical upset forging

2.2.5 **Electric Current Assisted Wire Drawing**

This process is very similar to the electrical upset forging, but in this instance a

current (several kAs) is pulsed through a wire as it is being drawn through the forming die (Figure 2.5). Pulsed current is used as current understanding is that the electro plastic effect (reduced yield stress) is mainly dependant on the maximum current[26], and high continuous current would cause excessive heating/melting. This process in not yet used on an industrial scale.

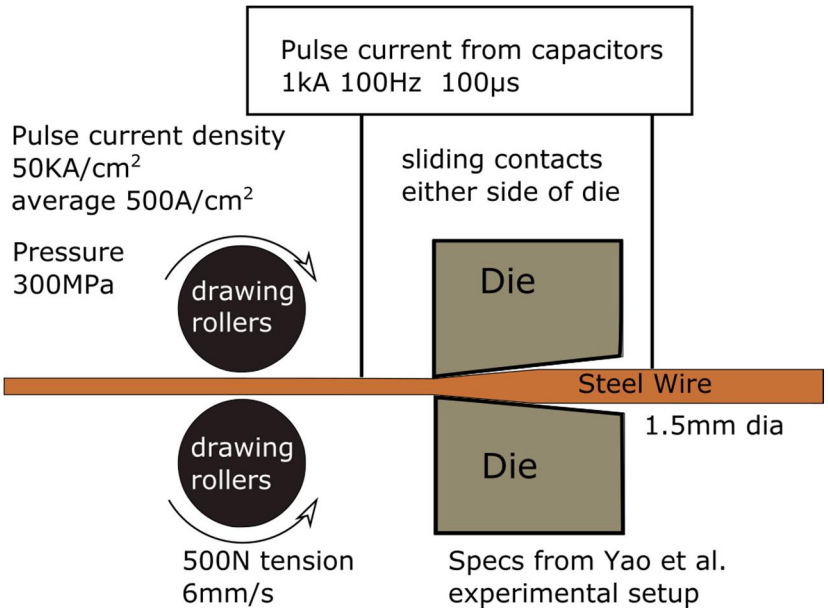

Figure 2.5 Schematic of Current assisted wire drawing

2.3 Plasma Processes

2.3.1 Electro Discharge Machining (EDM)

EDM is a process where controlled arcing and plasma generation is used for removing material for net shaping. A pulsing power supply is used to rapidly ignite an arc in the gap between an electrode and the work piece/sample. A dielectric fluid is used to fill this gap, often de ionized water. The fluid is needed to flush out the

removed material and to enhance the arc[27]. The effect of plasma in this process is undeniable, the voltage rises until breakdown of the dielectric fluid which causes a plasma to ignite in the gap. The large available current allows the plasma to rapidly

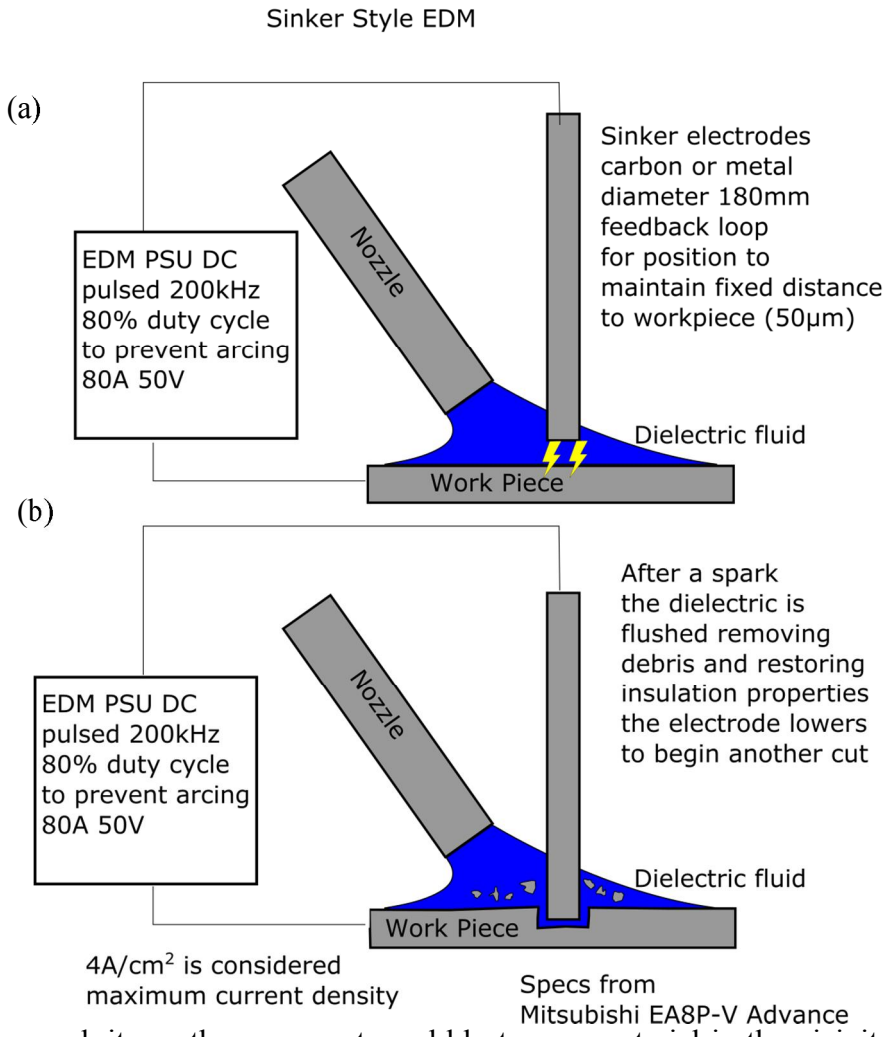

expand, it can then evaporate and blast away material in the vicinity (Figure 2.6 (a)). Once the pulse is over, the plasma extinguishes and the cycle can be repeated once the debris has been flushed away[28] (Figure 2.6 (b)). Local melting at the surface of the arc crater is visible and can affect the material to a limited depth[29]. Micro cracks are produced due to the rapid heating and quenching, the effect is much reduced at very low pulse power levels.

Figure 2.6 Schematic of the EDM process showing before (a) and after (b) a discharge

A unique derivative of EDM is Electro pulse coating, which is EDM in reverse. A target electrode is rubbed against a work piece, and as the current is pulsed material is blasted off the target and deposits onto the work piece[30]. The morphology of these coatings is determined by the electrical parameters which are in turn effected by the plasma properties. Another derivative is the explosion wire technique, in this technique a large current is passed through a thin wire in an insulating medium (water, kerosene or inert gas). When the pulse of current is applied the wire evaporates, from Joule heating, and a plasma ignites from the metal vapour. As the vaporised metal cools it forms very small spherical powders[31]. These are then collected in the insulating medium. In this technique the thermal and electrical properties of the plasma is exploited to achieve incredible heating rates[32].

2.3.2 **Arc Melting**

Used predominantly for homogenising/purify samples. Here a high current (up to 200 A for bench top units, Figure 2.7(a) and many kA for industrial billet making, Figure 2.7(b)) is passed directly through the sample using an arc. The sample is heated by the current flowing though it (Joule heating) as well as the heat transferred from the arc. However, the current is not distributed evenly, it is focused at the arc site and dissipates as the distance from the arc increases[33]. The region directly in contact with the arc is normally molten once the sample has heated up. The reason arc melting is used for homogenising samples is because by melting

only a portion of a sample at a time it is possible to sweep dissolved species around in the melt. Dissolved gasses can also be removed by arc melting.

The power of arc melting is to purify and homogenise materials. It has become an industrially important way to produce large billets (pictured in Figure 2.7a) of specialty alloys, like titanium and nickel super alloy. Another key feature of arc melting is maintaining the alloy composition. This is because there are no refectory surfaces for the alloy to react with, only water cooled copper. The water cooled surfaces also allow the microstructure to be controlled by adjusting cooling rate of the copper mould.

On the lab scale, smaller machines (Figure 2.7(b)) are an excellent way to produce small quantities of exotic alloys from pure elements, even with very reactive elements like titanium. Alloys can be produced with very little loss of material, ensuring the starting composition is the same as the final alloy. In arc heating a cleaning action can also occur as ion bombardment can etch and remove surface contaminants. This is most clearly seen in the cleaning action in TIG welding aluminium under ac[34]. Recently, this has been expanded to using a hydrogen plasma to selectively remove alloying elements[35]. Plasma has also been used to reduce metal oxides. By turning hydrogen gas into highly reducing atomic hydrogen species oxides can then be reduced into pure metal [36,37].

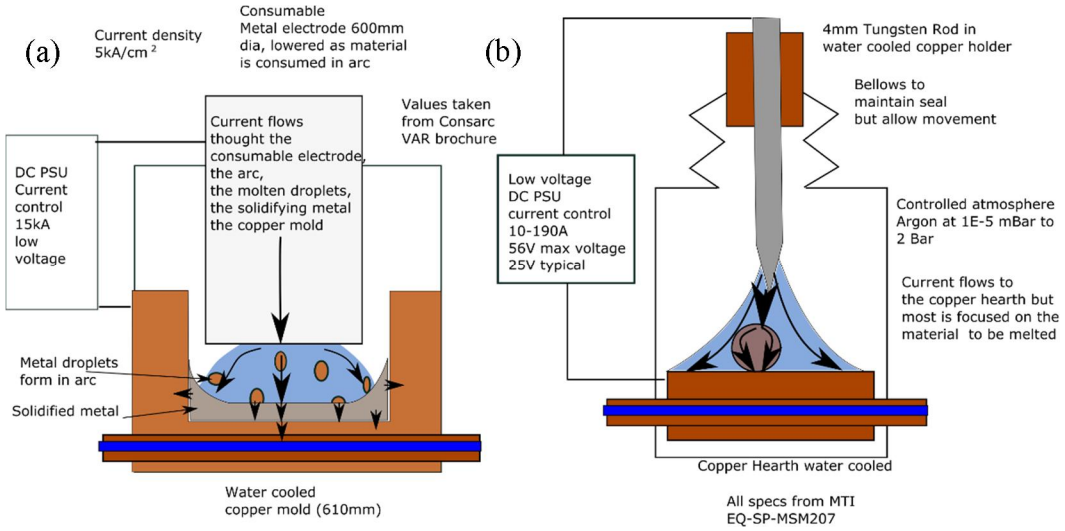

Figure 2.7 Schematics of industrial (a) and lab scale (b) arc melting apparatus, Plasma is shown in blue, current is signified by arrows.

2.4 Electromigration and Electrochemical Processes

2.4.1 Anodic Bonding

This is a process used in microelectronics where glass is bonded onto glass or silicon wafers to provide a hermetic seal. This is achieved by using polished parallel surfaces that are then pressed (low pressure) into each other at moderate temperatures (from 200°C to 500°C). This is insufficient to produce bonding, but on the application of a dc electric field (200V) the mobile species drift across the interface resulting in rapid bonding (10min) of the wafers/discs (Figure 2.8). When bonding Pyrex glass to a silicon wafer the sodium ions in the glass diffuse towards the electrode while oxygen drifts towards the Si. At the silicon wafer interface the oxygen will react with the Si forming silica glass, this results in a strong bond

between the glass the grown oxide layer. Concentration gradients of sodium and oxygen are visible in the sample on cross sectioning[38], this is clear evidence that electromigration has occurred and the ionic conductivity of the glass is responsible.

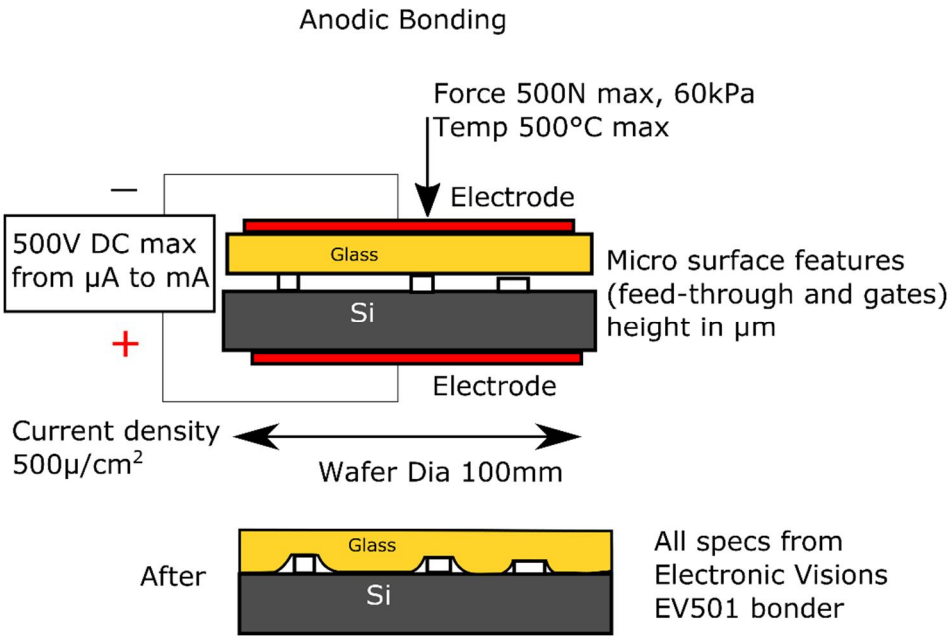

Figure 2.8 Schematic of the anodic bonding procedure showing before and after the bonding

2.4.2 Electrochemical Refining

Millions of tons of material are produced electrochemically each year. This most commonly involves reduction of metals from their ores[39], most obviously aluminium and now titanium[40]. Electrochemical methods are also used for purifying and plating many other metals e.g. copper. The principle is usually to dissolve or melt the material that is to be reduced, to produce free ions of the material, i.e. making the material an ionic conductor.

In an ionic conductor with two compatible electrodes on either side an applied

voltage will cause the ions to drift towards their respective electrodes (Figure 2.9(a)). Suitable electrode are needed as when the ions reach the electrodes they need to receive or loose an electron from the electrodes to be turned into their atomic form e.g. gas liquid or solid (Figure 2.9(b)). This process is very well understood for most basic reactions and electrochemistry is its own well established field and used extensively as an analytic tool[41]. In theory the reaction should require a set cell potential, however, in the real world a certain amount of over potential is required due to various losses inside the cell, e.g. polarisation[42]. For this reason predicting when and to what extent electrochemical reduction will occur in a scenario is no trivial task.

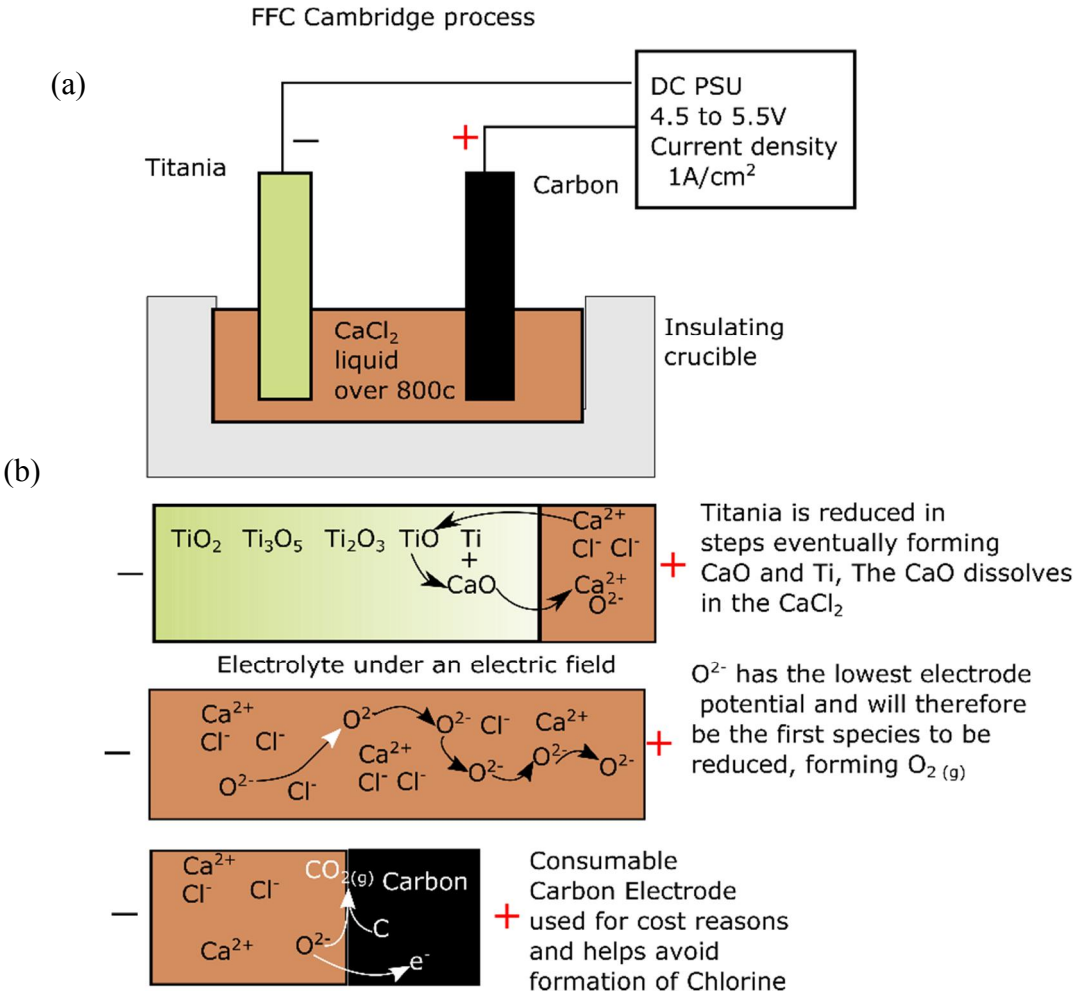

Figure 2.9 Schematic of FFC Cambridge process, showing overall schematic (a) and the movement and reactions between species at various points from cathode to anode(b).

2.5 High Frequency Processes

2.5.1 Induction Heating

Induction heating is a process where a sample is placed in an oscillating magnetic field. This induces a current inside an electrically conductive material which heats

the material via joule heating, and hysteresis for ferromagnetic materials (Figure 2.10). The main feature of induction heating is that the heat is not generated evenly like in traditional Joule heating. Due to the high frequency of the induced current the skin effect comes into play. The eddy currents in the sample generates an internal magnetic field, which repels the alternating current and causes it to become focused on the surface of the sample. The main reasons to exploit this effect is that it increases the local current density in the surface (potentially increasing ECEs), making the material behave as if its resistance was much higher. This higher effective resistance allows induction heating of copper and aluminium. The currents involved in induction melting metals is so high it can even allow them to be levitated, from the interaction of the induced current in the sample and the magnetic field from the coil. By levitation induction melting samples crucible contamination can be completely avoided[43].

The other key difference between dc heating and induction heating is the thermal gradient produced. This is exploited when heat treating steel, as it can produce surface hardened parts with a ductile and tough core[44]. Induction heating also allows much faster heating than radiant heating, and is one of the few non-contact way to heat a sample. Non conducting materials can be induction heated only by placing them in a graphite holder (a susceptor) which the transfers the heat to the sample. Using graphite tooling, where no current flows through the samples is how an induction hot press works.

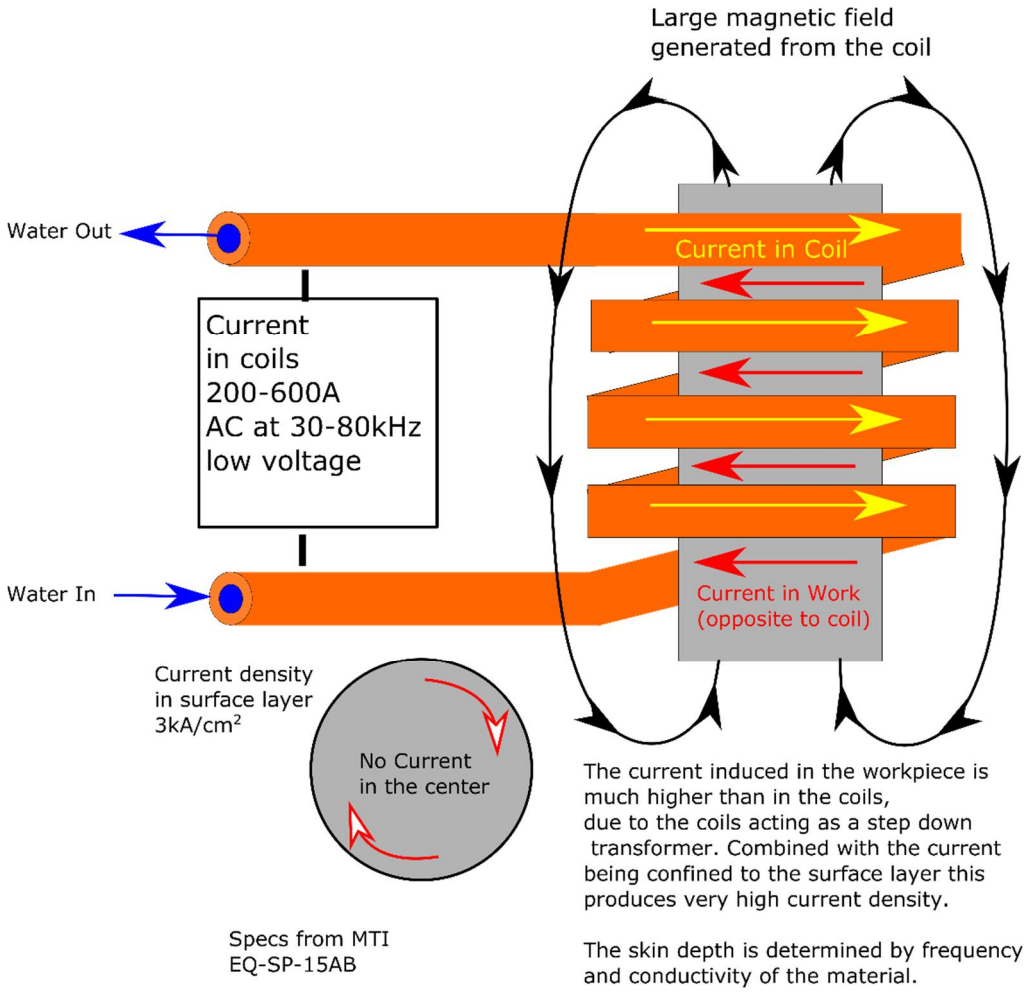

Figure 2.10 Schematic of Induction heating, showing current distribution inside sample

2.5.2 **Microwave and RF Heating**

Microwave heating for industrial materials processing is usually focused on sintering. While materials can be sintered in a modified kitchen microwave oven[45], purpose built industrial microwaves, both single and multi-mode exist.

Multi-mode industrial sintering furnaces are very similar to a domestic unit in operation, Microwaves are fed in to a metal cavity where they bounce around randomly. When processing poor absorbers of microwaves, or particular rapid

heating is required, single mode microwaves are used. Here the cavity is tuned so there is only one way for the microwaves to reflect around. The cavity resonates in a single mode allowing the EM field to build up resulting in a higher power density[46](Figure 2.11(a)).

Microwave heating can either be direct, the sample absorbs the microwaves, or indirect, where the microwaves heat a susceptor material that then reradiates the heat onto the sample. As no microwaves actually interact with the sample in the indirect method it will not be discussed further in this work. In some cases a susceptor is used to provide a preheating of the material until it is hot enough to absorb microwaves itself, this is often referred to as hybrid microwave heating[47].

For direct microwave heating a variety of effects can be seen depending on the type of material being heated (Figure 2.11 (b)). For conductive materials, dense metals etc., most of the microwave power is reflected. While this produces little heating it causes high voltages to be generated anywhere where there is a sharp point (particles in suspension). If the electric field is great enough it will cause breakdown of the atmosphere and arcing which means local heating at that arc points[48]. For more resistive materials e.g. SiC, graphite or powdered metal, the microwaves penetrate some depth into the material[49], inducing current flow in the material leading to joule heating. For dielectric materials there is no Joule heating but a different heating mechanism is possible. For ceramic materials like barium titanate or PZT while they are good insulators for dc in ac they show a frequency dependant resistance or dielectric loss. Because of the high field and frequency that microwaves usually operate at (2400 or 900 MHz), this dielectric loss is sufficient

to heat the material to sintering temperatures[50].

Looking at conceivable ECEs, there is always the possibility of arcing in microwaves, whenever any region experiences microwave induced electric fields exceeding the dielectric breakdown of the or atmosphere. However, as arcing is detrimental to homogenous processing and can even lead to damage of the microwave equipment[51] conditions are chosen to minimise this.

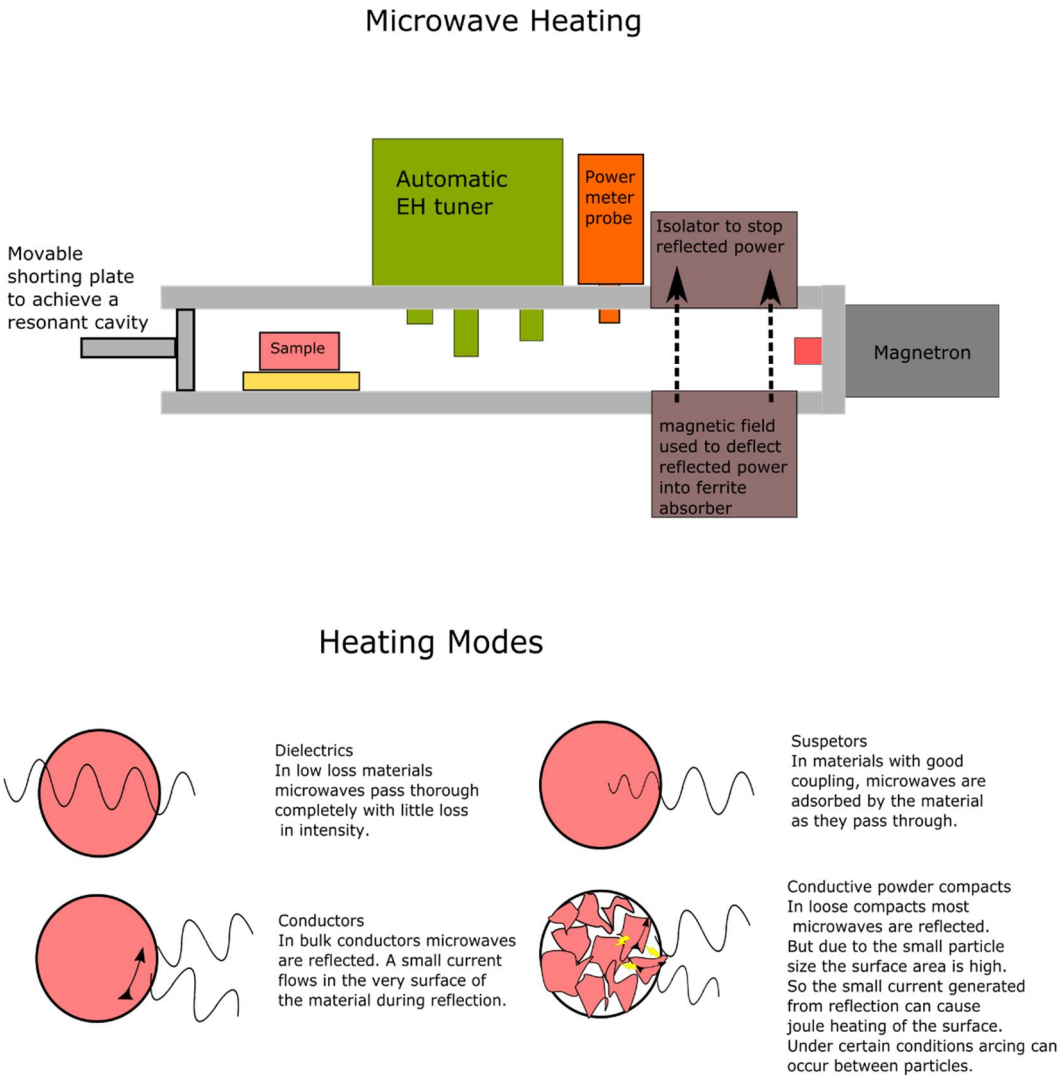

Figure 2.11 (a) Schematics of a microwave heating apparatus and (b) the possible interactions of microwaves with different materials.

RF heating is distinct from microwave processing as it uses flat plate electrodes, not a waveguide to couple the alternating field with the sample (Figure 2.12). Dielectric heating is due to rapidly activating the polarization mechanisms in the sample e.g. polarising one way then the other. The polarization will slightly lag the applied field, and as the frequency increases the lag becomes greater and greater and the loss increases accordingly. Therefore the ECE effects will depend on the polarization mechanism. Where ferroelectric domain switching is the main contribution to permittivity and dielectric loss it is possible for microware heating to affect the domain structure[52].

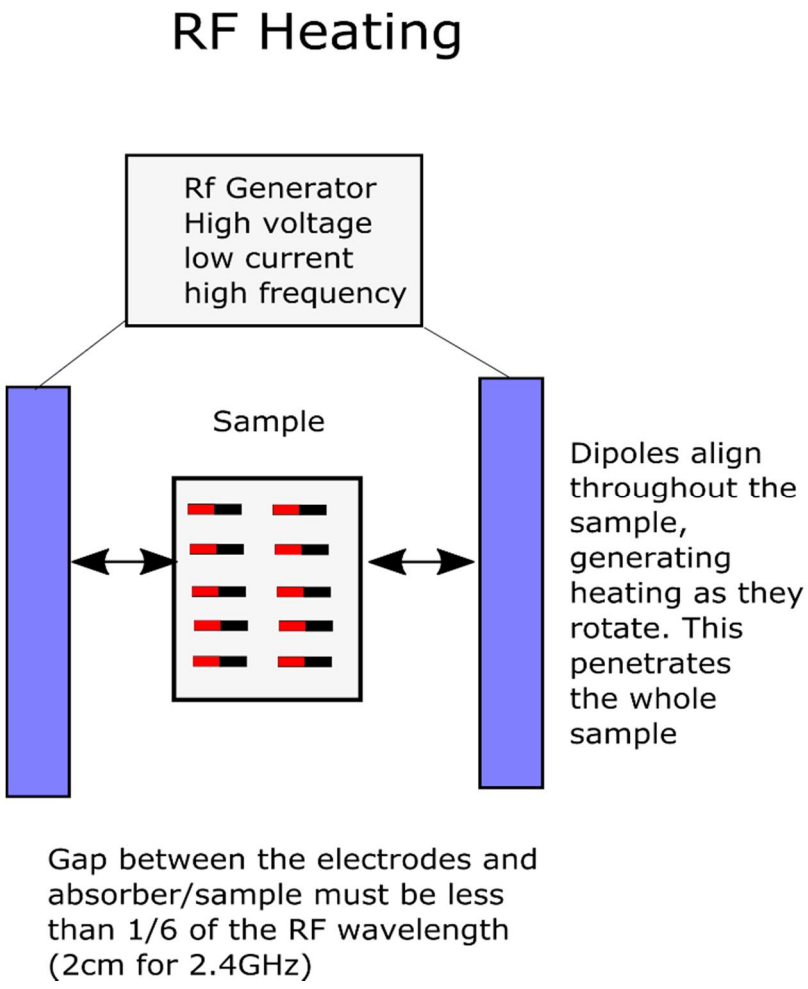

Figure 2.12 A schematic of RF heating

2.6 Secondary ECEs

These refer to effects that occur as a result of current flow, but are generally indifferent to the actual mechanism of conductivity.

2.6.1 Magnetic Effects

A magnetic field is generated whenever a current flows in a conductor. This effect is normally very small, however, for high currents this can generate a sizable Lorentz force. The induced magnetic field can also interact with the current producing it causing the current to concentrate on the surface of the conductor, this is called the skin effect. The Lorentz force can also generate a radial compression force on the conductor. For extremely high currents this force can implode the conductor. The radial Lorentz force can even be exploited to force a liquid metal to infiltrate a reinforcing body[53]. The magnetic field can also affect the magnetic properties of the material (switching domains) as well as interact with any magnetic defects etc. Induced magnetic fields can have further ternary effects due to magnetostriction effect, whereby the magnetic field physically distorts the material.

2.6.2 Peltier/Seebeck Effects

These are well known interrelated effects whereby a thermal gradient is generated by application of current (Peltier), and conversely a voltage can be generated by

the application of a thermal gradient (Seebeck). This is the working principle of a thermocouple. When heating thermoelectric materials with dc (for sintering etc.) the currents used can result in significant thermal gradients[54]. Even some structural ceramics show noticeable temperature gradients during processing. The temperature gradient can alter the microstructure causing material transfer by vapour phase (condensing on the cool side) or causing uneven densification[55].

As can be seen above there are a variety of ways an electrical current can interact with a material and alter its behaviour during processing, its final microstructure and properties. The following section looks in depth at the proposed mechanisms that might actually produce this interaction. Details on how the proposed mechanism might work will be discussed, evidence for and against, as well as requirements for the effect to occur e.g. voltages, current density material type etc.

2.7 **Different Proposed ECEs**

When talking about ECEs it is important to remember that Joule heating is an unavoidable effect. As the temperature gradient of internal Joule heating is practically impossible to recreate with external non Joule methods, it is very difficult to make true like for like comparisons. However, most of the effect discussed below show changes in materials response or properties that is far in excess of what any thermal affects could achieve.

Another important thing to bear in mind when discussing ECEs is that in sintering and to a lesser extent joining is the surface of the particles or joint. It can affect the

sintering rate, porosity and the final microstructure. So when discussing ECE a lot of focus is on the effect at the surface, interface or necks.

This focus on the surface is very justified as a surface coating is almost always present. If the particles are handles in air then they will rapidly grow a native oxide layer. Even oxide materials are not completely free from surface layers either. The atmosphere also contains moisture and carbon dioxide, which can be adsorbed or react to form hydroxides or carbonates.

For solid state sintering the effect is very pronounced as material will have to diffuse through the barrier that is the surface layer. This will tend to significantly slow diffusion, especially for metals as the oxides have much lower diffusion coefficient than the bulk metal[56]. However the oxides are not always stable so can dissolve or be reduced by the atmosphere, restoring higher sintering rates.

Surface layers don't have to be a disadvantage, by intently coating particles with an easy to decompose coating they can be protected from oxidation but allow easy sintering[57]. The surface layer can also be more active than the bulk enhancing sintering, for example adsorbed moisture can form hydroxide surfaces that are easier to sinter than oxides[58].

There has been substantial work on trying to manipulate the oxide layer or its behaviour. The choice of sintering atmosphere or how the powder is prepared and handled can play a large role in the surface layers and the resulting sintering. So it's no surprise that electric current has also been used in an attempt to affect these surface layers. This is why there is such interest in EC processes that occur at necks

and particle surfaces, anything that can disrupt or remove the surface coating can significantly affect the sintering.

2.7.1 **Plasma Generation**

Plasma generation has been proposed as a possible explanation for the experimentally reported enhanced sintering of metals in SPS. When two conductors make contact and are then separated (either by being physically moved or overheating to the point of evaporation) then an arc can be struck between them. For this to happen there must be sufficient voltage to support an arc (see Chapter 2.8.2 Table 2.2). The arc being very hot might evaporate and blast off any surface oxide on the particle surfaces and allow clean metal to metal (or ceramic to ceramic) contacts. This should produce superior sintering as there is no inhibiting oxide boundary. All materials have some surface coating be it oxide, nitride or adsorbed moisture. However the effect should be much more pronounced on materials with thick hard to remove oxide coatings, such as aluminium. For plasma generation and surface cleaning to occur various conditions must be met. The powder must be conductive, have an insulating oxide layer, contact must be made and then broken (via overheating or other ways), and the arc must extinguish rapidly (to avoid forming large nuggets). Given the voltage needed across a contact this is unlikely to occur in powder compacts without high voltages and currents.

2.7.2 Electrochemical Reduction

If a voltage is applied across an ionic conductor that exceed the redox potential then the material can be electrochemically broken down into its constituents. This is a very well understood process and underpins vital industrial processes, like the production of aluminium and chlorine. However electrochemical reactions can occur in material processing without being immediately noticeable. The threshold voltage (not field) needed to split a compound is usually very low, about 4V will reduce most materials[59]. This means that electrochemical reactions could occur in practically any ECAS process when used on ionic conductors. Electrochemical reduction could be expected to produce a second phase or change the stoichiometry of the sample. This change might allow sintering at a lower temperature[60] or compositional gradients to develop.

2.7.3 Local Melting

When two particles are in contact then there will be a contact resistance, due to the reduction in cross sectional area at the neck and also due to the actual interface/asperities. This will produce local heating at the regions or higher resistance. The degree of local heating this results in will depend on; the thermal and electrical conductivity at the interface, the time scale of the applied current and particle sizes. Various models have been made of contacting particles and the general consensus is that local heating is only significant for large particles and very short current pulses. This however is contradicted by several, papers have

reported experimental evidence of surface melting[20,61] of sub 10μm particles. However direct temperature measurements (time and spatial) on this scale are very difficult so true experimental proof is lacking.

2.8 Calculating the Scale of ECEs

Given the various ECEs that can occur when processing a sample it is important to have a sense of scale, i.e., which of these effect are liable to actually affect the material. For some ECEs this is relatively easy to determine, there are threshold values or simple equations, but for other effects complex models must be developed and verified with other experiments.

2.8.1 Evaluation of Ionic, electronic and mixed conductors

Some ECEs are limited to only one conductivity mode for example electrochemistry can only occur for ionic conductors. So being able to tell if a material is an ionic, electronic or mixed conductor can rule out some ECEs. The conductivity mode of a material can usually be found in literature, but for novel compositions or at nonstandard temperatures/conditions this must be found experimentally. Impedance spectroscopy is a powerful tool for understanding the source and mechanism of conductivity in a sample, but it requires significant expertise to properly interpret the data[62]. Alternatively blocking electrodes can be used to stop either the ionic or electronic conductivity to find the ratio of conductivity modes. This is often referred as the Hebb-Wagner method, but it has

many limitations and requires careful experimental setup[63].

To further narrow down the possible ECEs its necessary to look at the specific conditions used and how likely they are to activate a given ECE. Below is a collection of some relevant data and equations to evaluate the scale or likelihood of a given ECE effecting a sample.

2.8.2 **Plasma**

The topic of plasma physics is very large, so this section will focus only on the relevant information and simplifications will have to be made. But as plasmas formed the basis of two later chapters, significant depth is required. A plasma is an ionized gas, and will respond to an electric field. While it is possible to produce a plasma without the application of electricity (flames contain a small degree of ionized species due to thermal excitation), it is far more common to use electricity or EM waves to ignite and sustain a plasma. In the case of SPS or other ECAS processes, direct electrical discharge is the driving force for the formation of a plasma.

To calculate whether a plasma could affect a given electrical process its first necessary to know what kind of plasma could form. Plasmas are generally divided in to a thermal or non-thermal plasma. This is due to the fact that there are 3 types of species in a plasma, free electrons, ions and neutral atoms. As the free electrons are the lowest mass species, they are accelerated the most by the application of an electric field. This means that they absorb most of the applied electrical energy and then transfer it to the other species by means of collisions. In some of these

collisions a neutral atom will be ionised and in others an ion will capture an electron forming a neutral. It is this interaction that release a photon of energy equivalent to the ionization potential. This is the origin of plasmas emissions, which forms the basis of many analytical techniques, e.g. AES and ICPS. Due to the kinetics of the collisions there can be a difference in temperature (average velocity) between the plasma species if the equilibrium cannot be reached (pulsed or ac power). For this reason non-thermal plasmas are often referred to as non-equilibrium plasmas. Given the conditions of most ECAS processes, a thermal plasma is likely to dominate, as non-thermal plasmas requires some special technique to ensure the electrons do not have time to transfer significant energy to the other species. Thermal plasmas on the other hand have are very similar temperature for all of the species, due to frequent collisions. For a thermal plasma at room pressure the temperature is very high, with 5000K being near the lower limit of stability[64]. They can be produced with a simple dc power supply and are stable across a wide range of pressures.

Even in a simple dc discharge systems there are several different plasma types or modes. These can be generated when two plates are separated in a controlled pressure environment. A voltage is applied between the two and the current is controlled by the power supply. As the current limit is increased, the change in voltage is recorded. Current control is needed due to the nonlinear behaviour of the curve. The conditions under which the different plasmas are formed are illustrated in Figure 2.13.

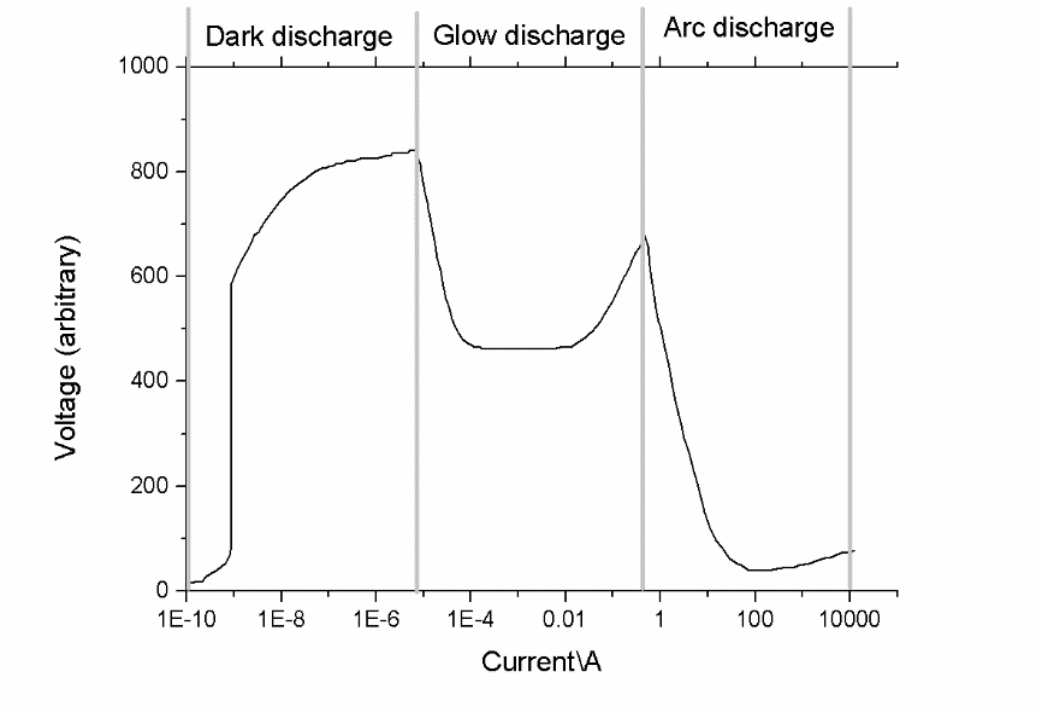

Figure 2.13 . I-V curve for gas discharge modes at 1mBar, adapted from figures from Edbertho[65]

The various modes of plasma operation are very affected by the atmospheric pressure. This graph is a typical one from literature, but is representative for most process that use a rotary vane vacuum pump (pressure near 1mBar). From Figure 2.13 the voltages required for a given plasma mode can be compared with typical

voltages found in industrial process.

However the details of the plot in Figure 2.13 are very dependent on pressure. At atmospheric pressure the glow and arc discharge modes overlap. This means that for a given voltage and current the plasma can either be an arc or a glow discharge. In reality at atmospheric pressure only an arc discharge is stable. This is because a glow discharge is diffuse, and an arc is localised, so the glow discharge can collapse into an arc [66]. The cause of this instability is because at low pressure (1mBar) the electron and ion/neutral temperatures are very different. However, as the pressure is increased the difference between them drops as there are more collisions[65]. As the neutral temperature increases (at pressures near 300mBar) the glow discharge becomes unstable as any hot spots result in thermal runaway. Hotter regions are more conductive so they draw greater current, giving the plasma a large NTC of resistivity.

While Figure 2.13 can be used to tell what mode a plasma is likely stable in a given electrical process there is more to plasma than just stability. A plasma will not spontaneously form without something to ignite it. As can be seen from Figure 2.13, even though an arc plasma is stable at less than 100V, if 100V is applied across a gap initially then only a dark discharge will be generated. To transfer from a dark discharge to an arc, the voltage must be high enough to forma a glow discharge, this can then degenerate into an arc. An arc is capable of being sustained with a low voltage because the plasma is very heavily ionized. There are lots of free electrons and the temperature is very high so it's easy to ionize a neutral. However before an arc is struck the gas is cold so there is no thermal energy to help

ionization and there are no free electrons. To ignite an arc electrons must be accelerated by a high voltage, this gives them sufficient kinetic energy so that in a collision with a neutral they can knock an electron off. The minimum accelerating voltage required to form an ion in a gas is called the breakdown voltage.

2.8.2.1 Non-Contact Ignition

For spontaneous breakdown, the required voltage is dependent on the gap distance, pressure and gas composition. This relationships is normally plotted on a Paschen curve. As illustrated in Figure 2.14.

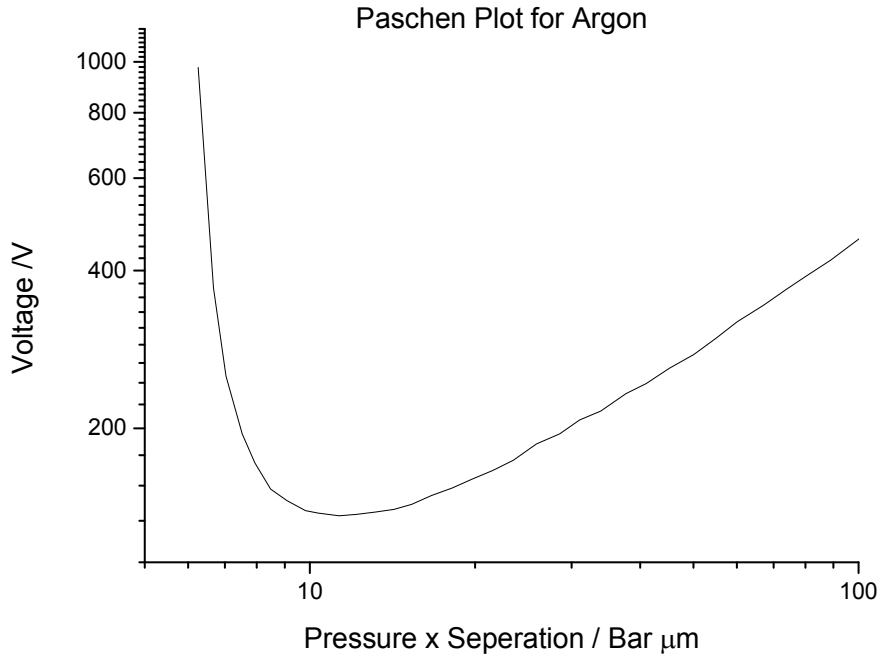

Figure 2.14 A Paschen Plot showing the minimum breakdown voltage of Argon adapted from Berzak et al[67]

From Figure 2.14 the minimum breakdown voltage can be found, due to the shape of the curve no change in pressure or separation can produce a lower breakdown voltage (not field). However, lower pressures do allow a given voltage (as long as it is over the minimum) to produce a breakdown over a larger gap. The Paschen plot for various gases has the same general shape but different minimum voltages and scaling, these variable are listed in

Table 2.1.

Table 2.1 Breakdown conditions for various gases at room temperature adapted from electrical contacts

Gas	Minimum Breakdown Voltage /V	Separation distance for minimum breakdown voltage (at 1atm) /µm
Gas	Minimum Breakdown Voltage /V	Separation distance for minimum breakdown voltage (at 1atm) /µm
$Air_{(g)}$	Voltage /V	breakdown voltage (at 1atm) /µm
$Air_{(g)}$	327	7.5
$N_{2(g)}$	251	8.3
$H_{2(g)}$	273	5.3
$CO_{2(g)}$	450	9.2
$O_{2(g)}$	450	9.2

principles and applications[68]

Plasma can be ignited by even lower voltages, the minimum breakdown voltage is much lower for metal vapours, however the metal needs to vaporized first. This can be achieved by passing a large amount of current through contact asperities. The current and voltage required to ignite an arc for various materials has been found empirically as it is of significant importance in the design of relays. Some of these values have been tabulated below in Table 2.2

Table 2.2 Arcing conditions for various metals, adapted from TE conductivity's application notes on relay life[69]

Material	Arc voltage /V	Arc current /A
$Cd_{(s)}$	10	0.5
$Cu_{(s)}$	13	0.43
$Au_{(s)}$	15	0.38
$Ni_{(s)}$	14	0.5
$Pd_{(s)}$	15	0.5
$Ag_{(s)}$	12	0.4
$W_{(s)}$	15	1

While these values have been determined experimentally the value for minimum arcing voltage can be roughly approximated as the sum of the ionization potential and the work function potential.

$$V_{min} \approx V_i + U_\varphi$$

Where

V_{min} is the minimum arcing voltage

V_i Is the ionisation potential

U_φ is the Work function potential

The physical reason for this is that for an arc to form sufficient electrons must be ejected from the electrode, the voltage must be greater than work function to saturate emission. These emitted electrons must be given sufficient kinetic energy to ionise the atoms of vaporized electrode surrounding them, this is equivalent to the first ionization potential.

2.8.2.2 Other factors

There are many other secondary factors that can affect the formation of plasma, perhaps the most important is the composition of the surface layer, the plasma formation is entirely dominated by the surface material (including oxides, adsorbed moisture etc.) not the bulk. While an arc can quite rapidly remove the surface layer it still dominates the ignition process, this is why relay contacts are often electroplated with noble metals.

Other factors include the geometry, especially the surface finish, play a factor as sharp points act to concentrate the electric field which can lower the breakdown

voltage (but not the arcing voltage). Any source of free electrons or ions in the gap can significantly lower the breakdown and arcing voltage, e.g. ionizing radiation, photoelectrons etc. Finally extreme temperature can effect plasma ignition as thermal ionization lower the voltage and currents needed, however over 2000°C is need for appreciable changes.

Practically all other factors will act to further increase the required voltage. For example the presence of a magnetic field will cause the flow of electrons to bend, resulting in them having to travel a further distance, increase the required breakdown voltage.

2.8.3 **Electromigration**

The type of Electromigration exhibited by a material is dependent on its conductivity mode. For electronic conductors indirect electromigration dominates, however, the required current density is very high 1MA/cm^2 [70] and significant effects only seem to be seen for very small conductors. The effect is much more pronounced at higher temperatures, especially if there is a liquid phase present, this lowers the required current significantly to 25kA/cm^2 [71]) but this current density is still very high compared to most ECAS processes. Another interesting feature is the effect seems to disappear under pulsed dc or ac, as the atoms can return to their equilibrium position when the current drops[72]. That is not to say that indirect electromigration can be completely ignored, in fact it has been exploited to separate out isotopes in molten metals[73].

The indirect electromigration force is the force applied to defects that is produced

from electrons scattering off them, and can be calculated according to the following equation[74].

$$F_{wind} = -\frac{\eta \rho_d m_0}{\eta_d \rho_b m_e} e\mathrm{E}$$

Where

F_{wind} is the force on the defects

η Is the electron density

η_d Is the defect density

ρ_d Is the resistivity of the defects

ρ_b Is the resistivity of the bulk

m_0 Is the rest mass of electrons

m_e Is the effective mass of electrons (due to relativistic velocity)

e Is the charge on an electron

E is the electric field applied to the bulk

While this equation explains the indirect effect due to electron collisions, there is still the direct forces felt by the charged metal ions in the lattice. This is normally much smaller than the indirect one (which is already minor).

$$F_{es} = -eZE$$

Where

F_{es} Is the electrostatic force felt by the ions

e Is the charge on an electron

Z Is the valence of the metal ion

E Is the electric field strength

While indirect electromigration dominates for metals the situation is reversed for ionic conductors. In ionic conductors the ions are not electrically screened by the delocalised electron sea, and there are no electrons to produce indirect migration. For ionic conductor's, direct electromigration can occur, in fact for ionic conductors electromigration must occur for current to flow. The application of a field will cause the ions inside the material to move under the applied electrostatic force. Under steady state conditions (source and sink of ions at both electrodes) this will produce a stable gradient in charge carriers, which follows the following equation[75].

$$\frac{dc}{dx} = \frac{I}{-D}$$

Where

$\frac{dc}{dx}$ is the gradient of species c (the charge carrier) over distance

I is the current

D is the diffusion coefficient of species c

While this is the situation for a steady state these gradients can easily get locked in place upon cooling. This has been exploited to stain glass with ions of another species, producing a surface layer with different optical and electronic properties[76]. The amount of the diffusion species can be calculated using the above equation, allowing electrical control of the resulting ion depth profile. Another issue is to know what happens at the electrodes, if and how are the ions replenished at the electrodes. To understand what happens at the electrodes and outsides of steady

state the key is to understand the electrochemistry of the system.

2.8.4 Electrochemical Reduction/Oxidation

Electrochemical reduction/oxidation is inherently linked to ionic conductivity/electromigration. Electrochemical redox occurs when an ionic conductor has been pushed too far, when the applied voltages is large enough to not only move an ion in the material, but also to oxidize/reduce it at one of the electrodes. If nothing replaces it then the material will become deficient in that species, sub stoichiometric. The voltage required to break the chemical bonding in a material can be calculated form standard electrode potentials found in relevant textbooks[77]. However, even for well understood systems there are many complications that can inhibit electrochemical redox e.g. concentration and bubble loses. The situation is only made worse when operating in non-standard condition, e.g. reactive atmosphere, mixes of compounds and complex electrode geometry. However, the standard electrode potentials are still a useful guide, as they are represent the lowest possible voltage that reaction could occur at, bar other sources of energy like thermal and chemical.

2.8.5 Electroplasticity

Electroplasticity is related to electromigration, it can be understood as electromigration of dislocations. Most of the literature on this subject is for metals and the required current density is very high, of the order of 1-10kA/cm^2 [78]. Also

electroplasticity is normally associated with a reduction in yield stress of at most half[79]. This means electroplastic effects will be hard to detect experimentally unless the applied stress is at least half the normal yield stress.

The most common explanation for electroplasticity is the electron wind effect. This is where electrons transfer momentum to dislocations and help to push them past pinning defects. The force the electrons transfer to the dislocations can be calculated according to the equations bellow. However for most materials the resultant force is insufficient to explain the results seen[80]. More recent work proposes that a magnetic field can accelerate this effect significantly[81].

$$\frac{\gamma_I}{\gamma_n} = \frac{B(B\tau b - B_{ew}^2 V_e)}{\tau b(B^2 - B_{ew}^2)}$$

Where

$B_{ew} = \frac{F_{wind}}{V_e}$ Is the electron push coefficient, for F_{wind} see Chapter 2.8.3

$B = \frac{\tau b}{v_D}$ Is the electron drag coefficient

γ_I Is the strain rate occurring under current flow

γ_n Is the normal stain rate

τ Is the applied stress

v_e Is the electron drift velocity

v_D Is the dislocation drift velocity

b Is the burgers vector

There is some work on electroplasticity in ceramics,[82] in most experiments the

current used is lower but the field/voltage is much higher than in metals. The mechanism at play is likely to be significantly different due to the different deformations mechanism in ceramics. One explanation for electroplasticity in ceramics is that when high voltages are applied on an ionic conductor electrochemical reaction occur. So the material might not be reducing its yield stress/becoming plastic, but forming a new phase at grain boundaries that allows the grain boundary sliding to occur.

2.8.6 Secondary ECEs

2.8.6.1 Skin Effect

The skin effect is the tendency of current to concentrate on the surface of a conductor when carrying ac. It is normally ignored but is important at high frequency and currents. Skin depth is the depth to which 63% (1 standard deviation) of the current flows within. It can be calculated using the skin depth equation given below[83]. A small skin depth with respect to the conductor size effectively increases the resistance of the conductor.

$$\delta = \frac{1}{\sqrt{\pi f \mu \sigma}}$$

$$r_{AC} = r_{DC}\left[1 + \frac{1}{48}\left(\frac{r_w}{\delta}\right)^4\right]\Omega$$

Where

r_{DC} is resistance of conductor as measured under dc

r_w is the radius of the conductor

$\delta$is the skin depth

f is the frequency of the applied current

μ is the magnetic permittivity of the conductor

σ is conductivity

This approximation is accurate when skin depth is moderate, less than half the radius. For higher frequencies (larger radius to skin depth ratio) the resistance is completely dominated by the skin depth.

2.8.6.2 Lorentz Force

Whenever a conductor carries a current it will generate a magnetic field. This magnetic field interacts with the current flowing, giving rise to the skin effect. It can also interacts with external magnetic fields, creating a force on the conductor called the Lorentz force. This force can be can be calculated from the below equation.

$$F = \mathrm{I}l \times \mathrm{B}$$

Where

F is the force experienced by the conductor in N ($Kgms^{-2}$)

l is the length of wire in m

I is the current in A

B is the magnetic field strength in T ($kgs^{-2}A^{-1}$)

The Lorentz force can also affect a material without the application of an external field. Here each part of the material is affected by the magnetic field of the other

parts. The net effect is a pinching effect that pulls material inward to the centre of the current. This is call z pinch and can be used to create massive forces that can crush metal tubes. This principle is very important in plasma physics as a means of confining plasma.

2.8.6.3 Peltier Effect

When a current flows through a materials it can generate a temperature gradient through the Peltier effect. The charge carrier's adsorb heat at one electrode and deposit it at the other, the effect is most pronounced for semiconductor materials. The effect can lead to uneven heating/sintering or thermally induced cracking[54]. While the Peltier effect is usually considered in reference to junctions between different materials, it is still valid for homogenous samples. This is because there is always a junction at the electrodes. To work out the magnitude of Peltier induced thermal gradients one can calculate the amount of heat pumped from one electrode to the other using the equation bellow.

$$\dot{Q} = (\Pi_A - \Pi_B)I$$

Where

$\dot{Q}$ is the heat generated at the junction

$\Pi_A$and Π_B are the Peltier coefficients of conductor A and B respectively

I is the electric current (from A to B)

The Peltier coefficient is not normally listed in literature but it can be calculated from the Seebeck coefficients that are more readily found in books on this subject [84]. The relationship is simply

$$\Pi = TS$$

Where

Π is the Peltier coefficient in V

T is the temperature of the material in K

S is the Seebeck coefficient in VK^{-1}

2.9 **Summary Table**

Table 2.3 A summary of industrial processes with possible ECEs

Process	Compatible Materials	ac/ dc/ Pulse	Current Density	Electric field	Sample Temperature	Proposed ECEs	Current Path

SPS	Metal, Ceramics	dc pulse	0 to 500A/cm^2	Low(1-5V/cm)	200-2000°C	Plasma Electroplasticity Electromigration Electrochemical reduction,	Through sample and/or die, dependant on conductivity.
Induction Heating	Metals, Conductive ceramics	ac HF	In the surface layer up to 3K A/cm^2	Low (10-100V/cm)	200-2000°C	Electroplasticity	Current flows in the surface of the sample, up to the skin depth
Microwave /RF Heating	Metal powders, Lossy dielectrics Ionic conductors	ac	Absorbed power is a more useful metric, due to difficulties in	Material and coupling dependant, maximum is	20-2000°C	Electromigration,	Through surface/ skin effect in metals. Through the bulk for dielectric and ionic

			modelling.	breakdown of atmosphere			materials.
Spot Welding	Metals	ac or dc	10kA/cm^2	10V/cm	20-2000°C	Electromigration, Local melting	Through the spot weld, current distributed unevenly, greater near the centre.
EDM	Metals, Conductive ceramics	dc	4A/cm^2	10kV/cm, over gap, before the spark.	Sample says cool. Plasma temperature >5000K	Plasma, Local melting	Current flows through the die, the plasma and into the sample surface.

Arc Melting	Metals, Conductive ceramics, Non-conductive ceramics (rarely)	dc or ac	5kA/cm^2	10V/cm, most of the voltage drop is across the arc.	Sample 200-2000°C Plasma temperature 5000K	Plasma, Electromigration	Current flows though the electrode, plasma and molten material.
Electro chemical Refining	Ionic conductors	dc	1 A/cm^2	Due to electrochemical potential, voltage is more important	Temperature depends on conduction point of ionic solution	Electromigration, Electrochemical reduction	Current flows through ionic conductor, relatively homogenous, some

				(1-5V).	(20-1000°C).		current focuses near electrodes
Upset Forging	Metals	ac or dc	4kA/cm^2	Low (1V/cm)	1000°C approx.	Electroplasticity	Through the sample, current density decreases as it deforms
Pulse Wire Drawing	Metals	dc pulse	Average 500A/cm^2 Pulse 50kA/cm^2	Low (10-100V/cm)	20-50°C	Electroplasticity	Through the bulk of the wire, minimal skin effect.
Anodic Bonding	Glasses, Semiconductors	dc	500uA/cm^2	High (500V/cm)	200-500°C	Electromigration	Though the bulk

Flash Sintering	Ceramics, Ionic and Electronic conductors	dc or ac	Material dependant 40mA/cm^2 for zirconia. Power density is a more useful metric	High (500V/cm)	300-1200°C preheating internal modelled at 2000°C	Electrochemical, reduction, Electrical defects, Grain boundary diffusion	Through the bulk

2.10**Aims**

The above literature review focused on the various industrial processes that involve an electrical current passing through a sample during processing. The various proposed ECEs were outlined to try and pinpoint areas of interest. From this review Flash sintering was found to be a very active research area, with many competing explanations, most of which hinge on ECEs. Flash sintering is still in development and has not yet been commercialised despite some early work from Lucideon[85]. This makes it an excellent area for further work.

SPS remains a very popular ECAS process and one of the most ill titled processes. While the current consensus is that there is no plasma or sparking there is still some controversy, a recent (2014) paper reports observing plasma effects[86]. Given the large volume of work on the topic ([61,87-89]), the topic could do with a more in depth understanding of the properties of plasmas, the conditions they need to form and some reliable ways to identify a plasma.

The industrial processes surveyed can be split into two types of process depending on how they were developed. There are processes where electricity was used as a convenient way to heat the material. They were often based on existing non electrical process, or where the current did not previously pass thought the sample. For these altered process once equipment had been developed interesting behaviour was seen and this was then explained as ECEs. Several of these process might not actually have ECEs, but simply different behaviour due to the thermal gradients/ heating rates that electrical heating allowed. On the other hand there were also

process that were designed from the ground up to exploit a particular ECE that was already understood to some degree. These ground up process can be further divided into two branches; plasma based processes, which include EDM and arc melting, and electrochemical process which include electrochemical refining and anodic bonding. While Electroplasticitiy might also be considered an interesting field of study, there is no simple means to isolate and identify the mechanism at play.

Both plasma physics and electrochemistry are their own discrete branches of science and there is little that can be added to the fundamental understanding of these processes. However, as can be seen by the various processes listed above, there is scope to develop novel processing techniques exploiting these processes.

With this in mind, the focus of this work was on gaining an understanding of plasmas with regards to material processing. This greatly informed experiments into plasma formation in SPS and related ECAS process. Once comfortable with the literature it was possible to develop novel uses for electromigration/electrochemistry and also plasma processing. These ECEs where chose at they have been shown to significantly alter the processing of materials, and the equipment needed is relatively modest, with suitable power supplies being readily available.

Chapter 3. Experimental Techniques

3.1 Intro

As mentioned in the aims section this work will focus on several different ECEs, as a result several very different experimental setups and techniques were needed.

To investigate plasma in SPS several experiments were undertake inside and SPS with fibre optic spectroscopy used to detect any spectral emissions typical of plasma. In an attempt to model a higher voltage SPS or other ECAS machine a mock sintering setup connected to a higher voltage PSU, with optical spectroscopy, was used. The voltages and currents applied were logged and spectroscopy was also used to evaluate the temperature at the powder contacts.

To investigate electrochemical effect an electric current was passed thought zirconium diboride while it was heated in air. The current and voltages was measured during oxidation. The samples were cross sectioned and the electrical data was related to the thickness of the oxide layer under the cathode and anode.

As a demonstration of the understanding gained from the earlier experiments on electrochemistry and plasma ECEs a Contactless flash sintering setup was developed. Here a slice of pours refractory ceramic (SiC and B_4C) was heated from both sides by arcs, once the sample was sufficiently hot current was passed through the arcs and sample. This resulted in rapid densification as seen in flash sintering, but without any electrodes touching the sample. Voltage and current was recorded during sintering and the samples were cross sectioned to evaluate density and

microstructure.

3.2 Sample Preparation

The purpose of this thesis is about the effect of electric currents on the processing of ceramics, but before anything can be processed a suitable sample must be prepared.

To investigate plasma in SPS powders were used for testing as plasma was most likely to form at the contact points between hard particles. Initial experiments were attempted with copper powder, however, it showed no plasma emission even at 50V. This could have been due to its low yield stress, melting temperature, resistively or other properties. This work informed the choice of ZrB_2 and W for the later experiments Commercial powders were available for the materials of interest (tungsten and zirconium diboride, so no ball milling of synthesis was needed. Tungsten powder with an average particle size of 0.5 μm, and ZrB_2 powder (Strack Grade B) with average particle size of 2.4μm were used in the experiments. In each experiment about 0.5-1.5g of powder was used. These materials were chosen because of their high melting points, 3683K for W and 3519K for ZrB_2, this means that melting is unlikely to occur without the formation of plasma . Both have low room temperature resistivity (5×10^{-8} Ωm for W[90] and 1.5×10^{-7} Ωm for ZrB_2[91]) and are significantly more conductive than the graphite punches. This meant that even in a conventional SPS configuration significant current should flow thought the powder.

For oxidation testing under an electric field dense samples were needed of zirconium diboride, commercial powder was available, and the material had been sintered before in our lab so literature sintering conditions could be used. SPS was used as it provides a powerful technique to sinter such a high temperature ceramic. The ZrB_2 used in this experiment was prepared by conventional SPS. ZrB_2 powder (grade B from H.C. Starck GmbH) and was sintered under vacuum using 16MPa for consolidation. The sample was headed at 100°C/min to 2100°C and held for 20mins before cooling (final relative density 98%).

After preparing the ZrB_2 it needed to be cut down to fit in the furnace sample holder. It was cut into 3mm cubes using a diamond blade. All the surfaces were polished with 1500grit diamond plates. The cubes were then partially oxidized in air using a tube furnace at 1200°C for 2h using a 10°C/min heating rate. This produced an even, thin (90µm) and continuous oxide layer, which was necessary to avoid short circuits when the field was applied.

For contactless flash sintering the samples had to be pre sintered to a low density, CFS could then be used to achieve further densification. Pre densification is common to other flash sintering techniques but could potentially be replaced with cold pressing in the future. The electrical parameters used for flash sintering must be careful tailored to the properties of the sample being processed. The most important sample property was probably the resistivity vs. temperature profile. Contactless Flash sintering being a newly developed process, meant lots of different materials were initially tested before settling on 3 materials for in depth investigations, pure SiC, SiC:B_4C and pure B_4C. The results of these preliminary

experiments is summarized in Table 3.1. Most of these samples did not survive the processing, so there was not any way to get meaningful microstructure analysis. However their behaviour during processing is summarised in to show the limitations of the CFS setup in its current incarnation. The main cause of problems was the high temperature of the preheating arcs. For this reason while this is primarily a table of failures it shows the potential of the process if different methods were used to generate more appropriate plasma electrodes.

Table 3.1 Table of the various materials that were tested with CFS and their behaviour under preheating arcs and FS PS.

Material	Sintering Behaviour
ZnO	Evaporated under the preheating arcs.
ZrO_2, 3YSZ	Thermal shock caused it to crack violently under preheating
Calcia alumina glass ceramic	Glass phase bubbled under the preheating arcs, boiled vigorously under even lowest flash currents.
ZrB_2	Required large current to heat, resulting in significant surface melting and issues with the tungsten electrodes melting.

The three main materials tested were chosen due to their high temperature stability, so that they were not damaged by the arc. They also have reasonable thermal

conductivity at high temperatures so that preheating can penetrate the thickness of the sample.

Commercial powers were available for pure SiC and B_4C and they were used as is, the composite material was produced by ball milling, a rotary mill was used as only mixing was required, not particle size reduction. The powders were 150g of each power was weighed and mixed in a 2L plastic jar with ≈600ml of ethanol (enough to form a low viscosity paste) 500g of SiC balls (diameter 2-10mm) were added. The jar and contents were milled of 18h at ≈200RPM,

Because of the choice of material for this work (SiC and B_4C, both high temperate hard to sinter materials) SPS was needed to produce 65-70% dense discs (60Ømm by 20mm. These were then ground and cut into thin slices, (18mm by 1.8mm by ≈40mm) using a diamond disc. After cutting, the samples were dried in an oven prior to flash sintering to ensure there was no residual moisture that could cause cracking under the arcs.

The materials used and the sintering conditions are summarized in Table 3.2 It is worth noting that the samples were partially sintered so that they had sufficient mechanical strength to be cut to shape. Potentially a cold pressing technique could be used instead to reduce energy, time and cost as has been used in other flash sintering work[92].

Table 3.2A summary of the different processing conditions and materials used

Material	Grade	Sintering maximum temp /°C	Sintering pressure /MPa	Sintering hold time /min	Relative density /%
SiC	Starck grade UF 10	2000°C	10	5	67
SiC:B_4C	Mix of both roller milled in ethanol 18hr	1550°C	40	30	65
B_4C	Starck grade HD 20	1600°C	20	5	70

3.3 Experimental Methods

3.3.1 Plasma in SPS

As this work is comprised of various different investigations this necessitated very different experimental setups. For investigating plasma formation in SPS data 2 types of experimental setups were used, with several minor variations on both. In the first a fibre optic spectrometer was places in a traditional SPS setup, in the second a higher voltage was used in a mock SPS.

Several preliminary configurations were tested before settling on the main two configurations used. These early experiments showed neither particularly rapid heating nor plasma emission but helped in the evolution of the work. The SPS used in this work was a FCT HP D 25 from FCT Systeme GmbH, Germany. The machine is limited to a maximum voltage of 10V but the power was limited to 50%. However due to the short processing time and the way the SPS is controlled the actual voltage and current varied. As mentioned earlier, the atmosphere can have a large effect on plasma properties and its ignition[93]. Normally SPS is used in vacuum but argon is sometimes used and has lower a breakdown voltage so both conditions were tested. All results discussed in later chapters were done at 0.9Bar argon but preliminary tests at 1mBar vacuum, showed identical results. The voltage and current were logged by the equipment every second. A fibre optic probe was placed inside the powder compact and logged 10x a second. Initially a standard 20mm diameter SPS graphite die and punch set was used and loaded with about 2mm of

powder and pressed under 20MPa. This configuration is typical of conditions used for most SPS sintering runs. This did not show any emission until the top pyrometer was reading over 1000°C and then only black body radiation.

As a result in an attempt to maximize the current density and voltage drop, the graphite die was removed so that all the current would flow through the powder. A side benefit of this setup was that it allowed a more direct quantification of electrical parameters acting on the particles. No plasma emissions were visible but a possible cause was found. The voltage measured across the powder was very low (<1V) because of the low resistance of the powder. The resistance of a powder compact is known to be very affected by the applied pressure, which lead to the final SPS configuration. The final SPS configuration (1) was designed to reduce the contact pressure acting on the particles; two glass slides of 1mm thickness were used as electrically insulating spacers. This configuration is sketched in Figure 3.1(a).

Since the upper voltage of our SPS equipment is limited to 10V, to apply a higher voltage a different dc power supply was needed. In configuration (2) a 50V PSU was used (model ZXY6020S), experiments similar to configuration (1) were carried out inside a quartz tube with flowing argon (4Lpm). To limit oxygen ingress a pressure of 1.1 Bar absolute was used. This setup is shown in Figure 3.1 (b). The power was supplied through the two sealed flanges and the fibre optic cable was fed through a hermetic port. The carbon punches where clamped together. The power supply was set to a voltage of 50V and the current limit was set to 60A. The available power was limited to 240W and was applied for approximately 5 seconds.

The voltage and current limits were chose to maximize the chance that the voltage drop at particle contact points would exceed the arcing values from literature (Table 2.2)

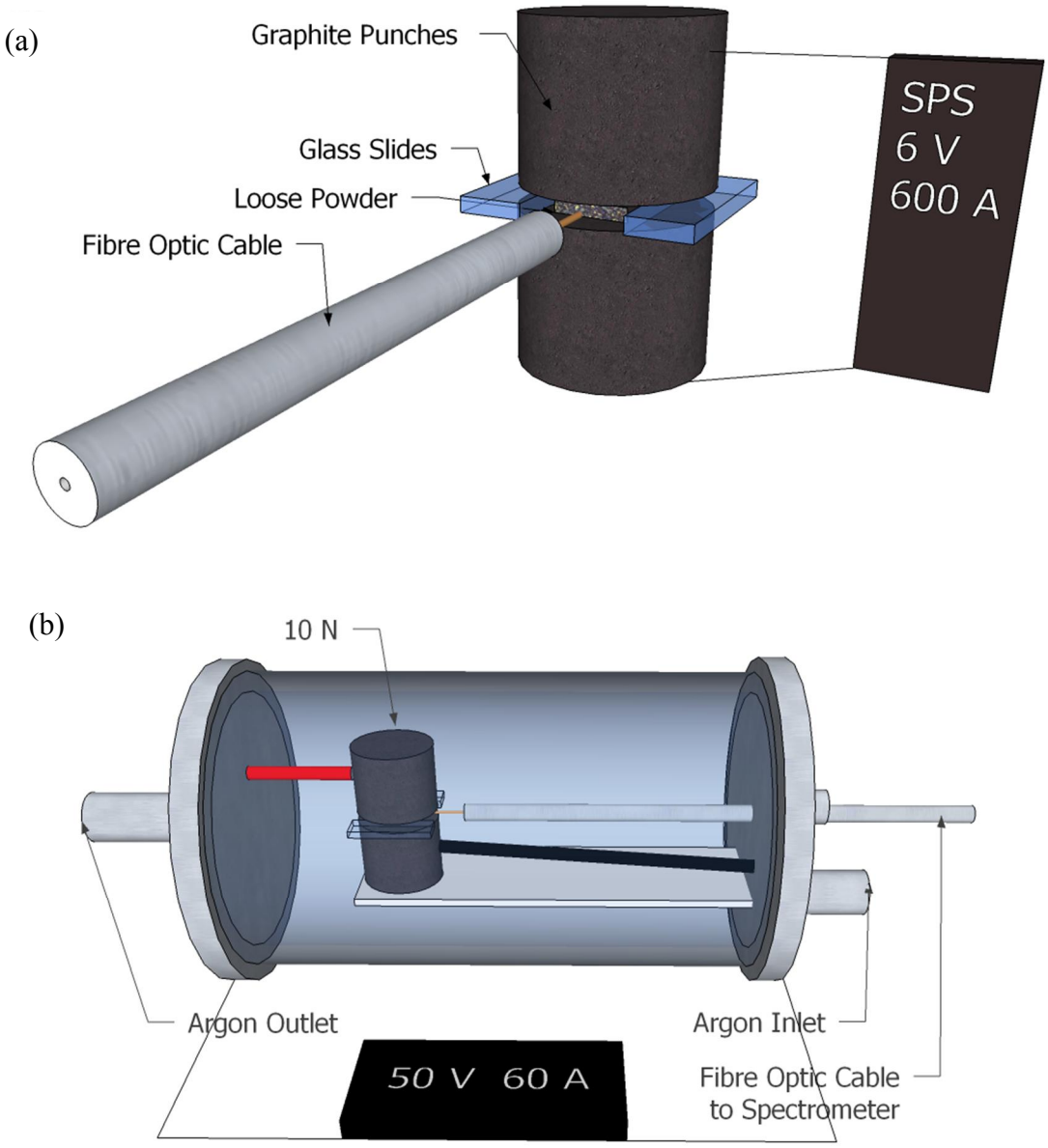

Figure 3.1Renderings of the two configurations used to detect plasma, Top (a) for use in SPS and below (b) using an external power supply

3.3.2 **Oxidation under an electric field**

Typically electromigration and electrochemical reduction require much lower voltages and currents than plasma effects, but take much longer time to produce noticeable changes, electromigration effects also don't require particle contacts, and the situation is simplified in the case of bulk materials. For this reason the configuration used in this electromigration oxidation experiment were very different from the Plasma in SPS work. In this work current was passed through a sample of oxidized zirconium diboride with the aim of exploiting the electromigration of oxygen in zirconia (the oxide that grows on zirconium diboride) to reduce the oxidation of the sample.

The experimental setup used in our investigation is shown in Figure 3.2. It allows the evaluation of the effect of field in both polarities at the same time. With a negatively charged ZrB_2 in the middle and a positively charge platinum foil at the top of the sample, and the reverse at the bottom.

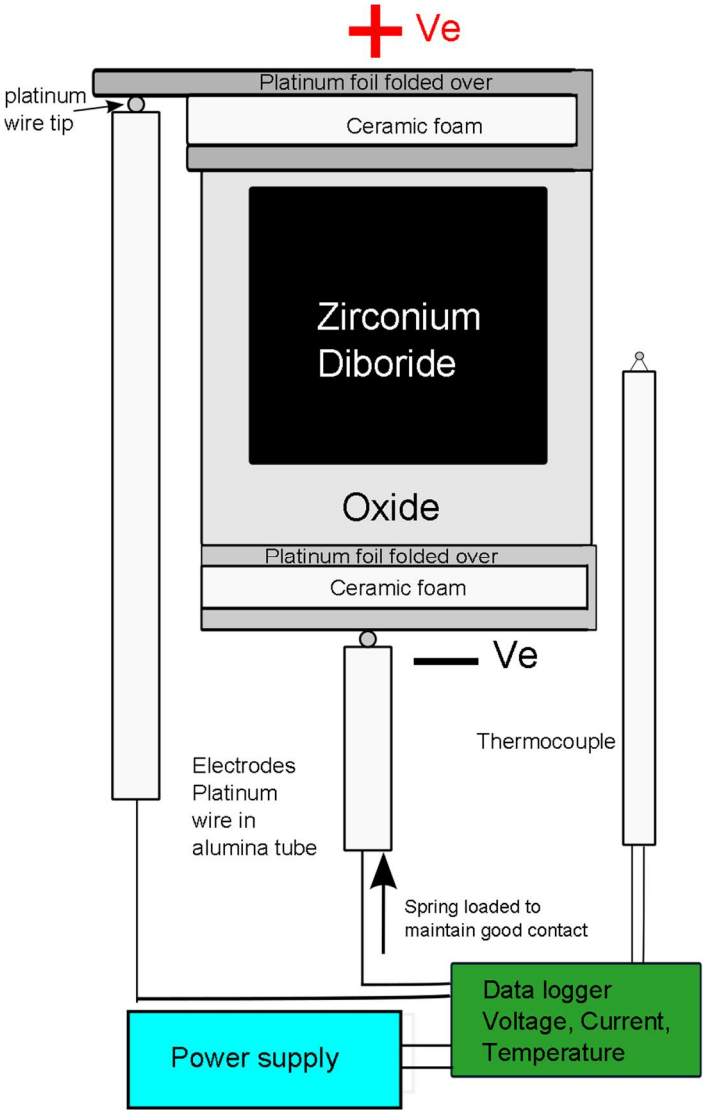

Figure 3.2 Schematic of the experimental setup used for oxidizing ZrB_2 under an electric field.

While it might have been preferable to have a platinum wire connected to the centre of the ZrB_2, this was not practical as at high temperatures (1400°C). The problem is oxygen can diffuse through platinum and

Electrical contact with the sample was made via platinum foil electrodes (Sigma Aldrich thickness 0.05mm, purity 99.99%). To ensure good contact, the platinum

foil electrode was pressed with a spring load against the top and the bottom surfaces of the ZrB_2. The platinum foil was folded over an alumina foam separator to allow the sample to be removed from the setup. This was required as otherwise the platinum foil and electrode welded together at high temperature. The assembly was then loaded into a vertical tube furnace, with an open bottom exposed to a normal air atmosphere. It was then heated at 10°C/min to 1400°C, it was held at this temperature for 5 hours, and then cooled at 10^0C/min to room temperature. The oxidation temperature was chosen after several preliminary experiments. It was found that lower temperatures produced too little oxidation to accurately quantify the electric field contribution and higher temperatures resulted in a very fragile samples. A 5 hour holding time was chosen as it shows a clear difference due to polarity without excessive growth of oxide under the negative electrode. During the duration of the heat treatment a voltage was applied to the sample using a power supply (Agilent E3645A) operated with voltage and current limits, 10V and 100mA. These settings were also chosen based on preliminary testing. Higher voltages were found to be unnecessary as the current limit dominates the behaviour. Lower current limits gave uneven samples as the current flow concentrated in certain areas. Higher currents lead to even greater acceleration under the negative electrode, producing samples that were too fragile. A data logger (National Instruments USB-6221) was used to record the local temperature next to the sample using a platinum type R thermocouple and to record the applied voltage and current.

3.3.3 **Contactless Flash**

The contactless flash sintering technique was developed to pass current through a sample without directly touching it, instead passing the current through plasma on either side. The configuration used was developed incrementally but only the finalized design will be discussed. A schematic of the experimental set up used for CFS is shown in

Figure 3.3. The experimental procedure was to load a pre-compacted sample into a ceramic holder. The sample was placed under the arcs using a 3 axis positioner. The two arcs were ignited in turn and the sample was then raised up so as to be in between the arcs, equidistance between them. The sample was preheated for 5s and then the flash power supply was activated with a set current limit (e.g. ≈6 a) for a fixed period of time (e.g. ≈2, 3, 4 and 5s). The hold time of 5s was chosen so the preheating temperature would be consistent and stable (see Figure 6.3). The electrode and torch spacing's were chosen according to some preliminary experiments discussed in chapter 6.3.1.

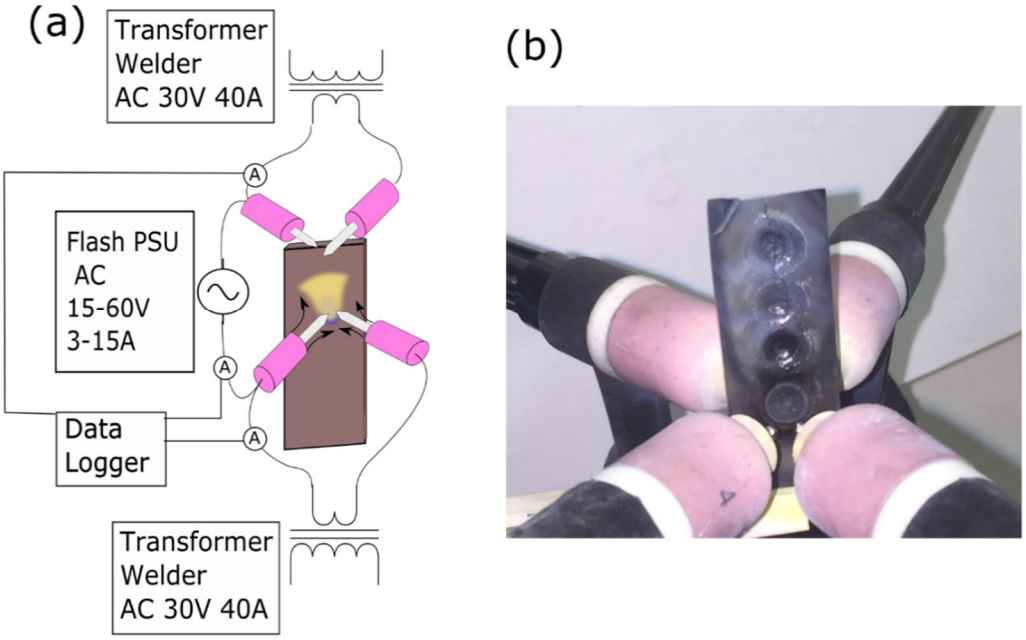

Figure 3.3 (a) schematic of the plasma flash experimental setup. Two isolated transformer welders were used to generate two electric arcs, a flash power supply was used to pass current through the sample. (b) A photo of two twin torches and processed sample.

To start the experiment an arc was struck between the two tungsten rods. This was achieved by shorting them out with a carbon rod and then breaking the contact. This is based on a common procedure in TIG welding called scratch start. Once both pairs of torches were lit, the sample was inserted between them. The distance between the two pairs of torches was critical, and 14mm was found to be optimal

and was used for all experiments unless otherwise stated. If the separation was too great then there was insufficient preheating. Another issue was that as the distance from the tungsten electrodes increased the conductivity decreased, for distances greater than 14mm there was poor electrical contact through the electrodes. The issues of preheating also affects the optimum thickness of the sample (1.8-2mm) for a particular configuration, thicker samples did not allow the heating to penetrate all the way through the sample.

The ac transformer welders (used for preheating arcs) were both set to 40A to control sample heating and wear of the tungsten electrodes. The arc gap (distance between the two tungsten rods in each pair of TIG torches) was chosen to produce a well-defined two zone plasma plume. It could not be too large or it destabilize the arc, 1-2mm was found to be a good range, only needing occasional adjustment as the tungsten rods wore down. The argon flow rate (1L/min) and cup size (no4 gas lens, diameter 6.35mm) were adjusted to provide sufficient coverage to avoid oxidation of the sample and tungsten. Gas flow speed had to be kept low to allow easy ignition of both pairs of torches. Under these conditions and given the resulting ac waveform, the calculated power is given in Figure 3.4 below.

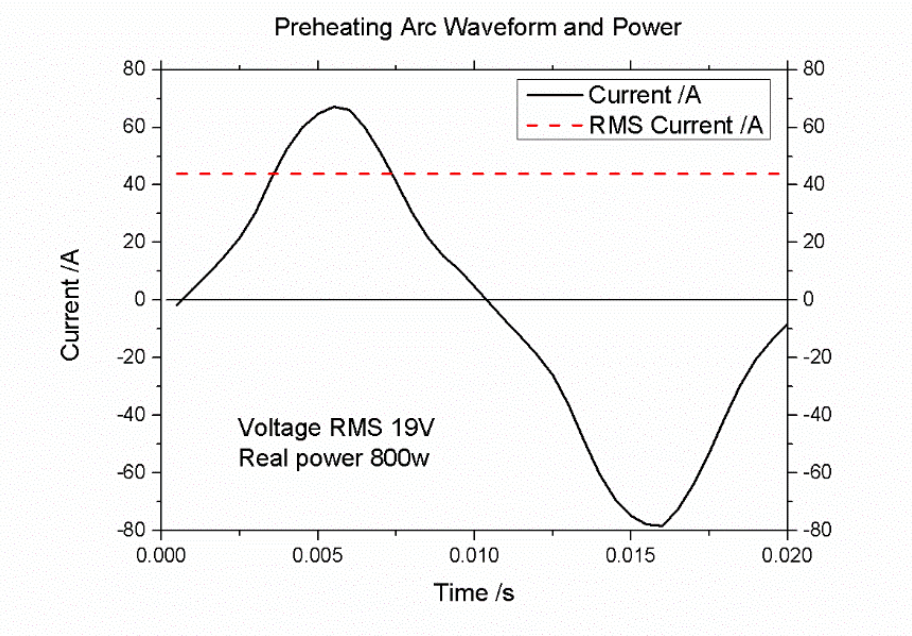

Figure 3.4 plot of the ac waveform of the transformer welder. The root mean square (rms) value of current is included for comparison. Combined with the rms voltage, measured from the isolated multi meter, the real power was calculated

The flash sintering current was supplied using a super 200p 4 in 1 welder. The currents in the two plasma arcs and the flash sintering current were measured using hall effect sensors (allegro microsystems, LLC acs758lcb-100b) connected to a data logger (national instruments usb-6221). The preheating temperature was measured in a separate experiment using a k type thermocouple 1mm in diameter embedded in the sample.

3.4 **In Situ Analysis**

During this work several measurements were made during processing and these

allowed understanding of the processes and also the sequence of events which provided invaluable insights

3.4.1 **AES**

Optical spectroscopy works by passing light through a fine diffraction grating, this causes the light to spread out according to its wavelength, just like a prism. The diffracted lights is then reflected by a series of mirrors that act as lenses, causing the wavelengths to further diverge. The light is then focused on a Linear CCD, a 1D camera. Each pixel only captures light from a very narrow range of wavelengths so the full spectrum of the light can be found by measuring the intensity of light at all the pixels.

Optical spectroscopy when used to detect atomic emission is called AES. Optical emission occurs whenever an electron drops from an excited state to a lower one. This can occur in plasmas, due to thermal excitation, and also from photoemission during charge recombination. The wavelength of light emitted is equal to the energy drop the electron experiences. This means that the wavelength is not only dependant on the element but also the charge state/ chemical bonding of the atom. Emission can occur from molecules as well as atoms and ions. While each emission is unique for a given atom due to the limited resolution of a spectrometer, theses peaks often overlap. This can make identifying species very difficult to do manually. The wavelength resolution of a spectrometer can be adjusted by using different size diffraction gratings and integrating times. But there is a trade-off, a

smaller grating produces more accurate resolution for wavelength at the expense of total light intensity. This lower intensity can in turn be compensated for by increasing the integrating time. Higher integration times come at the price of an increased thermal noise floor. For this reason it is often unavoidable to have overlapping peaks. Fortunately software exists to automate the peak identification process (plasus specline). When using software identification it is important to do some reasonable manual filtering by only selecting elements that are possible in the sample.

Optical spectroscopy can also be used in a more quantitative method to evaluate plasma temperatures. This requires some knowledge about the local conditions of the plasma and only hold for certain situations, e.g. thermodynamically stable conditions. Plasma temperature can be calculated by looking at the relative intensity of the various ionic species and using those values that in the Saha ionization equation[94]. The relative intensity of atomic emission peaks can also be used for chemical analysis, and this forms the basis of ICPS. The intensity of ion emissions peaks must first be calibrated against known values and can then be compared to a table of relative intensity (found experimentaly[95]) to calculate atomic concentrations. These relative intensity tables exist only for certain conditions of plasma that are used for ICPS. A similar situation exists for glow discharge analysis of metals, where a glow discharge is used to slowly erode material from the surface of the metal. Spectroscopy can then be used to find the composition vs. depth profile[96].

In these experiments the bare optical fibre was placed inside the powder, which

allowed direct observation of phenomena occurring during electric discharge. By placing the fibre inside of the compact, emission from particle contact points could be capture, as show in Figure 3.5. These emissions would likely have been missed if the spectra were collected only from the surface.

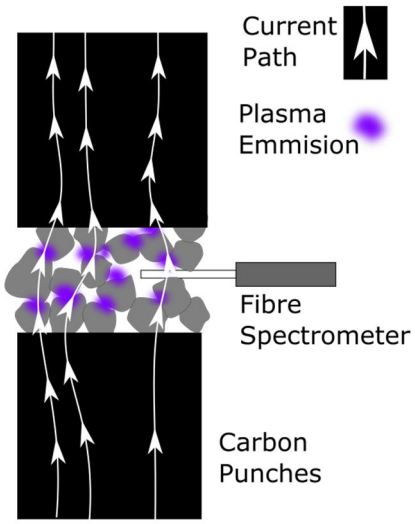

Figure 3.5 A schematic of how Fibre spectrometry allows collection of spectra inside the powder compact

To ensure that the very beginning of the sintering was captured, the spectrometer was set to start capture before power was applied. Aiming for reliable data, for each configuration five samples were tested. For each sample run 200 spectra were collected. Each spectrum was integrated over a duration of 100ms. The spectrometer collected emission spectra in the range 180-1100nm; data was mainly plotted over the range 300-925nm, where it could be accurately calibrated. The spectrometer used was an AvaSpec-2048 Fibre Optic Spectrometer supplied by

Anglia Instruments. It was used with a 2m long fibre optic cable with a bare fibre diameter of 650µm. A diffraction grating of 25µm was fitted to allow the maximum amount of light through the grating while still producing sufficient wavelength resolution. The relative intensity vs. wavelength was calibrated using an AvaLight-HAL, 10W Tungsten Halogen Light Source at a temperature of 2450K. Plasus Specline software was used to match the Atomic Emission spectral peaks. Specline uses several open access databases for peak matching [97-100] .

The temperature of the particles was calculated by plotting intensity vs. wavelength and using a fitting function based on Planck's law to interpret the black body radiation curves captured by the spectrometer[101].

$$I_\lambda \propto \frac{2hc^2}{\lambda^5}\frac{1}{e^{hc}/(\lambda k_B T) - 1}$$

Where

I_λ is the intensity at a given wavelength

h is the Plank constant

c is the speed of light in a vacuum

k_B is the Boltzmann constant

T is the absolute temperature

As the numeric aperture of the fibre optical cable and assembly is unknown the absolute intensity is unknown but the relative intensity can still be used. This meant there were two variable that had to be fitted for, an intensity scale factor and the temperature, as all the other parameters are constants. This allowed accurate

temperature measurement without knowledge of the emissivity, as the shape of the spectrum is analysed not the magnitude. This approach also means any deviation from grey body behaviour is easily spotted as the function will not fit properly. The accuracy of this method was verified by aiming the spectrometer at the graphite die surface and comparing the temperature measured to the side-entry pyrometer built into the SPS.

3.4.2 **Data logging**

While data logging is a relatively simple concept there are several pitfalls and limitations (studied in depth in books on the subject[102]). While one might expect a data logger to behave like a set of multimeters, most multimeters have various filters and signal processing built in. To achieve similar performance from a data logger the correct filtering and processing need to be designed. The raw nature of data logging is most obvious when analysing ac voltages/currents. A rough guide is the data logging frequency should be 10x the ac frequency to accurately recreate the shape of a sine wave. The required sample rate can be calculated for arbitrary waveforms using the Nyquist–Shannon sampling theorem[103]. Once the data is sampled, the true rms values should be calculated as its one of the most important factors, it is analogous to the equivalent dc value. Filtering is also important for small signals e.g. thermocouples. If one has an idea of the frequency range of interest, then a FFT filter can be used to remove noise outside of that range. This is normally used to remove high frequency electrical noise. To avoid needlessly large

data files, it is useful to capture at a high rate, perform signal processing and only save the processed data at a lower rate.

The other complexity with data loggers is isolation. Most data loggers share a common ground between the various channels, and even differential inputs are not fully isolated from one another. This leads to various issues when trying to measure several signals from the same circuit. Problems occur if there is a voltage between the grounds on the data logger. If this is the case then current will flow through the data logger potentially damaging it and definitely degrading the signal measured, introducing common ground noise. One countermeasure is to use fully isolated data loggers, but even they have limited capacity to resist high voltages. Alternatively, isolated current meters or optically isolated voltage measuring techniques can be used, but these bring limitations in response time and syncing. Throughout this work a National Instruments usb-6221 was used for data logging. It is rated for ±10V and each channel is isolated from ground up to 60V but the individual channels are not isolated from each other. The data logger was set to use differential measurements and was capable of reading thermocouples directly without an amplifier. When higher voltages were measured (for high voltage setup in Chapter 4 and the contactless flash setup in Chapter 6) the voltage was connected to 10:1 fixed resistor voltage divider. To measure large currents while maintaining isolation (needed in the contactless flash setup in Chapter 6) Hall current sensors were used. These use the Hall effect to detect the magnetic field induced by current flowing in a wire. By placing the wire inside the sensor but electrically insulated from the hall material the current can be read while maintaining isolation. To

measure ac or pulsed dc the data logger was configure to recorder 10k samples a second, a FFT filter was then used to calculate the rms value. The rms value was saved 10 times a second and that is what was plotted.

3.5 Ex situ Analysis

While as much data as possible was gathered during the experiments one of the most useful techniques in material science, imaging a polished cross section, has to be done after.

3.5.1 Cross Sectioning and Polishing

In this work it was necessary to evaluate the density and microstructure throughout the sample, due to inhomogeneous composition and density. To get a representative view of the sample internally there are two approaches, fracture surfaces where a sample is broken in two, or cross sectioning, where the sample is cut with a diamond saw and polished.

Only the samples processed in Chapter 4 were not cross sectioned, and this was because they were mostly loose powder with the occasional nugget of dense material, so could not be reliably cut. The value of cross sectioning is that it provides a much more representative view of the internal structure of a sample. As opposed to fracture surfaces, which are inherently biased as they form by a crack following the path of least resistance. Cross sectioning is also a much more reliable method to detect small sale porosity such as that trapped at the triple points.

Fracture surfaces do have some advantages when it comes to grain size analysis but only if the fracture is consistently intergranular.

One unfortunate limitation of cross sectioning is that it requires extensive polishing to reveal all the features. This is not always possible to achieve. When there are soft and hard material together the softer material will be removed before the hard one and it can end up smeared over the surface. Grain pull out can also cause problems in sample with weak bonding between grains or secondary phase's precipitating at the grain boundaries. This is particularly bad with porous samples which are inherently very weak at the grain necks. Issues with porous samples can be improved by embedding them in resin but this comes with its own set of drawbacks, the resin can cause charging during imaging and affect EDX analysis. However embedding in resin was required for the diboride samples in Chapter 5 as the samples were very fragile requiring resin to be applied before they could be safely removed from the equipment. The resin also ensured the electrodes stayed in position during cutting, allowing the contact points to remain undisturbed.

In this work superior results were seen using solid electroplated diamond discs of high grit number as opposed to more conventional felt pads. Felt pads were too flexible so tended to produce more uneven material removal. This was an issue when polishing dissimilar materials or porous samples such as the oxide scale on the diboride or the localized sintering seen in the contactless flash sintered samples.

3.5.2 Scanning Electron Microscopy

SEM is usually operated in two modes (secondary and backscattered) with a third EDX mapping being possible on some units. In this work, the Backscatter mode was used extensively for several reasons. The phase contrast provided is more important for polished samples, where there is limited topography. Back scattered mode also provides some advantages when dealing with porous samples. Due to the ballistic path of the backscattered electrons it effectively allows only the very top surface to be imaged. Higher voltage allow greater brightness and phase contrast. These trade-offs explain the conditions used in the different sections of this work. For imaging the loosed powder and nuggets in Chapter 4 secondary electrons were used with a low acceleration voltage (10kV) to get crisp topological imaging at high magnification. In Chapter 5 20kV backscatter imaging was used to get high phase contrast between the different layers in the oxide scale, and low magnification was mostly used. In Chapter 6 30kV backscattering mode was used to get the maximum phase contrast due to the small difference between Si and B. A spot size of 3.5 was used throughout as it was one of the least worn and provided a good trade off of resolution and brightness. Optical microscopy (Nikon smz-10) was also used on some sample as only low magnification was needed and it provided extra contrast showing the blackened region of the oxidized sample and the extent of arc damage in the contactless flash sintered samples.

Chapter 4. Plasma in SPS

4.1 Introduction

With the many various ECEs discussed earlier, it is important to focus on areas of particular interest. As mentioned in Chapter 2.3 plasmas have been exploited to develop processing techniques with unique and powerful features. EDM can machine materials irrespective of their hardness and has significantly changed the way dies are made for the plastic industry[104]. Because plasma formation can have such significant effects on materials, but is too complex to fully model (in most cases), it has become a go to explanation for any anomalous behaviour seen in any electrical material processing technique. Plasma effects have been proposed to occur in many processes without much regard for whether the conditions actually make plasma possible. Given that plasmas can be detected by spectroscopy, this means that with some careful experimental design it is possible to conclusively rule out plasma effects in various process, insomuch as it is possible to prove a negative. Plasma effects have always been discussed when mentioning SPS (it's in the name), although the current consensus is that they are non-existent or at most have minimal effects on the process. Most existing research has focused on whether there is or is not a plasma generated during SPS. In this work the conditions that are required to produce a plasma and the properties of the plasma that is liable to form in certain ECAS processes were investigated. The reason being that while SPS is a particularly common ECAS process, a wide variety of new processes are becoming

prevalent, from flash sintering to capacitive discharge sintering. The hope is that this work will provide a framework for others to evaluate the effect of plasma in other processes and conditions.

SPS is used extensively for densifying powders, especially for research [105]. However, scale up is happening as ever larger machines are being made[106], and increasingly companies are exploiting SPS's advantages for production manufacturing. The most obvious alternative to SPS is hot pressing, however, there are several advantages of SPS compared to hot pressing, including reduced grain growth and increased density for a given temperature. The improved properties of SPSed materials have been explained by several effects related to the process. These effects includes rapid heating and more unclarified field effects such as electroplasticity and electromigration, and plasma formation [107]. However, the line between SPS and hot pressing has become blurred recently with induction hot press machines able to achieve rapid heating similar to SPS. Over 100°C/min is easily achived[108] with induction hot press which is a commonly used SPS heating rate. In a more uncontrolled fashion even higher heating rates are possible over 500C/min[109]. Induction hot pressing does not apply a field or current to the sample, so the improved sintering performance cannot be attributed to ECEs. Induction heating has also been used in conjunction with SPS to form hybrid SPS. This uses induction or radiant heating to reduce temperature gradients during sintering[110], as induction and radiant heating are surface effects.

Even if the presence of plasma during ECAS remains to be proven, in the literature several theories about the generation and possible role of plasma in enhancing

sintering have been hypothesised. A common one is that when current flows through powders the contact points, having higher resistance, locally reach temperatures sufficient to boil or sublime at the surface of the particles. The resulting gases are ionized and form a plasma, through which a current flows. The electrical resistivity of a plasma is of the order of 10^{-2} Ωm to 10^{-4} Ωm [111] compared to an unsintered metal powder compact, which can vary from 10^{-4} Ωm to 1 Ωm [112]. So once a plasma is formed it can offer an effective path for current flow. Alternative theories suggest that the surface oxide coating on particles forms a dielectric barrier that breaks down under the applied electric field. Once the dielectric fails it generates an electric arc resulting in the formation of a plasma [113,114]. The plasma then promotes removal of surface material, cleaning the surface allowing improved diffusion and sintering.

Most theories of plasma enhancement in electric current assisted sintering suggest that a plasma would only exist in the first sintering stage. During the second and third stages the formation of a plasma is unlikely to happen because a relatively dense conductive sample simply behaves as an electric conductor. While a compressed metal powder compact's resistance might be 10^{-4} Ωm to 1 Ωm, once the sample is sintered and nearing full density the resistance is likely to be 10^{-6} Ωm to 10^{-8} Ωm. While plasma formation in SPS itself is still an open topic for debate in the scientific community, several papers have been published presenting indirect evidence of plasma formation [115], such as localized melting [116]. On the other hand, Hulbert et al [117] reported evidence of the absence of a plasma in SPS. One issue with this work is they attempted to observe plasma formation at a later stage of

sintering rather than in the very initial stage.

Within the field of ECAS a wide range of equipment designs have been developed [118]. Voltages ranging from 1 to 10^3V, and current densities of up to 10^6A/cm have been used. Furthermore, variations in the waveform, pulse discharge, pressure and atmosphere have been used. At present ECAS process of the SPS type, employing voltages below 10V dominate commercially. However there is a growing interest in higher voltage sintering techniques as demonstrated by a growing number of publications on flash etc. [119] . One explanation of the name SPS comes from K. Inoue [120] who patented a process named Spark Sintering in 1967. In this setup voltages greater than 50V were employed for sintering metallic powders. In the patent 50V dc was used with a 120V ac wave of frequency 400 Hz superimposed on it, the higher voltages used then might well have caused sparking and plasma. While this work focused on SPS and related processes, it is worth considering the various processes summarised in Table 2.3. A Wide range of conditions have been used, but low voltages (10V) and high current (<1kA) power supplies are the most commonly used.

This work attempts to observe in-situ the possible formation of a plasma when electric currents are forced to pass through conductive particles. Unlike previous investigations, special attention is given to the very first stage of sintering, before necks have formed. The effects of pressure (pressureless up to several MPa) and voltage (from 5 up to 50V) are also discussed.

4.2 Results

4.2.1 Low Voltage (SPS)

Experiments where a fibre optic cable was placed inside an SPS (configuration 1) only produced black body radiation from both the ZrB_2 and W powders, with a maximum temperature of 1200K. More interesting results were obtained from configuration 2 which used 50V in a mock SPS, and they are discussed in detail below. The higher voltages used outside the SPS resulted in a contact voltage drop great enough to ignite and sustain a plasma as reported in the literature [121]. Note that in most cases it is more appropriate to talk of voltage rather than field when dealing with arcs. Because even with the many contact point in a powder compact the plasma formation is limited by the arcing voltage of the powder or breakdown voltage of the gas. Both of these phenomena are not linear with distance and have minimums (137V for argon breakdown and 15V for tungsten arcing). One experimental issues is that even if an arc formed there would be no guarantee it would be captured by the spectrometer. This is due to various factors, the rapidness of plasma formation (50-100ms), arc wandering during discharge [122] and fibre optics occlusion by powder. In fact, careful preparation of the setup and multiple runs was needed to capture the plasma formation.

Typical current voltage profiles for tungsten in configuration 1 as recorded by the SPS machine are shown in Figure 4.1(a), and the corresponding spectra are shown in Figure 4.1(b). The graphs correspond to pure black body radiation curves, and

no evidence of a plasma can be seen. The calculated maximum temperature recorded was around 1550K and the voltage was 5-6V. According to the spectrometer readings, the heating rate was around 1000K/s (60000 K/min); the temperature rose from 1100K to 1550K in 0.4 seconds. The temperature then saturated and remained constant for several seconds. On the contrary to a thermocouple or pyrometer usually employed in SPS, the optical spectrometer allowed the real powder temperature to be measured in-situ in a small time interval. However, just like pyrometers, temperatures below 1000K are hard to measure due to the insensitivity of silicon detectors to long wavelengths and the limited energy emitted. Very similar results were seen when using diboride powder.

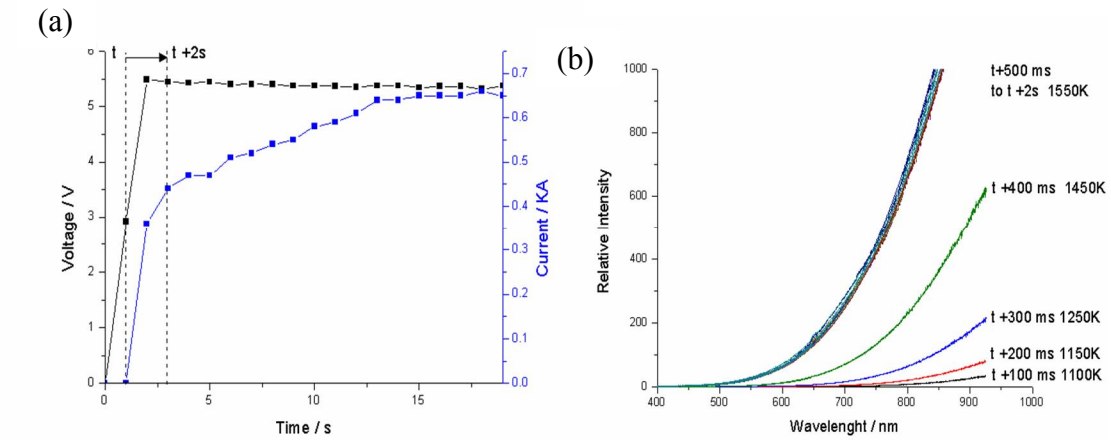

Figure 4.1 Data captured from SPS plasma setup with tungsten powder using configuration 1 (a) Current and voltage over time and (b) optical spectra over time with estimated temperatures, t refers to the start of the capture window as show in (a).

4.2.2 Higher Voltage

4.2.2.1 Spectroscopy

When higher voltages were applied in the case of configuration 2, bright flashes were visible with the naked eye during the first 2-3 seconds, as anticipated by the observation of K. Inoue in his patent [123]. These emissions were captured by the spectrometer Figure 4.2 and the spectral lines were identified in Figure 4.3. Similar experiments to those described above, but in the absence of powders between the punches resulted in an open circuit and no plasma was observed. From this we can conclude that the conductive W and ZrB_2 particles acted as a source for plasma ignition. It was not just breakdown of the gas across the gap or arcing form the graphite punches. Instead the current and voltage used were most likely sufficient to heat the powder to the evaporation point at the contact points. This metal vapour is much easier to ignite into a plasma (compare Table 2.1 against Table 2.2) and this is consistent with the emission peaks seen.

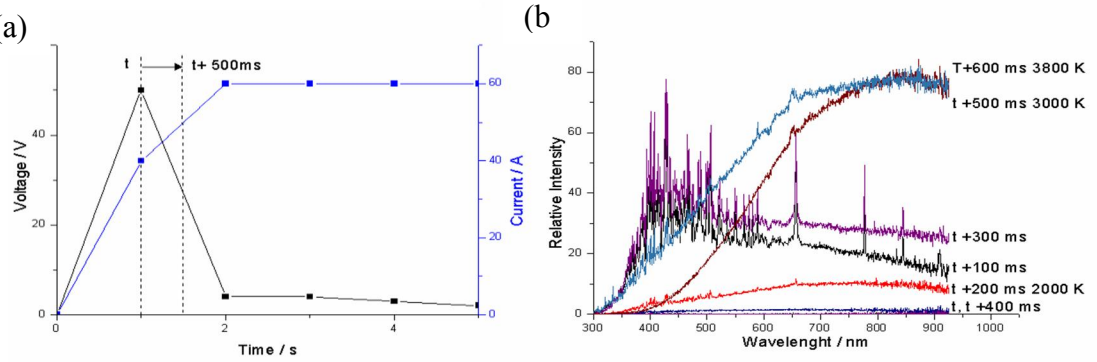

Figure 4.2 Data captured using configuration 2 with tungsten powder. left (a) current and voltage over time and right (b) optical spectra over time with estimated temperatures, t refers to the start of the capture window as show in (a).

Figure 4.2(b) shows the spectral emission data acquired during the in situ observation during the first 600ms of discharge. At 100ms and 300ms sharp spectral emission lines are visible, however, at times 200, 500 and 600ms no spectral lines are visible but high temperatures of up to 3800K were detected. After 600ms the temperature then fell as the power supply was in constant current mode at 60A, and the voltage and power dropped. The rapid change of the recorded spectra might be attributed to the arc wandering away from the fibre optic or extinction of the plasma. The high temperature emission and plasma formation could well be linked as material vaporisation was required to ignite a plasma. Alternatively the high temperature of the arc discharge plasma [124] could have heated the surface of the powder.

The optical spectra at 300ms was further processed by identifying the probable spectral lines in Figure 4.3. The presence of tungsten lines confirms that some of the tungsten must have been removed or sputtered from the surface of the starting particles.

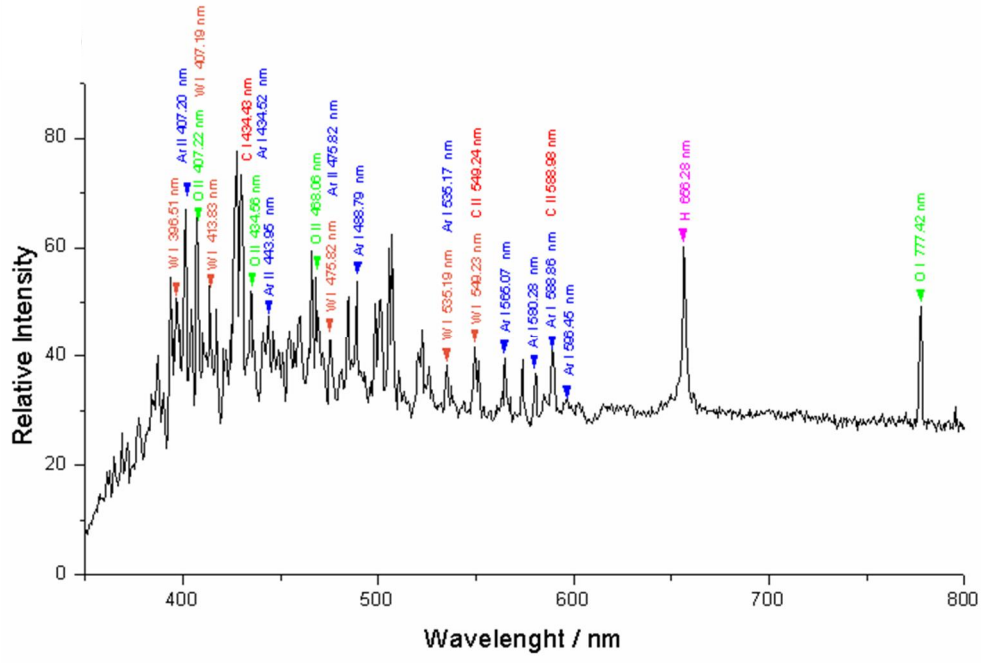

Figure 4.3 Spectra of tungsten in configuration 2 showing spectral peaks with identified species, the ionization level is signified by a roman numeral after the species

This kind of observation has not been reported elsewhere, and it clearly demonstrates the localized formation of a plasma. Obvious argon lines are also observed and they correspond to the ionization of the inert gas employed in the experiments. Weaker oxygen lines, shown in green, are also observed. They might have been generated from removed surface oxides, or from dissociation of surface water adsorbed on the particles. It's highly likely that at least some water was vaporised in the plasma as hydrogen lines are also present. The carbon peaks are most likely from the punches. The presence of oxygen in a plasma has been reported to alter the emission intensity of some species including argon [125]. The means that the relative intensities cannot be trusted to give a quantitative analysis and also certain species might not even be visible. Several double ionized species were present meaning that the ion temperature was high enough to produce significant ionisation. Even if the spectra at 100 and 300ms definitely confirm that a tungsten plasma was generated there is still no proof that the plasma was ignited at the contact point between particles. It is possible that the arc was ignited between the powder and the top or bottom punches.

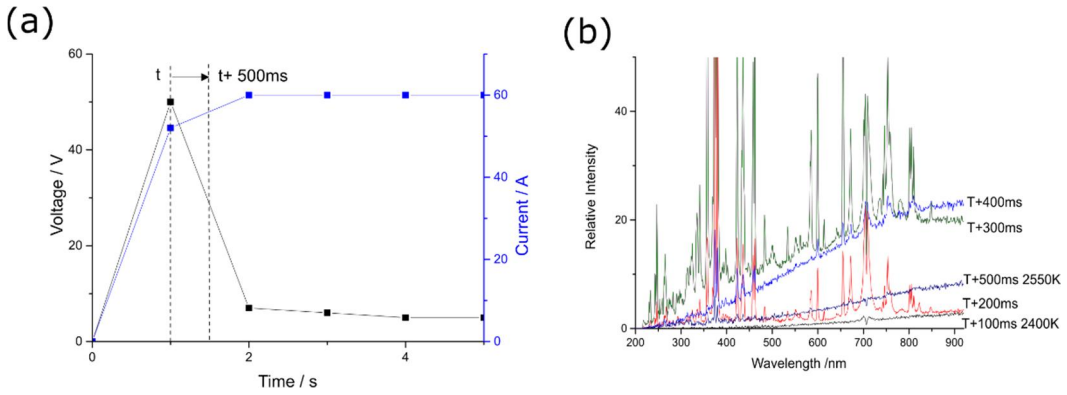

Figure 4.4 Data captured from diboride using configuration 2: (a) current and voltage over time (b) optical spectra over time with estimated temperatures, t refers to the start of the capture window as show in (a).

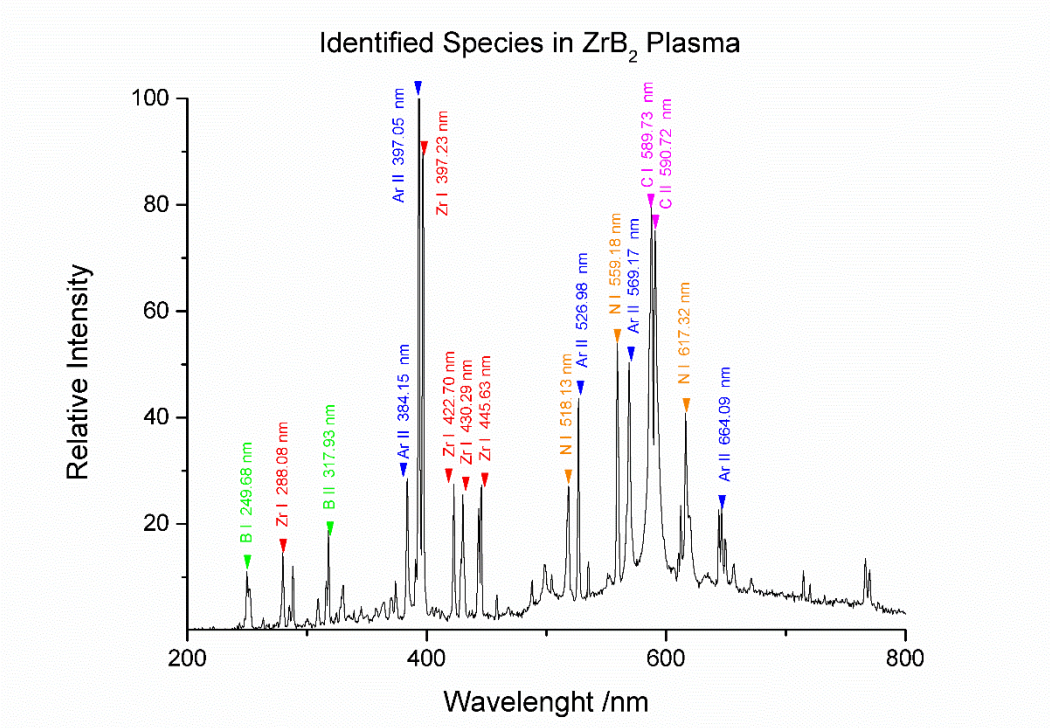

Figure 4.5 Spectra of diboride in configuration 2, showing spectral peaks with identified species

When the same experiments were performed with zirconium diboride it showed a similar emission behaviour (Figure 4.4(b)) to the tungsten sample. Black body heating was observed before the plasma ignited (2400K), and once the plasma ignited (t+200ms) the spectrum appears to show a mixed response of black body and plasma emission. In this situation the temperature could not be determined, after that the emissions decreased and then dropped rapidly with only minimal residual black body emission (2550K). Both materials showed that before plasma ignition there was little black body radiation, and after plasma there was minimal temperature rise. Significant heating only occurred after the plasma was extinguished. This is can be explained as the plasma has very little thermal mass, so is unlikely to heat the powder much apart from locally at the cathode and anode spots. After the plasma has been extinguished (due to the voltage drop) the particles are much more firmly bonded, (increased necking) so greater current can flow. The heating seen after the plasma is likely the result of increased Joule heating. However due to the unstable nature of an arc and the limitations of only sampling at one point with the fibre optic cable it is important not to over interpret the data.

Spectral lines for zirconium and boron species were identified in the first ZrB_2 spectra (t+100ms in Figure 4.5), implying that the diboride was also evaporated in the arc. Nitrogen peaks were visible, implying that there was either nitrogen impurities in the powder (powder specified at less than 0.25wt %) or incomplete sealing of the quartz tube allowed air to get in. However the lack of oxygen peaks implies the former. The carbon species could have come from the starting powder (0.2wt %) or from the punches.

From these measurements it is possible to infer the sequence of events that generated the plasma. When a voltage is applied a current immediately begins to flow through the conductive pathways between the contacting points of the particles. This causes local heating at the contact points. Either from the evaporation of the contact interfaces due to high local joule heating or from some movement that causes the particles to separate, an arc will strike. Due to the NTC of resistivity of the plasma and the relatively high resistivity of the loose powder, a sizable current will flow through the plasma. The plasma will then rapidly heat up and expand, it might even reach the top and bottom punches giving it an easier current path. The arc will then heat up, melt, evaporate and even ionise surrounding powder, generating the spectra we see in Figure 4.5 and Figure 4.3. The arc will wander around and several arcs could form, some might extinguish while others ignite due to changes in the local conditions. As the powder compact densifies it becomes more conductive and the voltage across the plasma will drop as more current flows through the lower resistance powder instead. Eventually the plasma will extinguish and none will be able to reignite as the voltage drops below the threshold required. In our case the voltage drop was also due to the current limit but the concept remains the same.

4.2.2.2 Microstructure

Figure 4.6 (a) and (b) shows SEM images of the as received powders of tungsten and diboride respectively. No difference in the microstructure was observed in the case of the W of ZrB_2 powders after being processed in configuration 1. The

materials were crumbly and were held together weakly, what little bonding there was came from the light pressure applied when hand loading the samples into the SPS. From the SEM analysis no necking or bonding was visible between particles, and the particle size was about 1μm and agglomerates composed of smaller particles were still visible. After the 50V discharge the bulk of the material was untouched and looked identical to the powder before processing. However, in certain regions a nuggets of densified material was found embedded in loose powder, this was removed and imaged in Figure 4.6 (c) and (d). The W and ZrB_2 nuggets likely correspond to powder that had melted. The melting is visible in the micrographs as evidenced by the large grain growth of tungsten, from around 1μm in the tungsten powder to about 10μm for the melted zone, as indicated by the white ring in Figure 4.6 (c). The diboride started with much larger particles (5μm) so the grain growth visible in in Figure 4.6 (d) could be caused by sintering. However due to the rapid heating and short processing time it is more likely from melting then recrystallizing. The melting seems to confirm that the temperatures measured by the spectrometer (2550K) are reasonable, and probably exceeded when the plasma ignites, the temperate cannot be measured during this time. On the edges of the melted zone, as shown by the black ring in Figure 4.6 (c) and (d), partially melted particles are visible. A close up of the partial melting is shown in in Figure 4.6 (e) and (f). There is a large variation in microstructure of the samples with some regions melting entirely while others are partially melted and some completely unchanged (dotted white arrow in in Figure 4.6 (d)). This uneven sintering/melting supports the hypothesis that current distribution during plasma discharge is highly

inhomogeneous. This resulted in localized heating with plasma formation in only some of the regions, at least in the first stage of sintering [61].

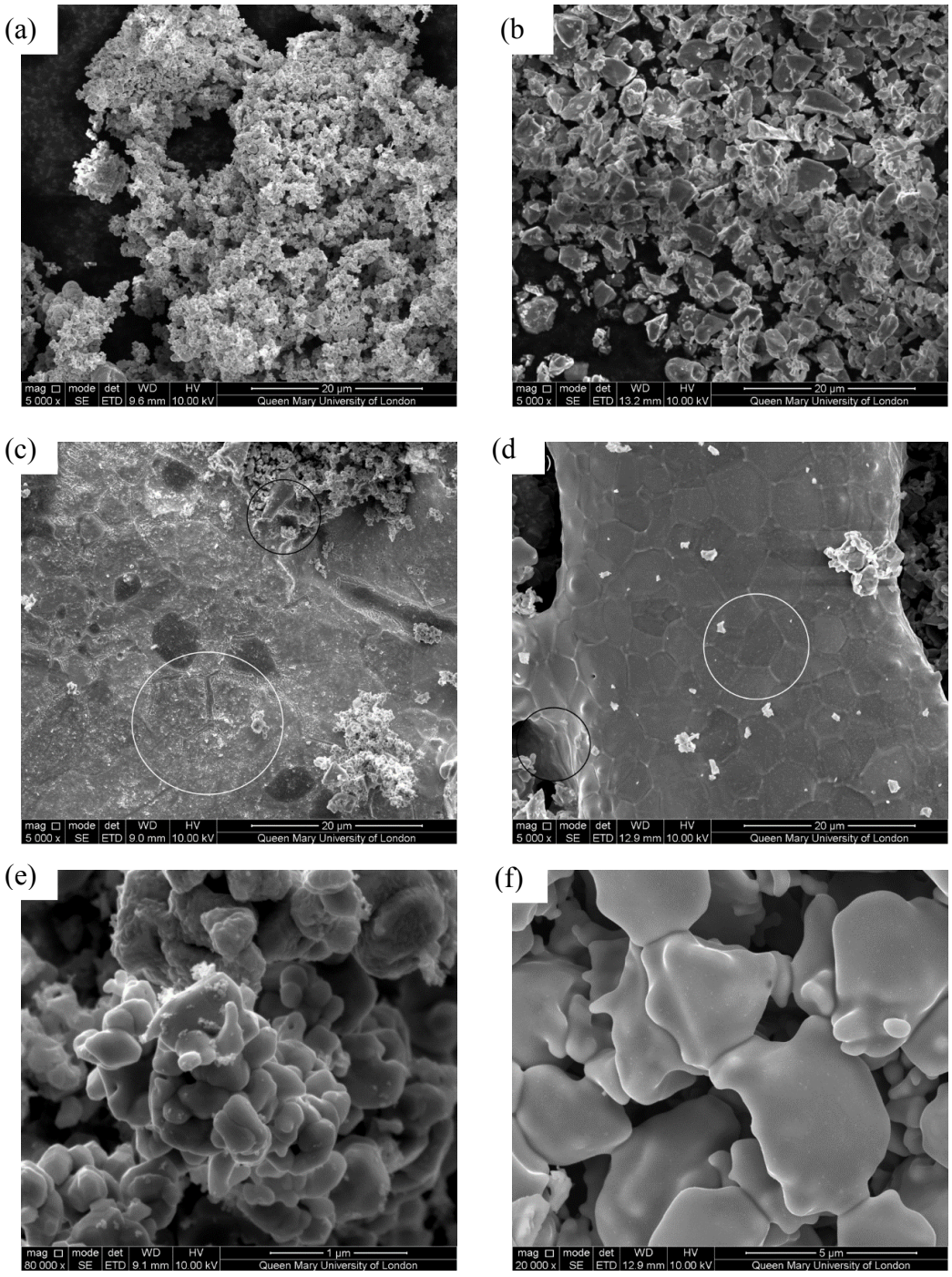

Figure 4.6(a) Micrograph of tungsten powder before processing (b) Micrograph of diboride powder before processing (c) Micrograph of tungsten sintered region after discharge in configuration 2, partially sintered regions circled in black and melted/recrystallized regions in white. (d) Micrograph of diboride sintered region after discharge in configuration 2, partially sintered regions circled in black and melted/recrystallized regions in white (e) High magnification micrograph of partially sintered regions, in Tungsten (f) High magnification micrograph of partially sintered regions, in diboride.

4.3 Conclusions

AES is a powerful tool for in situ temperature probing, it is capable of a rapid scan rate and small spot size (i.e. 650μm). It was also vital for detecting the formation of a plasma and identifying its species. The key findings of this work were identifying several of the parameters that affect the formation of a plasma. Contact pressure was found to be highly influential but most important was the applied voltage. In SPS processing at low voltages (< 10V) a plasma is unlikely to form. Despite the large amount of research on ECAS processing, this work presents the first direct evidence of plasma formation during ECAS. Evidence of plasma was detected when using tungsten powder under a low applied pressure in an argon atmosphere under a voltage of at least 50V. The developed approach has the potential to further understand the mechanisms operating during ECAS. The surface removal seen in the plasma could also be exploited for more controlled ECAS processing like in situ particle cleaning or even for in situ compositional analysis during sintering. Further work is needed to clarify how a plasma affects densification and how to optimise the conditions for increased plasma ignition and stability. Ultrafast ECAS [118] is a prime candidate for such a study due to the high voltages and controlled pressure used during sintering. AES has also been used recently to investigate emissions from samples during flash sintering[14],where a plasma is possible due to the high voltages used (500V). However, spectral lines produced during flash sintering can also be produced by solid state emission since the materials investigated are ionic conductors and semi-conductors. It is possible

to attempt to differentiate between the different mechanisms but it's not particularly reliable. In the case of an arc between two discrete electrodes with large separation, e.g. in welding. Then the emissions are dominated by the lines form argon or the inert gas, with limited emissions from the electrode materials. In the case of a short arc or arcing in a powder then the majority of emissions are from the metal vapour, but with some emission from the atmosphere as well. The atmosphere is ionized by the metal plasma and will mix in very quickly. In the case of solid state emission or oxidation reactions then there is lots of emission from the material but none from the atmosphere. The data provided from flash sintering shows no atmospheric peaks, only form the solids, implying it is not a plasma emission.

Chapter 5. Oxidation Electric Current Effects

5.1 Introduction

The earlier chapters in this thesis were on proposed ECEs on which there is still much debate on the mechanisms at play (see Chapter 2.7). This chapter will focus on electromigration, which is one of the few well understood ECEs. Electromigration forms part of conventional understanding of ionic conductivity. Most work on ECEs has focused on what is and is not happening in a particular process. This is often tricky as it's very hard to separate out the different effects since they often occur simultaneously. However, in this work the focus is on designing an experiment to exploit the well understood phenomena of electromigration in a novel manner to alter the oxidation rate of an ionic material.

The ever growing interest in flash sintering has stimulated research on understanding the mechanisms at work. A better understanding of ionic conductivity and how the flow of ions and neutral species might explain the sintering behaviour seen [3,126]. Due to this recent interest some of the more peculiar or niche applications of zirconia, the first and most commonly FSed material, has resurfaced. For example Nerst lamps have been referenced in several recent publications[14,127] despite their near complete obsolescence over 100 years ago. Another interesting type of behaviour is oxygen pumping. In all ionic conductors

on the application of a sufficient voltage the mobile ions will flow through the material, even against a concentration gradient. For zirconia at high temperatures the flow of oxygen through the lattice is significant and has been exploited to pump oxygen form a gas stream to control the PO_2 accurately[128].

Another type of material of significant academic interest at the moment is UHTCs, of which zirconium diboride is perhaps the most common. With the great interest in the oxidation behaviour of zirconium diboride, and the fact that the oxide layer that protects the diboride is mostly zirconia a promising link was found. In this work the oxygen pumping of zirconia is used to pump oxygen away from the diboride surface by applying an electric field through its oxide scale (zirconia).

The technique developed in this work is not just applicable to one particular material and configuration, the same concept could potentially be applied to a wide variety of materials to alter their oxidation behaviour. Any improvement in oxidation resistance is significant as the oxidation of materials operating at high temperatures is often the limiting factor in many applications. Many non-oxide structural ceramics, with good high temperature strength, cannot be used in air due to their poor oxidation resistance. In order to increase their operating temperatures, a considerable amount of work has been done on the development of protective coatings. These work by inhibiting diffusion of oxygen into to the bulk material. When operating in the ultra-high temperature (UHT) regime (>2000°C), this approach has had limited success. This is because most oxide scales tend to be either oxygen permeable/porous (e.g. zirconia) [129] or otherwise unstable at ultra-high temperatures (e.g. silica based materials derived from the oxidation of SiC

and Si_3N_4 tends to sublime[130]). This is a major hurdle to greater application of UHTC ceramics, and something better than a silica oxide layer is needed. This work will focus on ZrB_2, a typical UHTC with a large gap between its operating temperature in an inert atmosphere and in air

5.2 Electric Field Effects on Oxidation in literature

A variety of experimental setups, material combinations and temperatures have been proposed to investigate the role of field effects during oxidation. The possible methods can best be grouped according to their electrode configuration as illustrated in Figure 5.1 (a-d)[131-135]. Figure 5.1 (a) refers to Direct Contact Electrode (DCE) methods, where electrodes were attached to the sample and the top of the oxide layer. Figure 5.1(b) and (c) refer to Non-Contact Electrodes (NCE) methods, where an electrode was attached to the sample but not directly to the oxide layer. Figure 5.1d) refers to External Charge Source (ECS), where the charge needed to produce a field was applied without electrodes.

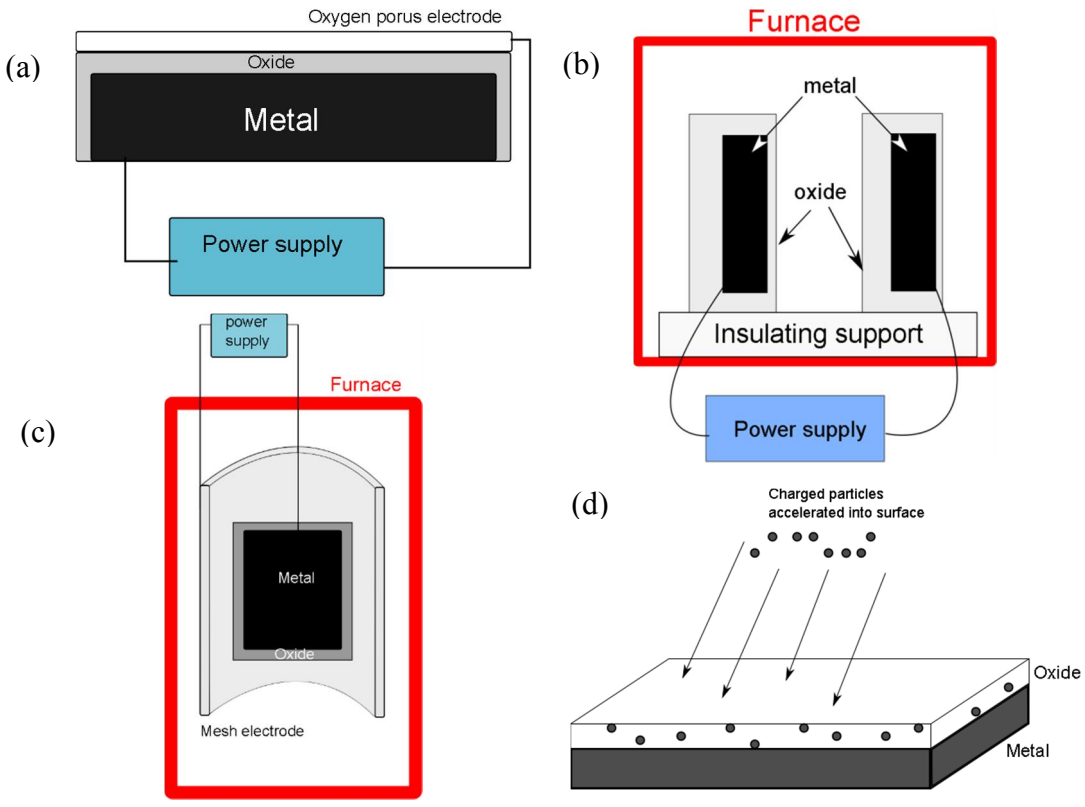

Figure 5.1 Illustrates the various configurations as surveyed in the literature: (a) Depicts the DCE configuration using oxygen permeable metal electrodes directly applied to the oxide; (b) Illustrates the parallel plate NCE configuration where both electrodes are also sample; (c) Refers to concentric NCE with a cylinder sample and tube electrode; and (D) Shows the ECS configuration, where electron bombardment charges the surface of the oxide.

5.2.1 **Direct Contact Electrodes (DCE)**

Typically, in the direct electrode experiments an electrically conductive porous oxygen permeable electrode (e.g. platinum mesh) was attached to the oxide (Figure 5.1a). A voltage, usually in the range of 1-10V, was applied across the oxide scale.

When the electrode was negative with respect to the sample the oxidation rate was observed to increase, and the reverse was found if the polarity was inverted. This method allows direct application of an electric field over the growing oxide layer [136].

Using the configuration schematized in Figure 5.1(a), Jorgensen[133] performed experiments to confirm whether the diffusing species during the oxidation of silicon were oxygen ions. It was demonstrated that the oxidation rate was strongly affected by the application of an electric field, which would only have been possible if oxygen ions were the diffusing species. In Jorgensen's experiment, a silica layer was grown on a block of silicon and porous platinum electrodes were attached to opposite sides of the block. A voltage of 2V-5V (corresponding to a field of 100V/cm) was used and oxidation took place in air at 850°C. The oxide layer thickness was measured during oxidation by interferometry. It was found that the oxidation rate was reduced when the surface electrode was positive with respect to the sample. In some cases oxidation completely stopped, when the voltage was above 4.5V. This is significantly above the theoretical electrode potential to reduce silica into silicon and oxygen gas (2.1V), but there is likely significant loses in the system. Conversely, when the polarity was reversed the oxidation rate increased.

5.2.2 **Non-Contact Electrodes (NCE)**

Figure 5.1 (b) and (c) illustrate NCE configurations. In these configurations the electrode was not in contact with the surface of the oxide scale, but was instead

separated by an air gap. This requires much higher voltages (>100V) to achieve similar results to DCE. In this case there is an electric field across both the oxide layer and the air gap. The majority of the voltage drop likely occurs across the air gap. The field across the air gap might produce other effects not seen in the direct electrode configuration. Such effects include ion wind [137]or corona discharge, which might alter the oxidation rate. Parkansky et al used this type of set-up to investigate the effect of electric field on the oxidation of copper. In their experiment two copper plates were held at a fixed distance apart and 500V was applied between them [135]. The whole assembly was heated in a furnace to 500-600°C for an hour. In this case no change in the Copper oxide thickness was observed but the valence of the oxide layer was changed as well as the grain size.

Lawless et al. [132] employed a cylindrical non-contact setup as shown in Figure 5.1 (c). Here a cylinder of metal (e.g. nickel, molybdenum, or 304 stainless steel) measuring less than 1 cm in diameter was suspended, using platinum wire, in a heated chamber (700°C-1140°C). The samples weight change was measured using a microbalance. A 5cm diameter platinum mesh electrode was suspended concentric to the metal cylinder. Potential differences ranging from 100 to 250V were applied between the inner cylinder and the outer mesh electrode. Their results variable massively depending on the material tested. Nickel showed no change in weight gain, the weight of stainless steel reduced in both polarities. The behaviour of molybdenum was more complicated, it showed increased evaporation (MoO_3 is volatile) at low voltages (<100V) and reduced evaporation at higher voltages (>100V) with polarity having little effect. The authors attributed the oxidation

behaviour to the electric field changing the activation energy of the rate limiting step (ionic vacancy diffusion).

5.2.3 External Charge Source (ECS)

From the literature above its clear that having an electric field across the oxide layer is sufficient to alter the oxidation rate, or alter the stoichiometry (i.e. reduction/oxidation) of the oxide phase. Some novel experiments have been performed where the field across the oxide layer was generated by charging the top surface using an electron beam (Fig. 1.1(d)). In the setup employed by Popova et al. [131] a thin oxide layer was grown on an aluminium single crystal by electron enhanced oxidation. This is a common micro fabrication technique where electron impacts cause dissociation of adsorbed surface oxygen, making the oxygen more reactive, so growing the oxide layer [138]. After the initial oxide layer was grown a, 100eV electron beam was rastered over the surface. This resulted in electrostatic charge building up at the surface of the alumina layer, which generated a field through its thickness. The effective voltage across the layer was 1V. When oxygen was readmitted to the chamber, the oxidation rate was increased even though the electron beam was switched off. The authors explained this result according to enhanced diffusion of oxygen ions through the oxide layer due to the electric field. The thickness of the layer was measured using X-ray photoelectron spectroscopy and all of the steps were performed at cryogenic temperatures.

5.2.4 **Literature Summary**

While several investigations have been carried out on the effect of electric field effects on oxygen transport, the only practical applications is limited to zirconia cells for oxygen pumping and sensing [139,140], [128] . This configuration is similar to the one in Figure 5.1(a). While zirconia is described as being oxygen pumping this is no different from electromigration of oxygen. Oxygen pumping can occur in other oxides and the only difference is the magnitude of the gas/current flow. For this reason one can expect that zirconia should show very different result with and without field. The lack of recent and more systematic studies shows the field is relatively immature, despite is a great variety of literature surveyed there was no obvious pattern in the results in Table 5.1.

Table 5.1 A Summary of the effects of an electric field on the oxidation rates of a wide range of materials. Electrode configuration, substrate composition and its resulting oxides, temperature, applied voltage and the effect of the polarity are listed

Electrode Configuration	**Reference**	**Substrate**	**Oxide**	**Temperature /°C**	**Voltage /V**	**Oxide –V Substrate +V**	**Oxide +V Substrate -V**
Direct Contact Electrode	[133]	Silicon	Silica	850°C	2-5V	Increased oxidation rate.	Reduced or stop oxidation.
Direct Contact Electrode	[136]	Vanadium oxide	Vanadium oxide	20°C	10V	Alters oxide valence, polarity not given.	Alters oxide valence, polarity not given.

Non-Contact Electrode	[135]	Copper	Copper oxide	600°C	500V	Increased O/Cu ratio, decreased grain size	Decreased O/Cu ratio , increased grain size
Non-Contact Electrode	[132]	Stainless steel	mixed oxides	1140°C	300V	Reduced weight gain	Reduced weight gain
Non-Contact Electrode	[132]	Molybdenum	Volatile molybdenum oxide	700°C	250V	Bellow 100V increased evaporation above 100V reduced.	Bellow 100V increased evaporation above 100V reduced.

Non-Contact Electrode	[132]	Nickel	Nickel oxide	1040°C	195V	None	None
Electrostatic	[131]	Aluminium	Alumina	-193°C	1V	Increased oxidation rate.	Not applicable.
Direct Contact Electrode	This Work	zirconium diboride	Zirconia	1400°C	10V	Increased oxidation rate	Reduce and /stop oxidation
Oxygen Pump	[128]	Platinum	Yttria stabilized zirconia	800°C	1V	Higher PO_2 near platinum(e.g. increased oxidation rate).	Lower PO_2 near platinum (e.g. reduced oxidation rate).

This variability is likely due to various configurations resulting in different and unknown voltages across the oxide layer. Things are further complicated by the presence of gaseous oxides, and the use of temperatures without reference to the conductivity of the oxide. The almost universal lack of information on the actual current flow through the oxide is also worrying as current density should determine oxygen pumping rate. With this in mind it is not surprising that several different mechanisms have been proposed to explain the various effects seen at each electrode. Another complication is that electromigration and electrochemical reduction are related phenomena. As voltage is increased migration becomes reduction/oxidation, and both can occur at the same time and at different rates. This gets particularly convoluted when there are multiple valences of the cations and sub stoichiometric phases. A useful property of zirconia for the study of electromigration/electro reduction is that it has only one stable oxide. It has very limited tolerance of sub stoichiometry, and the only phase formed by reduction is metallic zirconium.

The literature survey suggested that the most suitable setup for performing high temperature oxidation tests for ZrB_2 in the presence of an electric field is the DCE mode. This is because the electrical parameters, voltage and current, can be precisely measured and correlated to the oxidation mechanisms. Another advantage is there is no interaction of the field with the oxidizing atmosphere.

5.2.5 Oxidation Under Field, Experimental Complications

While this experiment is most closely related to the work of Jorgensen[133] on the oxidation of silicon, there are several differences. The porous nature of the zirconia oxide being the main one, but the composition of the oxide was also an issue. The silica layer grown by Jorgensen was very pure and silica is a very highly studied material. In contrast, while there is a considerable amount of work on yttria stabilized zirconia[141-147], there very little is reported for pure zirconia[148]. This is due to the destructive phase transition on that can occur on cooling of zirconia. The situation is even worse for zirconia with liquid phase boria, where no reliable data could be found. The addition of dopants (yttria, ceria, etc.) significantly increases the ionic conductivity of zirconia, reducing its effectiveness as a conventional oxygen barrier. Doping also changes the ratio of ionic to electronic conductivity and their temperature dependence[149]. For this reason the literature data on doped zirconia cannot be used a reliable guide to the properties of the grown oxide layer.

5.3 Results and Discussion

5.3.1 Microstructural Analysis

Figure 5.2 shows images of cross sectioned ZrB_2 samples before and after oxidation with and without the application of an electric field. The measured

thickness (taken from cross sections) of the oxide layers are given in Table 5.2. Ten measurements were taken perpendicular to the surface evenly spaced on each of the 4 sides, the mean and standard deviation were then calculated.

Table 5.2 Thickness of grown oxide layers on ZrB_2 after oxidation testing

Sample 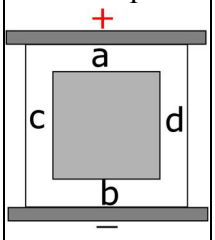		Thickness (a) \µm	Thickness (b) \µm	Thickness (c) \µm	Thickness (d) \µm
Pre Oxidation (1200°C, 2h)	Mean	92	92	97	91
	Standard Deviation	7	7	5	6
Control (1400°C, 5h)	Mean	387	423	590	599
	Standard Deviation	41	43	40	40
Applied Field 10V 100 mA (1400°C, 5h)	Mean	217	1402	1045	983
	Standard Deviation	84	67	30	70

Measurements were taken in several locations to show the asymmetry produced. The difference locations are described in the inset of the table, (a,b,c and d). All the micrographs are aligned in the same way so the polarity and location of points

a, b, c and d are consistent.

The pre-oxidised (1200°C for 2 h in a box furnace) sample is shown in Figure 5.2 (a). It had a well adherent oxide with an even thickness (**a**=**b**=**c**=**d**=92μm) and small standard deviation (5-7μm). The boria layer did not evaporate at this temperature, so the oxide layer was dense and consisted of boria filling the gaps between the zirconia grains. The pre oxidised oxide microstructure is visible in the high magnification micrographs (Figure 5.2 (c)). The samples at higher temperature without field, (Figure 5.2 (d)) showed a typical two layer structure, the top being free from boria.

The control sample which was oxidised (at 1400°C for 5 h) in the set up in Figure 3.2, without the application of an electric field, is shown in Figure 5.2 (b). The sample developed a symmetric oxide scale (a≈b≈400μm), however, the sides of the sample were significantly thicker (c≈590μm). This suggests that the Pt foil acted as a diffusion barrier and limited the oxygen diffusion through the top and bottom.

Before the effect of an electric field can be investigated a clear understanding of the oxidation process is needed. When heated in air ZrB_2 reacts to form boria and zirconia, boria is a liquid above 600°C and will wet and dissolve some zirconia [150]. The oxidation mechanism is temperature dependent, as modelled by Parthasarathy, et al [151]. At low temperatures the boria will coat the outer surface of the material and form an effective diffusion barrier. As a result oxidation follows a parabolic rate curve dependent on oxygen partial pressure and is proportional to the thickness of the boria layer. At higher temperatures (>1000^{0}C)

the boria will start to evaporate and will retreat into the interior of the zirconia scale. At this point the outer porous zirconia layer acts as a Knudsen diffusion barrier (a weaker barrier) due to its geometry of long elongated pores. The interior boria continues to act as the main diffusion barrier so the oxidation rate is dependent on the boria evaporation rate. Above a certain temperature the boria evaporates too rapidly to be an effective barrier and the oxidation rate becomes rapid.

As shown in Figure 5.2(e-f), when the sample was oxidized in presence of an electric field (10V and 100mA) at 1400°C for 5 h a clear field effect was observed. The layer thickness **a** (under the + electrode) grew to 217μm with a standard deviation of 84 μm. The diboride was curved with the thinnest oxide occurring in the middle. This could have been caused by uneven current distribution, once an area has started oxidizing it will be more resistive and hence get less protective current. At its narrowest point the oxide layer was only 120μm which is similar to the peroxidised sample at 92μm, (Figure 5.2(a)). This indicates that the application of the electric field was sufficient to significantly retard the oxidation. Conversely, there was significantly acceleration oxidation at the negative electrode as well as on the sides of the sample (b=1402 and c≈d≈1000μm). The increased oxidation seen on the sides of the sample was not anticipated but could have been a side effect of the enhanced oxidation at the bottom electrode. The oxygen pumped towards the top electrodes did not all react with the diboride, much of it would likely diffuse away. As the oxygen would be deposited near the diboride surface, inside the scale it's reasonable that it would diffuse up the sides

of the sample. So the sides might experience a higher local PO_2, but there is no direct evidence of this.

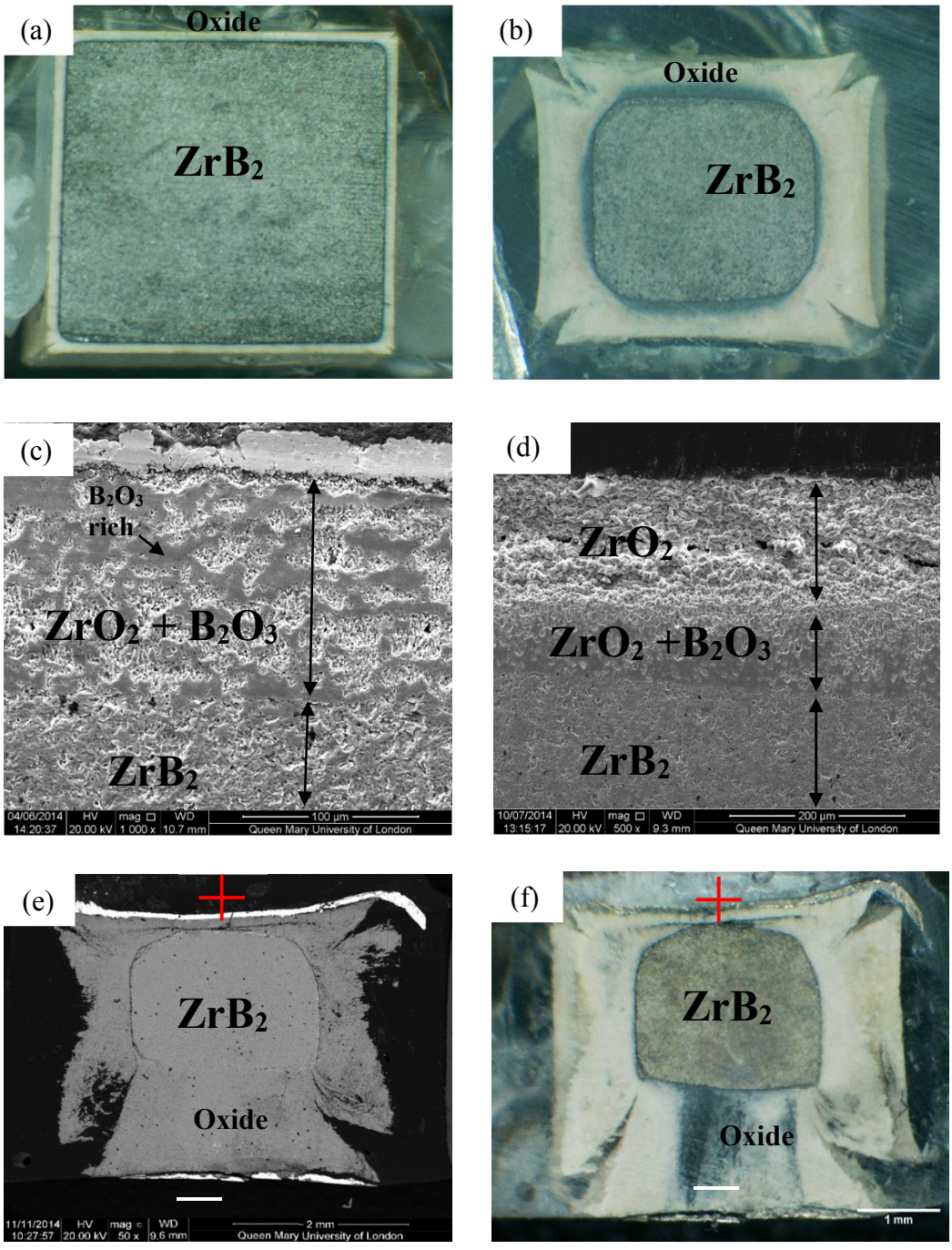

Figure 5.2 (a) Low magnification optical micrograph of Diboride sample after peroxidation step (1200°C for 2 hours)(b) Low magnification optical micrograph of Diboride sample after oxidation (1400°C for 5hr) without an applied field (c) high magnification micrograph of oxide scale after pre oxidation at 1200°C showing boria throughout (d) high magnification micrograph after oxidation at 1400°C showing boria receded (e) Low magnification micrograph of Diboride sample after oxidation (1400°C for 5hr) with an applied field (10V 100mA) polarity as marked (f) Low magnification optical micrograph of Diboride sample after oxidation (1400°C for 5hr) with an applied field (10V 100mA) polarity as marked. With electrochemical blackening visible.

5.3.2 Electrical Data and Electrochemistry

From observation of the current and voltage curves during heating (Figure 5.3) some useful information on the mechanism of oxidation can be inferred. During heating, below 1200°C, the measured current is negligible, but above 1200°C the oxide layer became conductive. The lack of dopants in the zirconia scale formed meant that it had a low oxygen vacancy concentration, which limited the current flowing until 1200°C. Above 1200°C the intrinsic oxygen vacancy concentration was sufficient to produce significant current. It is worth noting that most oxygen pumps can operate at as low as 600°C because they are doped and so have relatively high oxygen vacancy concentration. Above 1200°C the voltage dropped from 10V to between 1 and 2V as the current limit of 100mA was reached. As the temperature of the sample continued to rise the thickness of the oxide layer (b) continued to increase. This lead to an increase in the resistance of the system, as seen by the increasing voltage. Unlike the current, the voltage signal was noisy due to the instability of the oxide layer, as it cracked and spalled the resistance changed. During cooling, the current only dropped after the sample had cooled below 1050°C, implying that some change had occurred to the composition or structure of the oxide layers.

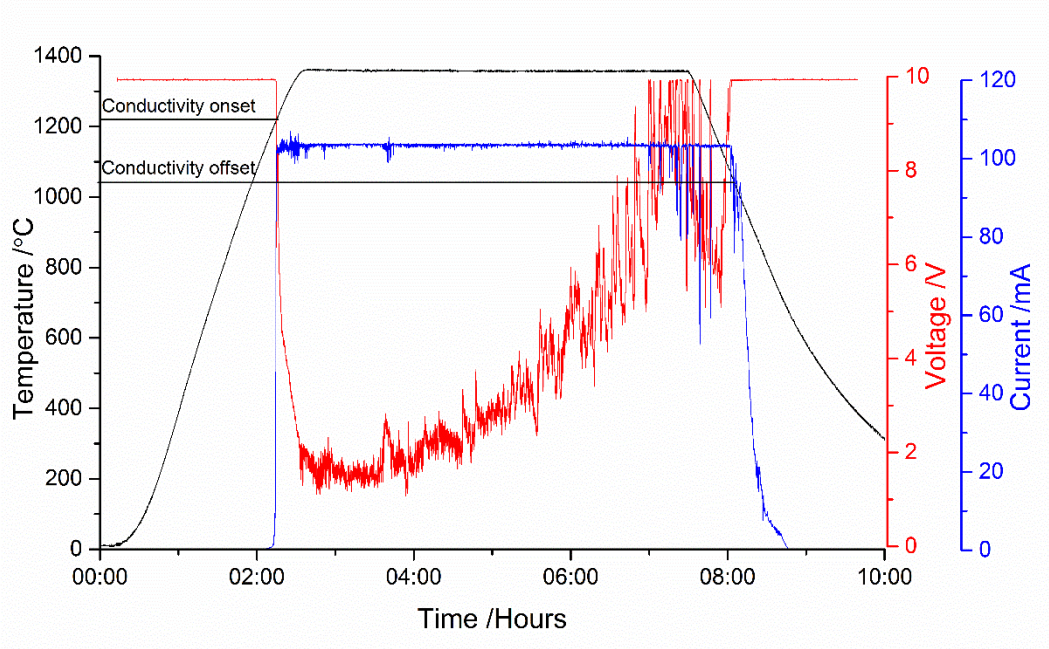

Figure 5.3 Electrical parameters recorded during the oxidation under 10V 100mA

The Initial voltage of 1 to 2V was in the range of the Nerst potential based oxygen pumping (0-1.25V [140]), considering that there are two junctions and the voltage drop was split between them. As the voltage increased above 2V (after 2hr) it became increasingly likely that electrochemical reduction occurred. This is when zirconia is reduced to sub stoichiometric zirconia and possibly metallic zirconium. The electrochemical reduction potential of zirconia is 2.1V at 900°C [152]. This could explain the change in electrical properties of the zirconia during the cooling. Any over potential (voltage exceeding that needed for electrochemical reduction) will produce voids and zirconium metal precipitates that influence the conductivity [153]. Electrochemical reduction should be visible as blackening of the

zirconia. The situation at the sides is more complex, the edges tend to crack, which means there is no path for current to flow. Despite the lack of current the oxide layer did grow

A reasonable assumption, especially during the initial stages of the oxidation test, is that the voltage drop at both layers is the same. Initially the oxides layers (a) and (b), should have the same thickness of about 90µm, and an applied voltage of 0.9V (1.8V divided by 2). At the end of the oxidation the thickness ratio a:b was 1:6.46 (217µm:1402µm) so the applied 9V was split 1.2V(a) and 7.8V(b). This analysis makes some questionable assumptions, mainly that the resistance of the zirconia is relatively stable throughout the oxidation process, but is the best that can be achieved with the data at hand. It also implies that there was no electrochemical reduction on the top surface (<2V) while the electrochemical reduction is expected on the bottom (>2V). This theory is supported by the visible blacking near the bottom (-ve electrode) in Figure 5.2 (f).

5.3.3 Idealized Model to Understand Oxidation under an Electric Field

As described in chapter 5.2.5, a complex oxide scale was formed on the ZrB_2. However, for the purpose of understanding the effects of electric field on the oxidation mechanisms, a simplification is to assume that the scale was a dense zirconia layer. In pure zirconia, $\ddot{V_o}$(charged oxygen vacancies) form intrinsic point defects. These increase in number with increasing temperature and decreasing

PO_2. The mobility of the oxygen vacancies (substantially higher than the cations) is the major diffusing species through the zirconia [154]. For all conditions an equal counter flow of O_0^x occurs for each $\ddot{V_o}$, so it is reasonable to talk about oxygen vacancies and ions interchangeable. However it is important to note that the $\ddot{V_o}$ is the species that actually feels the electrostatic forces, even if it's simpler to imagine it as an $O_0^{"}$.

To understand the basic oxygen pumping phenomena it's easiest to ignore the diboride and just look at a solid sheet of zirconia, with platinum electrodes, separating two atmospheres at different PO_2. The flow of oxygen across this interface would be expected to be from high PO_2 to low PO_2, however the flow rate and even direction depend on the electrical situation at the electrodes. This is explained in Figure 5.4 .

(a)

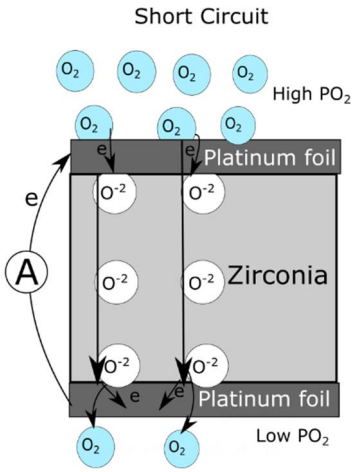

If there is a path for electrons to flow then oxygen flows from high PO_2 to low PO_2, the electrons flow the opposite direction.

(b)

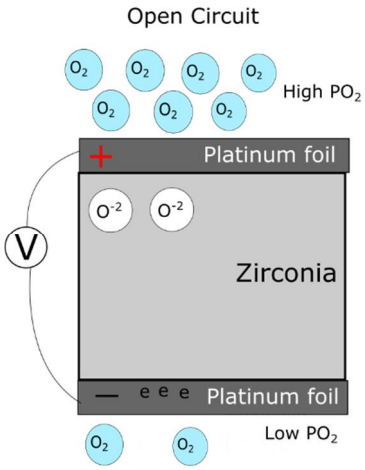

Initially oxygen can flow across the gradient but rapidly the top foil gets depleted in electrons, and the lower foil gets saturated. This generates an electric field in the zirconia, stopping the flow of oxygen ions. The charge that builds up (voltage on electrodes) is proportional to the difference in PO_2 described by the Nernst equation.

(c)

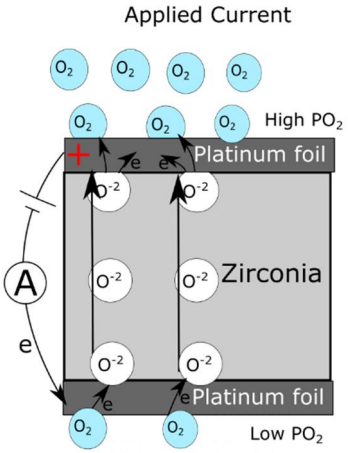

If an external voltage is applied it generates an electric field in the zirconia, this causes the oxygen ions to flow to the positive electrode, where they lose an electron becoming gas. The applied field can even cause the ions to flow against the concentration gradient

Figure 5.4 A diagram showing oxygen diffusion thought a zirconia interface under (a) Short circuit conditions (b) Open circuit conditions (c) With an applied current

Once oxidations starts (oxygen admitted into atmosphere) a concentration gradient of oxygen is produced across the zirconia layer. This forms as oxygen is rapidly consumed at the ZrB_2 /ZrO_2 interface (effectively very low PO_2). This causes a gradient of oxygen vacancies to form inside the zirconia, as the vacancies and oxygen try to reach local equilibrium at each interface. Oxygen flows across the vacancy gradient producing a net flow of oxygen towards the ZrB_2 surface. This flow produces an electric field, which under open circuit conditions is proportion to the PO_2 gradient. On the basis of this effect, zirconia is used as an oxygen sensor [140]. The voltage generated across the oxide layer can be calculated according to this Nerst equation [140].

$$E = 0.0496T \log_{10} \frac{P_1}{P_2}$$

Where

E is the measured voltage across the zirconia membrane

T is the temperature in

P_1 is the partial pressure of oxygen on one side of the electrode

P_2 is the partial pressure of oxygen on the other side of the electrode

This system can be driven in reverse. The application of an external electric field can cause the oxygen ions to drift in the direction of current flow, which results in oxygen being transported in the opposite direction[155]. Oxygen can diffuse across the zirconia despite the fact that this can be against the external oxygen PO_2 gradient. The zirconia is effectively pumping oxygen from one side to the

other. The pumping voltage determines the equilibrium oxygen concentration gradient (between the two sides) and the current determines the rate of pumping.

5.3.4 Oxidation under an Electric Field in the Presence of Porosity in the Scale

Because of the formation of a porous zirconia scale, the behaviour of the system deviates from the Nerst equation. By combining the results of microstructural analysis and electrical measurements we can build a more complete understanding of the phenomena. Upon heating above a critical temperature (1200°C) the zirconia became electrically (ionic) conductive enough to reach the experimental current limit of 100mA. The flow of current corresponds to oxygen being pumped by the applied potential. The zirconia layer formed during oxidation was porous, so some oxygen diffused through the pores. In fact during the whole oxidation cycle the total amount of oxygen pumped grossly exceeded that needed to react with total mass of the ZrB_2. This is only possible if the oxygen was leaking through the porosity. The current flow reduced oxidation on the top side (positive electrode), where oxygen was pumped out, and increased the oxidation rate on the bottom (negative electrode) where oxygen was pumped in.

A schematic of this is shown in Figure 5.5. The loss of boria was ignored in this case as it tends to evaporate at 1500°C and does not interact with the electric field. Figure 5.5 shows the model without (a) and with (b) an electric field. In summary the oxidation retardation in presence of an electric field can be divided in four stages shown Figure 5.5. **Stage 1** diffusion of O_2 thought the platinum foil and

surface of the sample. **Stage 2** diffusion of O_2 into the zirconia lattice, becoming O^{-2}, but also O^{-2} being ejected from the lattice as O_2 gas. In parallel some oxygen will also diffuse through the pores. **Stage 3** due to action of the electric field O^{-2} in the zirconia lattice diffuse back toward the platinum foil. The O_2 in the pores, however, continues to diffuse towards the ZrB_2. **Stage 4** limited oxygen reaches the ZrB_2 surface as it is constantly being pumped away by movement of oxygen vacancies.

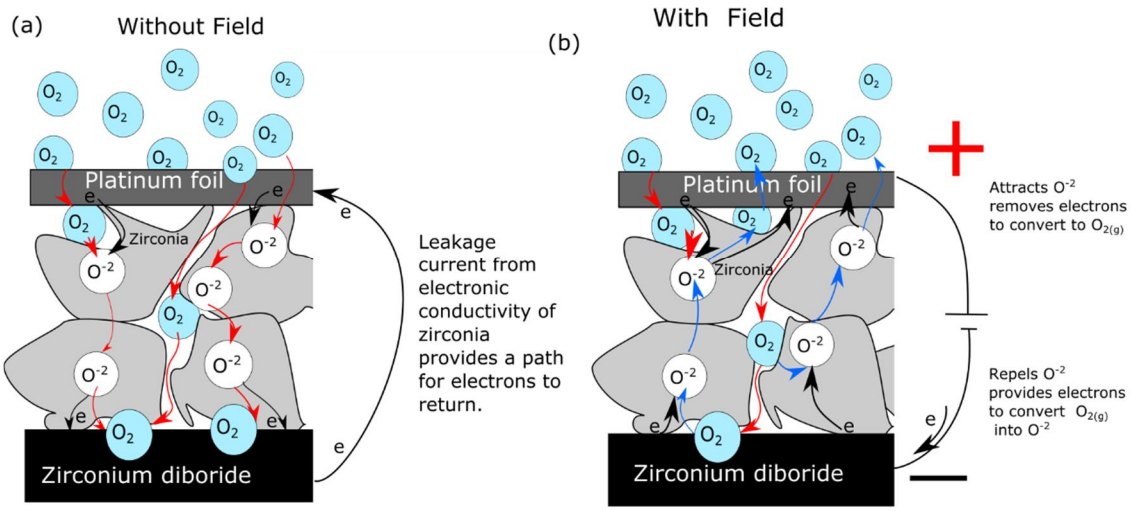

Figure 5.5 . A diagram of hypothesized model of oxidation of ZrB_2 under the condition of this experiment, (a) without and (b) with electric field. Oxygen gas (light blue colour) and Oxygen ions (white colour) diffuse through both the pores and bulk zirconia toward the ZrB_2 surface causing oxidation as shown by the red path. With the application of a field the flow of oxygen ions can be reversed, the blue path, giving a reduced oxidation rate.

5.4 Conclusions

Microstructural and electrical data analysis showed that by applying a voltage across the zirconia scale (positive polarity) on a ZrB_2 sample (negative polarity)

oxygen transport can be restricted to reduce oxidation. Comparing the growth in thickness of the oxidation layer with (125μm) and without electric field (300μm), the oxidation resistance was enhanced by 240%. Reduced oxidation occurs despite the zirconia being porous. The oxygen pumping effect reduces oxygen partial pressure at the ZrB_2 interface resulting in very low oxidation rates. By careful choice of sample and electrode geometry it should be possible to extend their service temperature of ultra-high temperature ceramics in oxygen rich atmosphere. This work exploited two ECEs, electromigration and electrochemical reduction. While it might have been preferable to have operated with pure electromigration the amount of oxygen that need to be pumped to avoid oxidation was too great due to porous zirconia scale. The voltages need to pump that amount of gas was too high so electrochemical reduction was inevitable. The reduction of zirconia transformed it into a more conductive form[156]. This process achieved its stated goals of exploiting an existing ECE to significantly alter the behaviour of a scientifically interesting material (UHTCs). But there are several hurdles to overcome if the process is to be significantly improved or exploited for commercial use.

For this reason this work is best viewed as a stepping stone towards the next chapter in this thesis. While the particular setup used in this chapter might ultimately be a dead end, the lessons learned proved invaluable in developing the contactless flash sintering setup described in the next chapter.

Chapter 6. Contactless Flash Sintering

6.1 Introduction

During the last several years there has been ever increasing interest in flash sintering. From the academic side more and more materials have been investigated and the optimum conditions for flash sintering have been found for many [3,6,157-161]. There is still much debate about the mechanism involved, but there is growing confidence that it is related to rapid Joule heating and thermal runaway [8,162]. Understanding the mechanisms at play in flash sintering has been complicated by the fact that most flash sintered materials are ionic conductors. The issues is they are being operated far outside the conditions that they are usually studied, much like the issues discussed in Chapter 5.2.5. From the commercial side there has been interest in scaling up the process to realize the potential energy and time saving properties of flash sintering on an industrial scale. Lucideon[85] is already testing a commercial scale flash furnace.

However, there are many complications that flash sintering brings, which limit its commercial application. The need to have electrodes attached to the surface of the sample is a challenging issue. The initial choice of electrodes was platinum[157] with obvious cost issues and alternatives like carbon rolls (used by Lucideon) brings its own issues and requirements. The use of electrodes inherently adds several extra steps to the FS process, since conductive electrodes have to be attached and then removed after sintering. The requirement for electrodes also

limits the geometry of sintered parts. A uniform electric field and current flow is required to achieve homogeneous heating. This means complex geometries (having non-constant thickness) cannot be sintered homogenously. The development of Contactless FS (CFS) technology would not only overcome these problems but might also allow continuous sintering. This can be achieved by passing current through a material that is in relative motion with respect to the non-contact electrodes. To the authors' best knowledge, there are at least two ways to achieve FS in contactless mode, plasma electrodes or microwaves sintering. Microwave FS, especially in single mode cavities, is capable of rapid sintering (with a heating rate of a few thousands of degree per minute) [46,163,164]. However, the use of microwaves has limitations, with hotspot formation limiting either the speed of sintering or the homogeneity/size of the samples[165].

There was no published work on plasma electrodes for sintering. With the work already done on understanding the physics of plasma discharge and how it relates to materials processing, (Chapter 2.3, 2.7.1 and 4.1) it was decided to try and develop a technique based on this principle. One possible advantage of using plasma electrodes is that they might also integrate the preheating of the material (plasma usually being thermally hot). In existing FS technology, preheating (to a temperature above which the electrical conductivity suddenly increases) is usually done in conventional furnaces. This greatly adds to the processing time and energy requirements, making FS less energy attractive. A Plasma can be used as an electrode in flash sintering as the main requirement for an electrode is that it is electrically conductive and does not contaminate/react with the sample. A plasma

being composed of ions and free electrons can carry current and conform to the surface it is in contact with. If an inert gas plasma is used their there is also no possibility of contamination. The simplest design is to have two metal electrodes and the sample held between them with a gap. Two independent plasmas are generated at the electrodes as depicted in Figure 6.1, and current can then flow through the sample across the plasma. However, this configuration is not practical, as each plasma electrode would require so much support equipment that two could not be placed even relatively close together. The plasma used must also be sufficiently conductivity and meet other requirements.

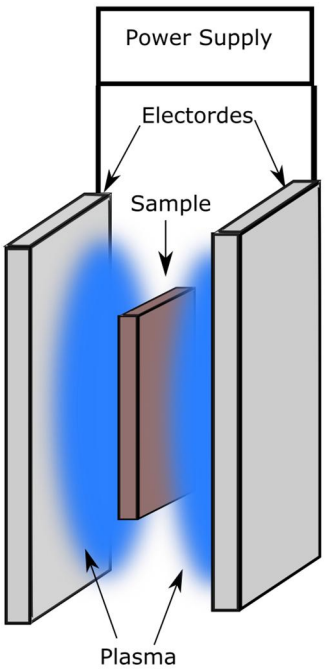

Figure 6.1 schematic of essential components to realize contactless flash sintering based on plasma electrodes.

6.2 Development of the Experimental Setup for Contactless Flash Sintering (CFS)

As discussed earlier (in Chapter 2.8.2), there are a variety of different modes of plasma they can have very different properties [166-169]. For the purpose of this work, the thermal and electrical properties of the plasma are most important as well as the equipment required to generate them. The electrical conductivity of a plasma is complex and it depends on many different environmental conditions/parameters. However, if all that is needed is a broad comparison of orders of magnitude, electrical conductivity can be considered to be proportional to the electron number density. Electron number density is the number of free electrons in the plasma per unit of volume and is listed in Table 6.1

Table 6.1 summary of different plasma generation techniques and the properties of the plasma that they produce

Plasma source	Electron number density / m^{-3}	Background pressure/ Torr	Nominal power* /W	Reference
dc glow discharge	10^{16}	0.10-5	100-300	[168]
RF glow discharge	10^{17}	0.05-1	200-500	[168]
Electron	10^{18}	10^{-4}-0.01	300-1,000	[168]

cyclotron resonance				
Inductively coupled	10^{18}	10^{-3}-0.1	500-2,000	[168]
Helicon	10^{18}-10^{19}	0.01-0.1	500-2,000	[168]
dc plasma jet	10^{20}-10^{23}	750-7,5000	1,000-20,000	[170]
dc welding arc	10^{19}-10^{23}	750	500-2,000	[171]

To allow CFS, the plasma should have a temperature suitable for preheating the sample. So a cold plasma would be preferred (low neutral temperature) for materials having low sintering temperatures (below 1000°C). A plasma with a high electrical conductivity is preferred as it would result in a low voltage drop across the plasma. A plasma that could homogenously cover a large surface (on both sides of the sample) would allow the entire volume of a sample between the electrodes to be sintered. A RF glow discharge or inductively coupled plasma are the most likely candidates to meet the above requirements. However, both of these methods require a completely controlled atmosphere and complex plasma generation equipment. A further complication is the presence of an external electric current in the plasma (the flash sintering current), which can change

drastically the proprieties of the plasma. By looking at the traditional voltage current curve for gas discharge[169] (Figure 2.13), it is likely that the plasma will degenerate into an arc discharge under normal flash sintering conditions, when the current exceeds 1 a. To avoid the catastrophic degradation of the plasma electrodes, it is necessary for the electrode materials to be compatible with the high temperature of the arc discharge. Due to the issues of all plasmas to degenerating into an arc plasma it is pragmatic to use arc electrodes, at least for this initial work. An advantage of an arc plasma is that it only requires simple equipment; a step down transformer with a magnetic shunt as is used in a traditional welding power supply. There is good reason to use a simple transformer style welder instead of more modern transistor systems. By using an ac welding transformer the three power supplies are effectively isolated from one another by their magnetic cores (see simplified electric schematic in

Figure 3.3). This avoids issues where common ground faults would short out the power supplies with disastrous results. The choice of arc plasma electrodes is not without its disadvantages, the high neutral temperature (over 5000K[172]) of the arc plasma will transfer significant heat into the sample. One upside of this is that the samples will already be heated by the arc electrodes. This renders external preheating unnecessary which further simplifies the experimental setup. ac power supplies were used because arc heating is affected by polarity; in dc operation the

+Ve surface of the sample would adsorb 70% of the heat. As results of this, ac allows a more even and symmetric heating compared to dc arcs.

6.3 Results and Discussion

6.3.1 Preheating Arcs

Before discussing the results in depth, it is useful to clarify what is happening during contactless flash sintering. Before the flash sintering occurs the arcs heat the sample from the surface. This preheating is so that a discrete sample volume is hot enough to be electrically conductive (above or near the flash sintering threshold temperature). On application of the flash power supply an arc is struck between the electrodes and the surfaces of the sample. This results in heating of the surface due to radiation from the plasma and electron bombardment, but also joule heating inside the sample. It is this internal heating that distinguishes this method from simple arc heating/melting and makes it a flash sintering process.

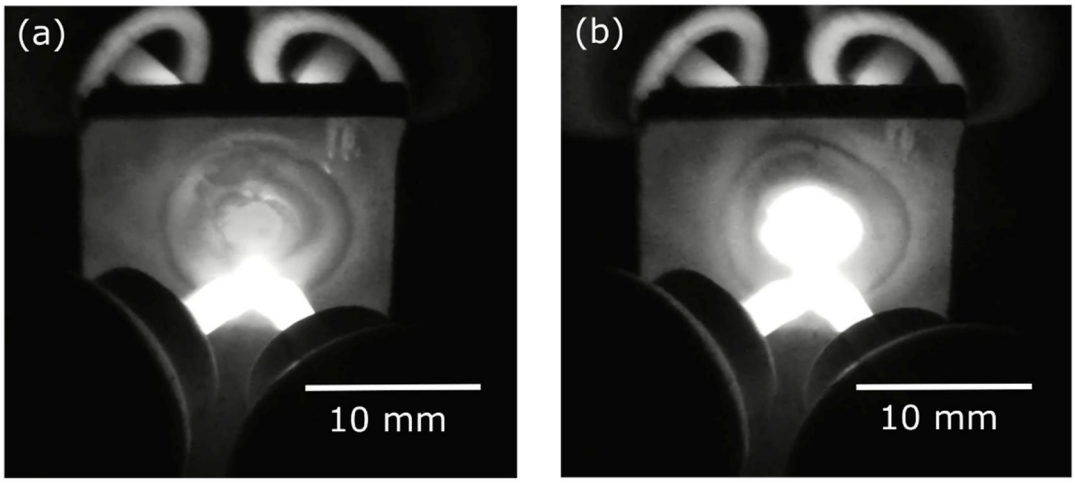

Figure 6.2 showing stills from a video of the contactless flash sintering process, (a) before and (b) 0.5s after the application of the flash power supply reaching a current of 6A..

An attempt was made at quantifying the preheating temperature reached, and this is plotted in Figure 6.3. For this test the sample was correctly positioned between the torches, by which time the sample had already reached 400°C. Once in position the temperature rapidly rose to 1400°C in just 5s. For this reason the sample was preheated for at least 5s in the actual experiments to ensure an even and repeatable preheat.

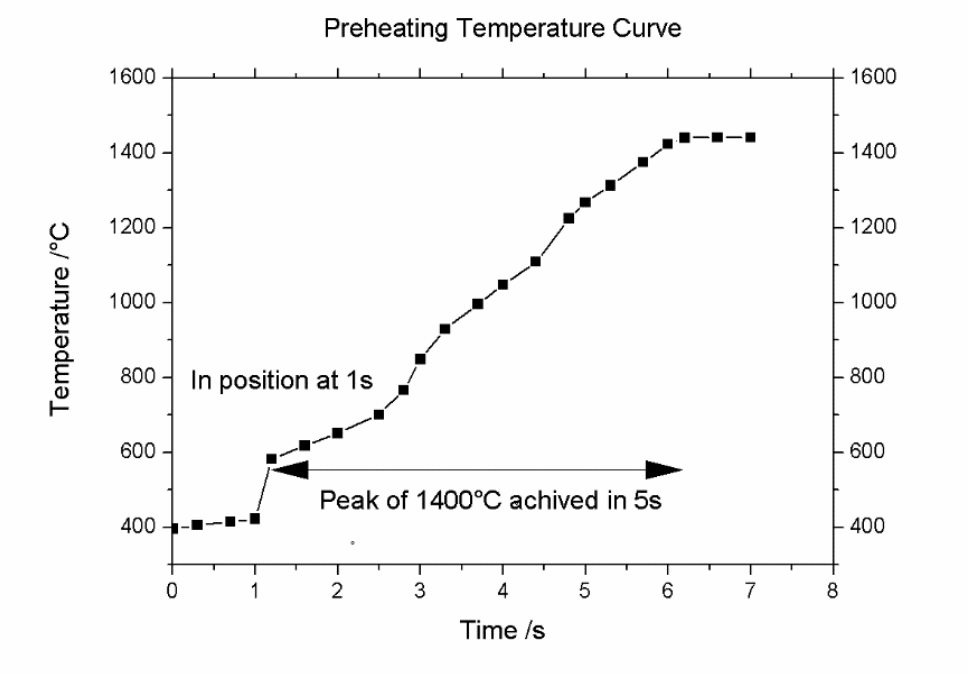

Figure 6.3 time temperature preheating curve measured using an embedded thermocouple.

The total power supplied by the welding transformer to each twin arc was ≈800W (19V and 43A rms, see Figure 3.4). Despite this high power, when the sample was held between the arcs for 60s no densification was observed. Arc preheating caused the temperature to rapidly rise to 1400°C within 5s (as shown in Figure 6.3) and stabilize. This temperature, which was lower than the pre-compaction temperature of the sample (1550°C), was not sufficient to further densify the material, as seen in Figure 6.4.

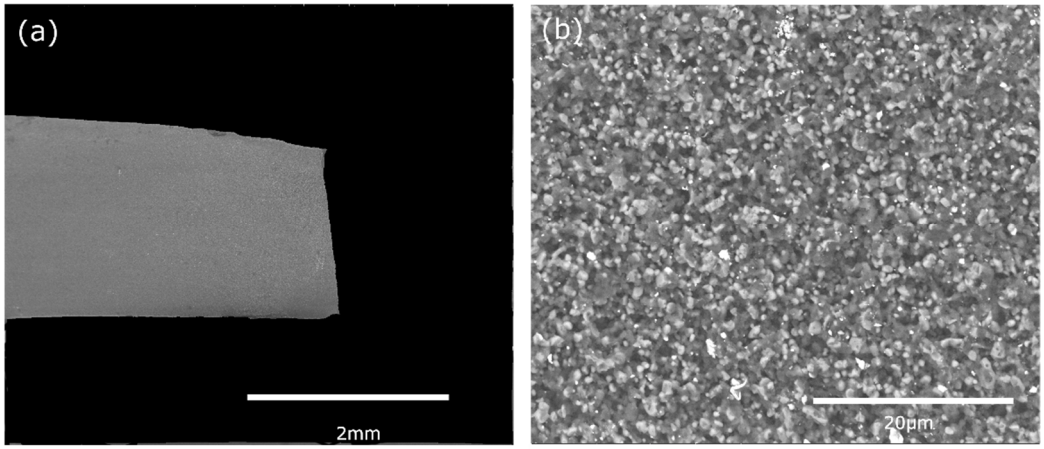

Figure 6.4 , micrograph of cross sectioned SiC B_4C sample after 5s under preheating arcs.

This is due to the poor thermal coupling of the (preheating) arcs with the sample. In an arc the heat is mainly carried by the electrons, so most of the heating was localized at the tungsten electrodes. The CFS power supply produced much better coupling by a combination of internal joule heating and from electrons striking the surface of the sample. This explains the rapid heating seen in Figure 6.2, where a ripple (4-5mm diameter) of heat was seen spreading across the surface of the sample within 0.5s of the flash power supply (≈200W) being switched on.

6.3.2 **Typical Results**

While the various materials and conditions used produced a variety of samples and behaviours, there was some clear common traits. The arcs always produced some surface damage. Figure 6.5 shows a representative example of a sample directly after CFS. The surface in contact with the plasma was modified by

electron bombardment which resulted in excessive local heating. The discoloration located outside the crater (visible in the inset of Figure 6.5) was produced by a thin oxide layer formed as the sample cooled outside of the argon flow.

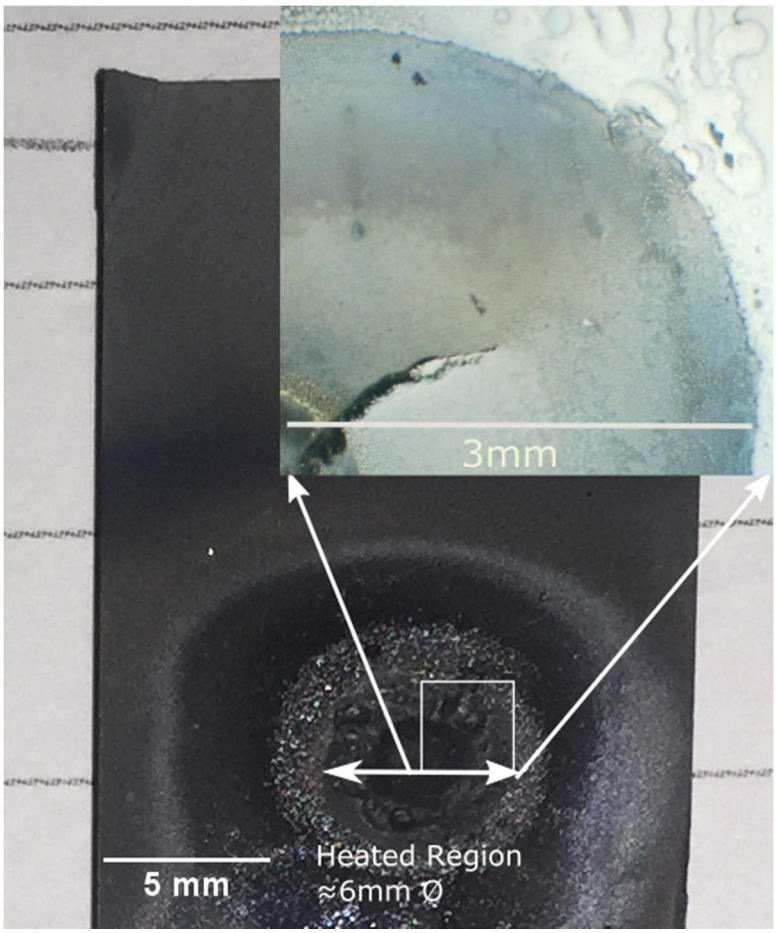

Figure 6.5 photograph of the SiC 50 wt% B_4C sample CFSed for 2s and inset showing optical micrograph highlighting surface modification induced during the processing.

The surface, however, was not representative of the underlying material, so the samples were cross sectioned about the centre of the crater. A schematic of the

different zones typically seen is shown in Figure 6.6. These zones are discussed below with regard to the SiC:B_4C composite but the basic structure remains the same for different materials.

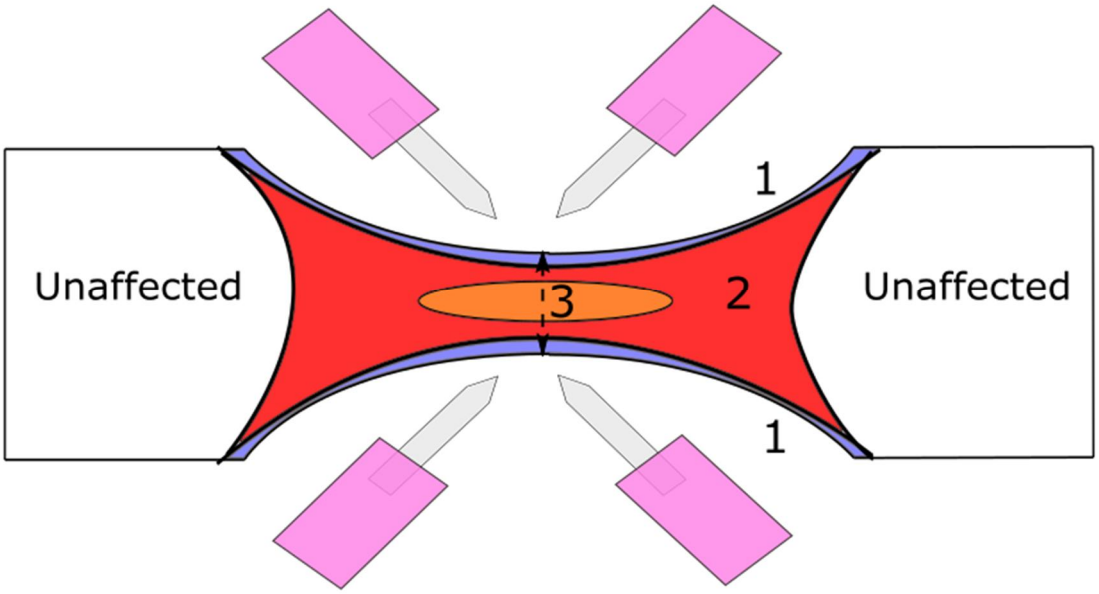

Figure 6.6. Schematic of a typical CFSed sample illustrating the location and relative size of the resulting zones (described in the text).

6.3.3 **Composite SiC:B_4C**

Of all the materials processed, the SiC:B_4C composite sintered at 6A produced the best microstructure and showed a clear pattern of behaviour. For this reason it was investigated in the most detail and will be discussed first.

6.3.3.1 Comparison of Different Times, the Progression of Sintering

Depending on the processing time, up to three different zones (Figure 6.6) were visible in the microstructure. The heating was generated both internally, by Joule heating and externally from the arcs. Due to the very short times used the sample did not reach thermal equilibrium and was heated inhomogenously. A significant amount of heat was carried by the arc electrons bombarding the surface, hence the surface (zone 1) was overheated (showed signs of melting/ eutectic structure). This molten layer does not change significantly with the different times because it has a small thermal mass and is capable of dissipating excess heat as radiation, so it saturate in under a second. The internal Joule heating however is much more dependent on the time and current. If the sample resistivity was fixed then the heat would be generated homogenously. This would lead to even temperatures but there is external heating from the surfaces so the material near zone 1 should heat up quicker, this region is referred to as zone two. Material in the centre of the sample (zone 3) is thermally insulated from the surface heating, so even with internal Joule heating it heats up at a slower rate. This general pattern can be seen in Table 6.2, which was constructed from measurements taken from the micrographs shown in Figure 6.7(a-d). The 2s and 3s samples were very similar, the only major difference was the porosity in the middle (zone 3) seen in the 2s sample. As seen in the micrographs, Figure 6.7, and optical images, Figure 6.5, almost all of the samples showed cracking induced by the differential shrinkage during CFS processing. This issue is inherent to any local densification method

and could be solved by sintering a larger portions of material.

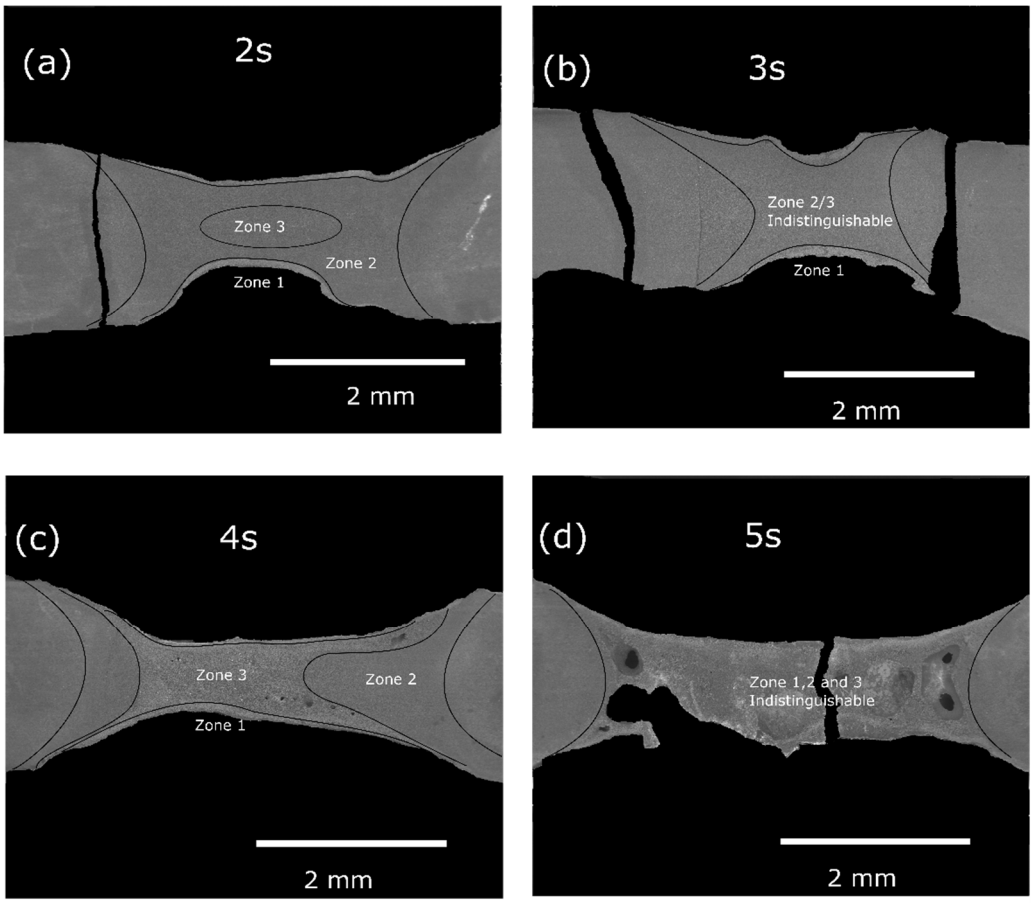

Figure 6.7 micrographs of plasma flash processed SiC:B_4C showing the progression of sintering over CFS discharge time: (a) 2s; (b) 3s; (c) 4s; and (d) 5s, with the zones labled.

From Figure 6.7 and Table 6.2 it is possible to piece together the sequence of events that occurred as the samples were CFSed. First, the sample was preheated up to 1400°C by the arc torches, which produced a diffuse heating over a region of ~10mm in diameter (see Figure 6.3). When the CFS power supply was switched on it generated an arc against the surface of the material. As the arc was transferred to the sample, the surface was bombarded by electrons and ions, causing rapid

heating of the surface. As seen in Figure 6.2 the hot spot rapidly expanded within 0.5s to 5mm in diameter, melting a thin layer of material (zone 1). The temperatures reached in zone 1 must have exceeded the eutectic temperature of SiC - B_4C which is 2300°C[173] as evidenced by the needle like precipitates seen in zone one of Figure 6.9(b). These precipitates are typical of solidification from a eutectic liquid in the SiC - B_4C system[174]. The pseudo binary phase diagraph for SiC B_4C is shown below in Figure 6.8

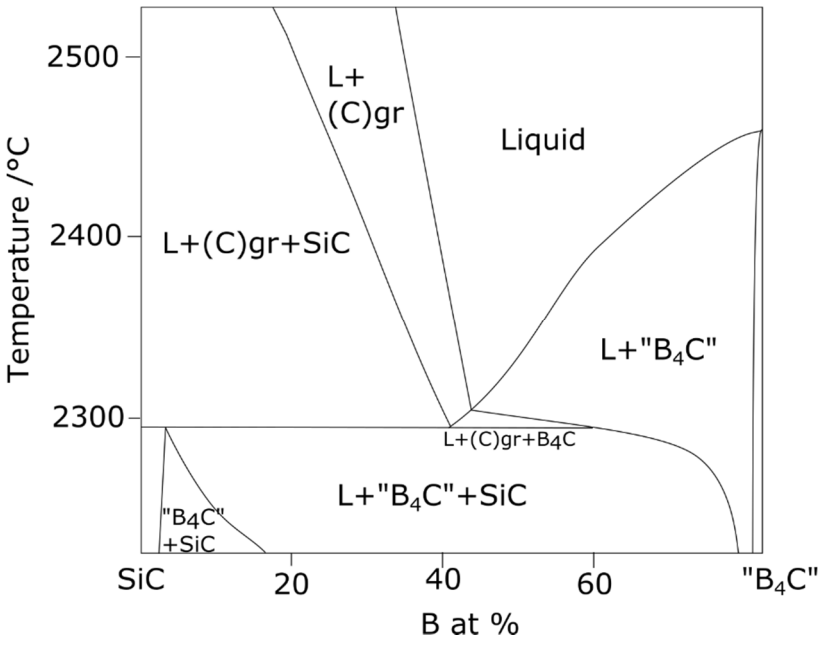

Figure 6.8 Phase diagraph for SiC B_4C, adapted from Korniyenko, K. I[175]

Two seconds after the initial arc transfer the surface heating had diffused deeper into the sample, which caused the melted zone 1 to grow to 80µm thick. Material near zone 1 began to sinter, forming zone 2, with a thickness of 170µm. Zone 3 (400µm thick), was still relatively cool and so remained highly porous. The sample was about 1200µm thick at its most narrow section.

Given more time (3s) the melted layer (zone 1) grew thicker (100µm), consuming more of the sintered region (zones 2). Zones 2 and 3 were now indistinguishable (labelled as zones 2/3 in Figure 6.9) as both were dense with no bubbles or abnormal grain growth, with a thickness of 900µm.the sample was now 1100µm thick at its most narrow section. The theoretical thickness predicted for fully dense material (starting from 1800µm (65% dense)) is 1170µm. So the small deviation from the measured value suggests little material was lost during CFS.

Given even more time (4s) the molten layer (zone 1) expanded to 160µm and the sample started ablating and thinning, and the total thickness was now 700µm. Hotspots formed inside the sample at the boundary between zones 1 and 2/3. These regions overheated to the point where SiC started to sublime, forming bubbles as the gas was trapped by the molten zone 1. This also indicated that the temperature inside the sample had reached at least 2200-2400°C, the point at which SiC sublimes rapidly [176]. In zone 2/3 (now 380µm thick) the temperature continued to rise which caused significant grain growth.

Given further time (5s) the entire sample melted, and platelets formed by precipitation form the liquid phase and bubbles formed throughout. This actually caused the sample to expand to 1100µm thick, even as material was being lost by sublimation/ablation.

Table 6.2 Summary of microstructures observed in the different Zones of the sample processed by CFS after 2, 3, 4 and 5s. The layer thickness and diameter (Φ) of the different Zones are also given. Initial sample thickness 1.8mm

Time /s	**Zone 1 Surface**	**Zone 2 Interior**	**Zone 3 Centre**
2s Microstructure Thickness (900µm total)	melted 80µm	sintered porous 170µm	sintered highly porous 400µm
3s Microstructure Thickness (1100µm total)	melted 100µm	fully sintered (900µm) Zone 2 and 3 indistinct	
4s Microstructure Thickness (700µm total)	melted 160µm	sintered bubble (380µm) Zone 2 and 3 indistinct	
5s Microstructure Thickness (1100µm total)	melted and bubbles (1,100µm) Zone 1-3 are indistinct		

6.3.3.2 In Depth Analysis of the 3s Sample

Because of its more homogenous microstructure, the sample CFSed for 3s is described in more detail. From the low magnification micrographs (Figure 6.7 (b)) it was evident that Zones 2 and 3 were indistinct. Figure 6.9 shows the microstructure in more detail for each of the Zones. Zones 2/3 were nearly fully

dense with no pores visible even at 20,000X magnification and in the TEM image. Consolidation occurred over a sizeable region of the flash sintered sample with a volume of 14mm^3. This was derived from SEM analysis supposing a cylindrical sintered region of thickness 1100µm and diameter of 4000µm. Only a thin layer of overheated material (Zone 1), showed signs of having melting, and this was limited to just the surface (≈100µm thick).

The microstructure visible in Figure 6.9 shows many interesting features. In Zone 2/3, the phase volume fraction measured by SEM phase analysis was 61% B_4C and 39% SiC. This is close to that expected of a 50wt% SiC:B_4C mixture (57 vol% B_4C: 43 vol% SiC). This confirmed that the molten phases on the surface of the sample, visible as zone 1 in Figure 6.9(b), did not significantly affect the bulk composition as measured in zone 2/3 from Figure 6.9(d). In the higher magnification image of zone 2/3 in Figure 6.9(d) it is possible to clearly see the two phases and how they were distributed. B_4C (dark phase) formed a continuous network matrix with the SiC (lighter phase) forming the secondary distributed phase. The phases were not entirely segregated; several individual isolated grains of SiC were visible within the B_4C matrix.

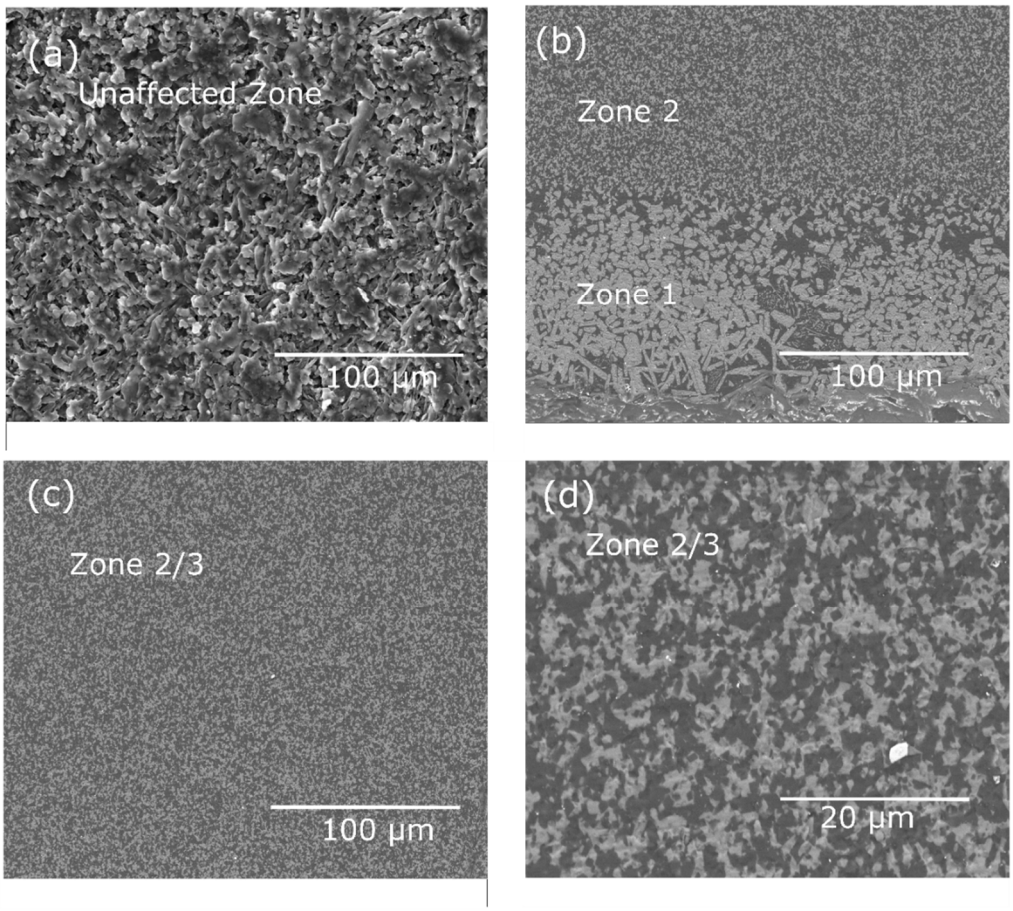

Figure 6.9 SEM micrographs of SiC 50 wt% B_4C sample CFSed for 3s: (a) unaffected Zone; (b) boundary region between Zone 1 and 2/3 (the Zones were indistinct); and (c) (d) higher magnification of Zone 2/3.

The grains were multifaceted and the grain boundaries remained well defined with a marked sharp compositional gradient between the two phases. Similarly, sub-micrometre SiC grains were present in the matrix. The sharp small grains confirm that the material did not have a chance to reach equilibrium as sharp grains are a high energy interface and thermodynamically unfavourable. This is most clears in the TEM image in Figure 6.10 (d).

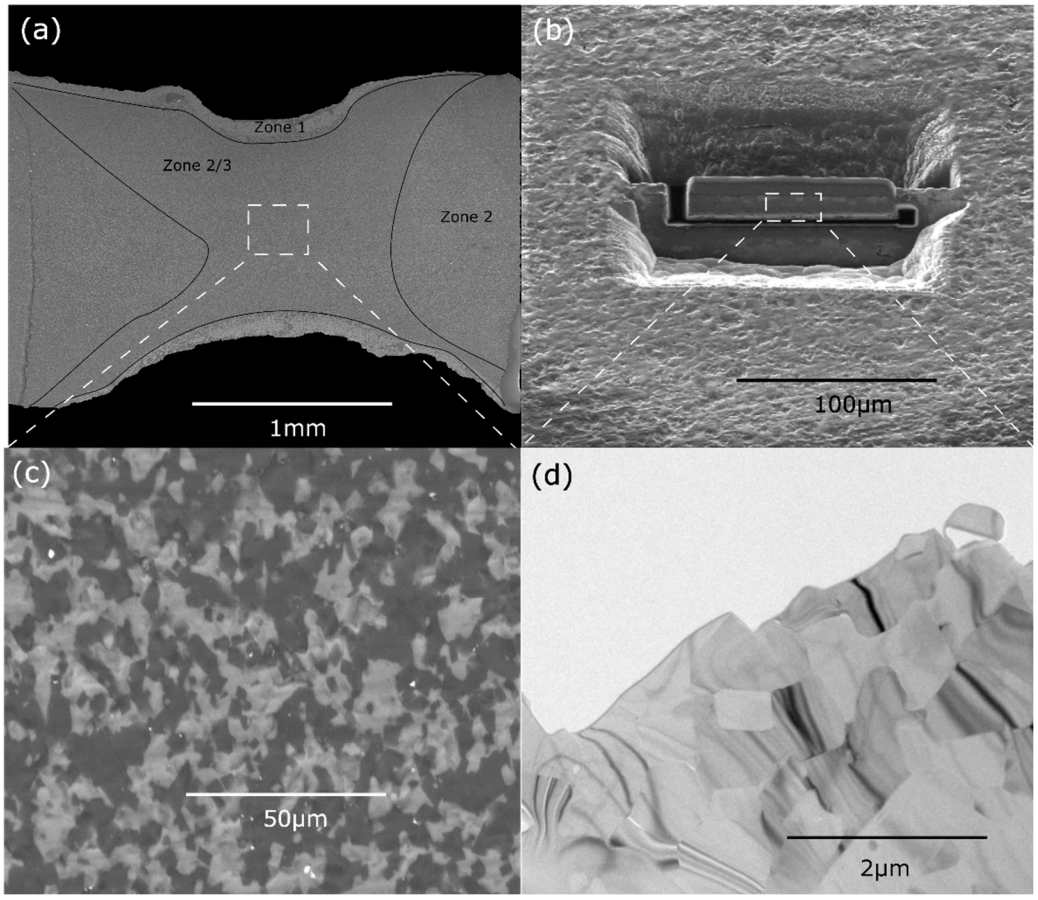

Figure 6.10 SEM and TEM micrographs of SiC 50 wt% B_4C sample CFSed for 3s: (a) low magnification micrograph showing all zones, (b) high magnification micrograph of zone2/3 being prepared by FIB for TEM. (c) High magnification SEM micrograph of zone 2/3 (d) TEM micrograph of foil prepared in (b).

If the material was allowed to reach equilibrium it would have suffered increased segregation, eventually becoming more like materials processed in more traditional conditions, such as those reported by Lankau et al[177]. They produced SiC - 40% volume B_4C composites with 98% relative density by sintering the material in argon at 2150°C for 75 minutes. The resulting SiC grain size ranged from 2 to 5µm. In this study, the initial average particle size of the starting powder was 0.7 and 0.5µm for SiC and B_4C respectively (according to manufacturer's

specification). For the sample CFSed for 3s the grain sizes, estimated using the method developed by Wurst and Nelson[178], were 1.1μm for SiC and 1.4μm for B_4C (Figure 6.9 (d)). The reduced grain growth of the SiC compared to B_4C can be attributed to the constraining grain growth effect of the matrix. In comparison with pressureless sintered samples[177] the finer SiC grain size of samples CFSed for 3s (Zone 2/3) can be explained by the very short processing time.

6.3.3.3 Electrical Data

Electrical data from the samples processed by CFS for 2, 3, 4 and 5s (those discussed above) are shown in Figure 6.11 (a-d). For all of the samples the arcs were stable (i.e. no current oscillations or cut offs) and there was no obvious trend in current or voltage over time. There was minimal incubation time, when the voltage was applied the current suddenly increased within 1s. The lack of an incubation period implies that the preheating provided by the arc electrodes was sufficient to heat the sample above the thermal runaway temperature. The times given are for the intended times, however, the actually time of applied current was slightly variable due to the delay in arc ignition and in the control equipment.

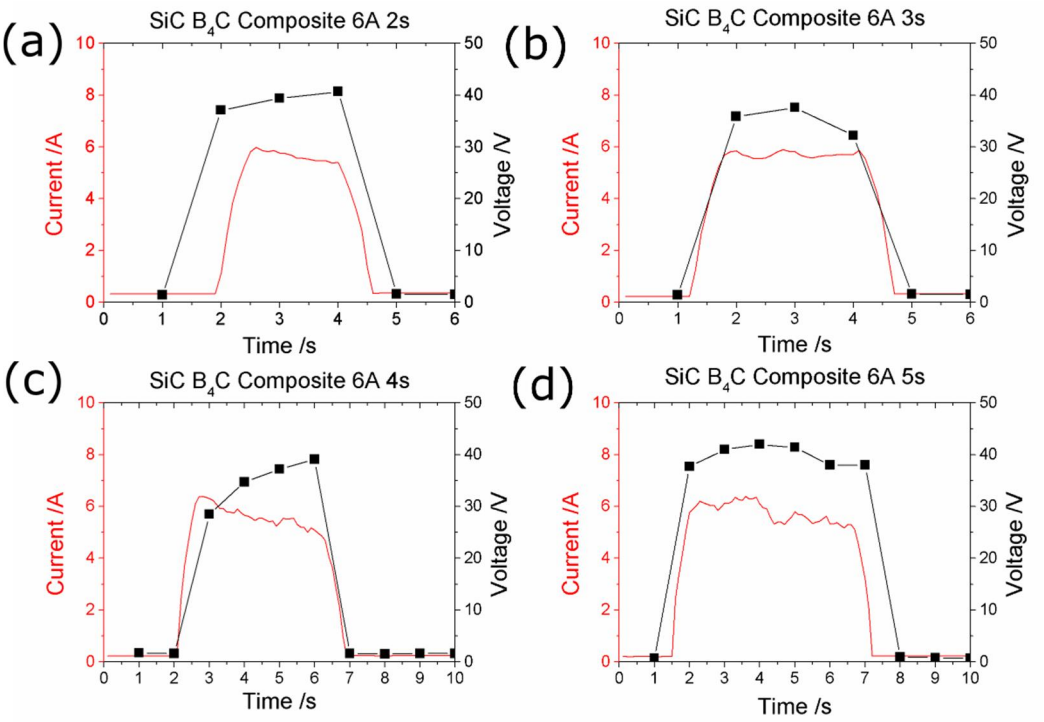

Figure 6.11 Comparison of the current and voltage over time for samples SiC 50 wt% B_4C contactless flash sintered at 6A for; (a) 2s: (b) 3s: (c) 4s; and (d) 5s

6.3.3.4 Temperature Estimation

As in most flash experiments the actual sample temperature is unknown and there are likely significant gradients inside the sample. This lack of data is due to the extreme difficulty in measuring samples where there is a combination of high temperatures, rapid heating and small sample sizes. Another practical issue is the surface is often occluded or unrepresentative limiting non-contact temperature measurement methods. However, an educated guess can be made from microstructural evidence. The temperature in the bulk of the sample (Zone2/3) CFSed for 3s was most likely in the range of 2100-2300°C. For this estimation,

the lower temperature limit of 2100°C comes from the fact that it is difficult to achieve dense materials in pressure less conditions below this temperature. Similarly if the region was above 2300°C the material should have shown evidence of the formation of eutectic phases. Eutectic phases were seen in Zone 1 (Figure 6.9 (b)), but not in Zone2/3 (Figure 6.9 (c)). As a result of this estimation, the Zone 2/3 was heated from 1400°C (preheating temperature) to 2100-2300°C in 3 seconds. This corresponded to a heating rate between 14000 and 18000°C/min. This extreme heating rate is likely linked to the very rapid densification

6.3.3.5 Low Current SiC:B_4C

Now we have a clear understanding of the process for the SiC:B_4C composite at 6A we can compare this behaviour to that at a lower current of 3A. By reducing the current one might expect the process would be slower and so more easily controlled. However, the actual process is much more complicated as can be seen from the microstructures in Figure 6.12.

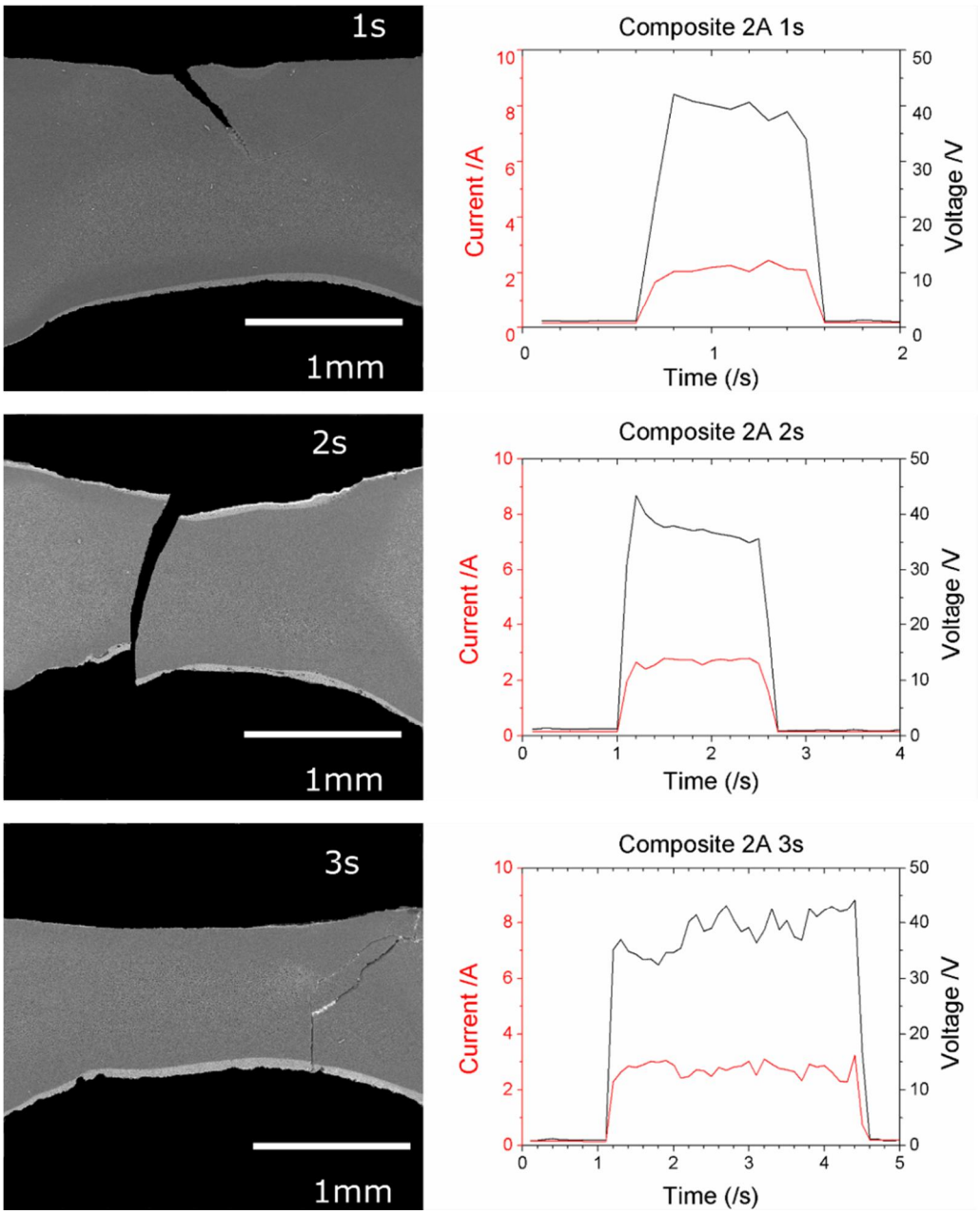

Figure 6.12 Micrographs and electrical data for CFS composite material at a lower current (3A) for a variety of times showing the progression of the process

The reduction in thickness seen in Figure 6.12 is less rapid than in samples prepared at higher currents, as might be expected since a lower current means a lower temperature. However, the sample never achieved full density, and only zone 2 densified, and as time increased the pores in zone 3 actually grew in size. This can be seen more clearly in the high magnification images in Figure 6.13. This is hypothesized to be due to the different temperature gradient produced with a lower current. Due to the lower current there is less internal Joule heating and this lead to the sample mostly heating from the surfaces. If a dense crust formed that would seal in the porosity in the 3rd zone, which would explain why it did not densify even at the longest time sintering time 3s (actually 3.5s).

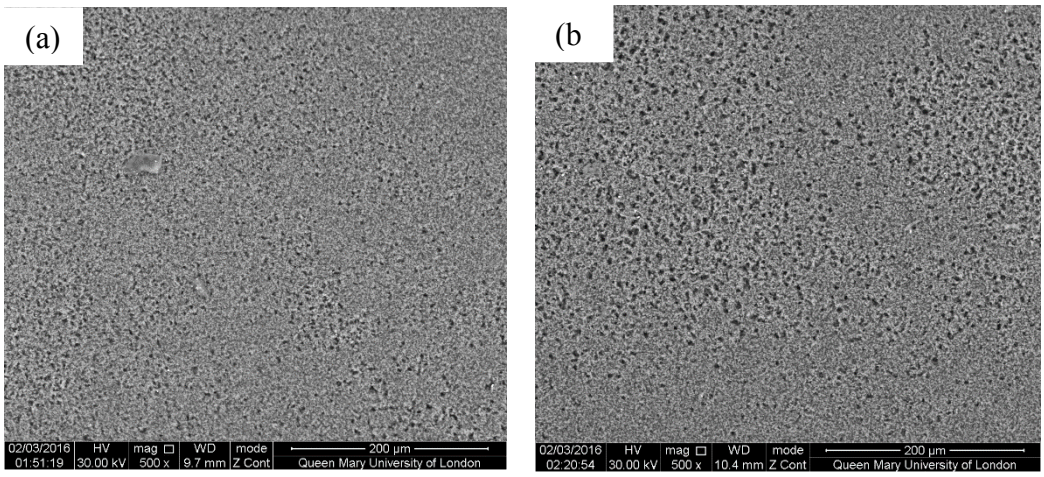

Figure 6.13 High magnification micrographs of zone 3/2 in composite processed at (a) 2s and (b) 3s showing growth of large pores at longer times

6.3.4 Pure B_4C

6.3.4.1 Microstructure

Pure B_4C is normally sintered at higher temperature than the composite as it does not form a liquid phase (melting point of B_4C is ≈2450°C). Given this, one might expect the conditions required for CFS to be much harsher than for the composite. However, due to the unusual nature of arcs resistance, as mentioned earlier, the actual conditions used were the mildest of the materials trialled. From the microstructures shown in Figure 6.14, it is obvious that the material is very sensitive to time. Two seconds produced the best microstructure, 1s being too short to produce even modest densification and 3s producing bubbles from overheating in zone 3. Also, it is worth noting the absence of a zone 1, which was very clear in the composite. This is likely due to the increased stability of the surface phase. In the composite, zone 1 is obviously discoloured in the micrograph, due to preferential SiC evaporation leading to a B_4C rich zone (Figure 6.9(b)). This did not happen with pure B_4C as the pure material has a higher melting point, and the surface was not melted by the arcs, making zone 1 and 2 the same. Due to the rapid processing, just an extra half a second of current induced bubbles. The sintered region was also smaller. This might explain how a higher temperature material sintered faster at a similar power to the composite, because it had a higher effective power density.

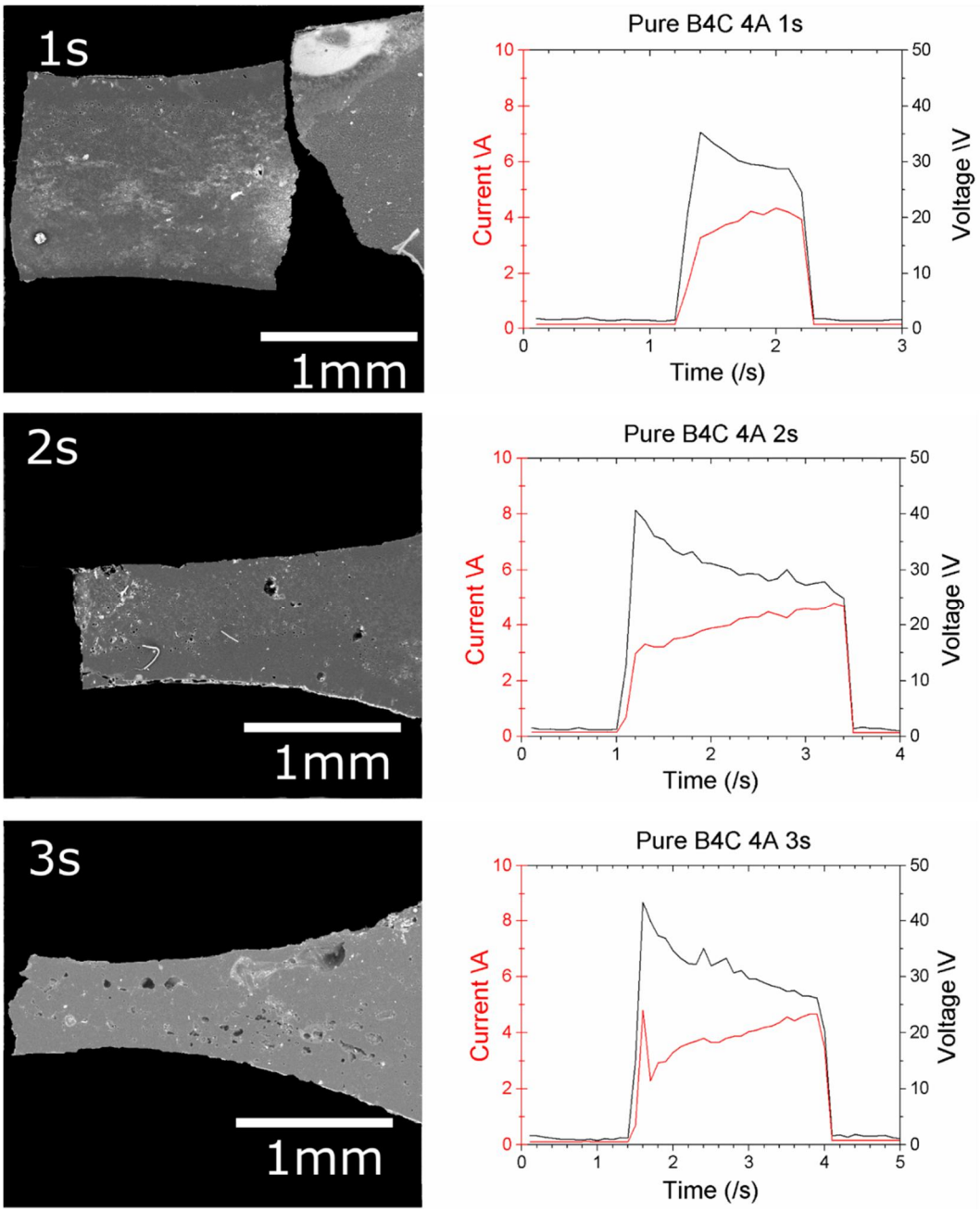

Figure 6.14 Cross section SEM micrographs and electrical data for pure B_4C showing the progression of the sintering process.

The B_4C samples showed significantly different microstructure compared to the composite material, with spherical pores were visible at both low and high

magnification. Using the FIB to etch the polished samples in Figure 6.15 revealed much greater grain growth than the composite. The reduced grain growth in the composite is likely due to the second phase acting as a barrier to grain growth.

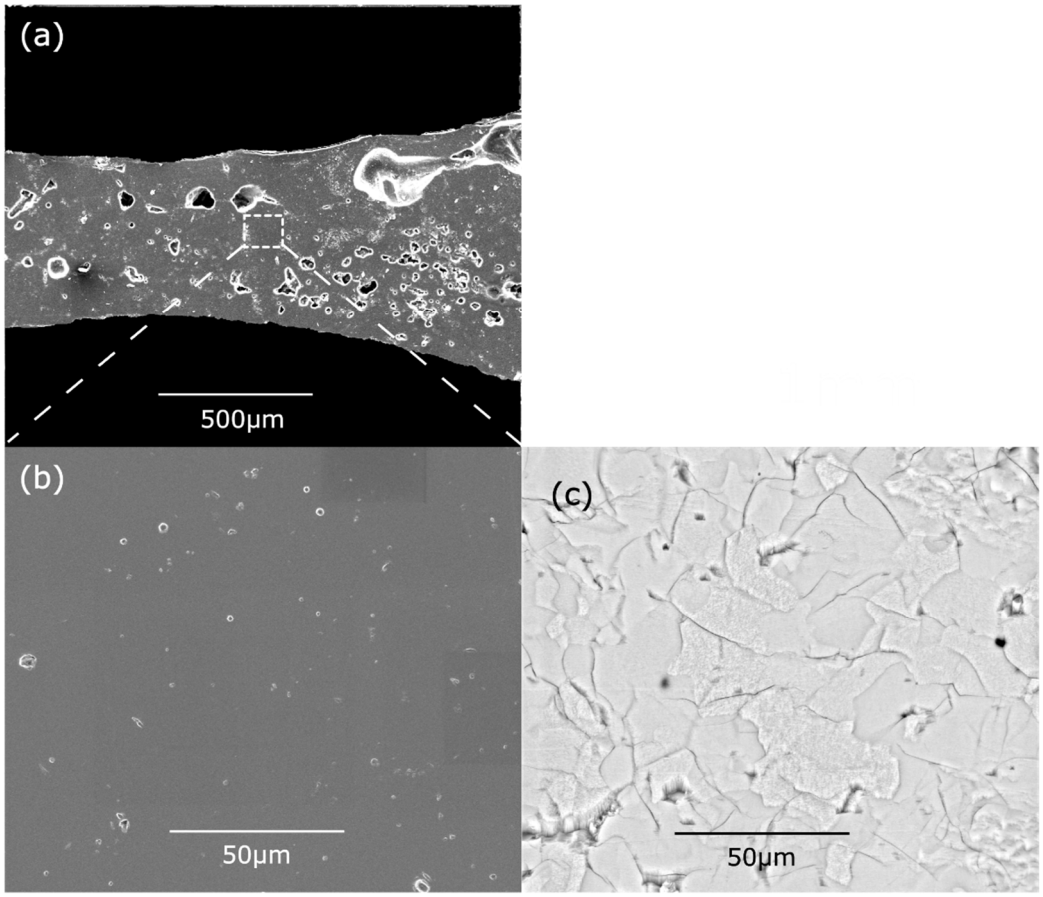

Figure 6.15 SEM micrographs of the pure B4C sample after 3s of CFSing: (a) Low magnification SEM micrograph, (b) high magnification micrograph of a relatively dense region, (c) the region shown in (b) after light etching using a FIB.

6.3.4.2 Electrical Data

A possible explanation for the more focused sintering might be found in the

electrical properties of B_4C, particularly the gradient of the temperature vs. electrical resistivity curve. A steeper curve (higher temperatures significantly increase conductivity) should tend to cause the current to focus as the sample heats up. However, in this particular situation some interesting behaviour occurs. One might expect that if the conductivity of a sample increases it would heat up more, the same voltage and lower resistance means more power. The actual behaviour depends on the setting in the power supply. For a given voltage and current limit there is only one resistance that optimises the maximum heating, if the resistance is higher or lower less power is applied. So the effect of a change in resistance (due to temperature or other) depends on whether the PSU was in current or voltage limit mode. Considering the nonlinear arcs in series with the sample this situation is even more complicated.

Looking at the literature data for electrical behaviour for SiC B_4C and composites[179 180] is not particularly helpful as semiconductors like SiC and B_4C are heavily dependent on doping. Literature values can easily differ by an order of magnitude or more depending on the degree of doping (accidental or intentional).

While the resistance of the CFS system (sample with preheating arcs in series) is not a reliable indicator of the resistance of the sample some useful information can still be extracted. Despite the difficulty of measuring the temperature, the general trend is higher temperate means lower resistance. The power supply is like a constant current source, this is not perfect approximation, but the PSU is definitely not a constant voltage. This means that the current will tend to focus

into the centre region at the expense of the periphery. Once the centre is heated it has less resistance so current concentrates there, the PSU is in constant current mode, so the total current stays the same. This should result in the sintering process slowing at the edge of the sample as it progresses. The fact that the measured power remains relatively constant implies that the arcs are compensating for the drop in sample resistance, so surface heating should increase.

6.3.4.3 Incubation Period

Given the interesting electrical properties of the pure B_4C, a brief investigation was made into the preheating of the sample. For all of the samples discussed so far, when the flash voltage was applied the current immediately jumped to the set limit. This is in contrast to conventional flash sintering, which normally shows a significant delay between the application of the voltage and any significant current flow. In traditional flash sintering this behaviour has been explained by the small current flowing initially slowly heating the sample until it becomes significantly conductive i.e. thermal runaway. Recent work has shown the amount of incubation time is related to the sample temperature before applying the flash voltage[8]. To investigate this behaviour and to verify that both the contactless flash sintering setup and ceramic showed normal flash sintering behaviour, the setup was modified. To increase incubation time (so it is visible) the preheating temperature had to be reduced. For this, the separation between the preheating arcs and the sample was increased, the distance between the electrodes was

increased to 16mm. With this arrangement the sample should have reached a lower stable temperature before the CFS power was applied. The exact temperature reached could not be verified as the measured value was very sensitive to thermocouple placement, and the thermocouple itself altered the temperature. This change also made the flash sintering very unreliable with most of the samples failing to flash.

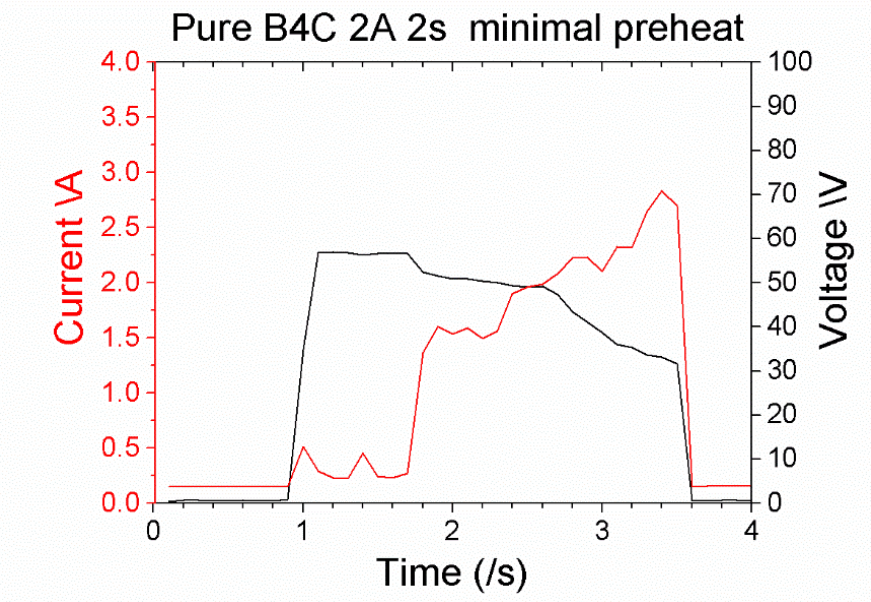

Figure 6.16 Electrical data for low preheating pure B_4C, showing incubation time

By increasing the separation distance to 16mm an incubation period of 0.4s was visible in Figure 6.16. However a power spike was not visible. A spike in applied power is normally seen during the transition from a voltage to a current limit and is associated with an incubation period. Even though the voltage dropped slightly once the current stared flowing it was not as dramatic as seen in traditional flash

sintering[161]. This can be explained by the arc being in series with the sample and its resistance is likely to dominate the behaviour of the system. From this result it can be surmise that for all the other experiments (performed with 14mm separation) the preheating temperature was well above the flash sintering threshold (for the applied voltage).

6.3.5 **Pure SiC**

Of the materials trialled, SiC proved to be the most challenging to CFS, and despite our best efforts refused to sinter. Perhaps that is to be expected, as even advanced processes like flash and FSPS require substantial pressure to achieve full density SiC [6,181]. CFS is by its nature pressureless so even with the rapid heating rate is unlikely to sinter SiC.

From the sequence shown in Figure 6.17, it is obvious that very little densification of SiC took place, as the sample did not thin. Closer inspection showed that the SiC merely sublimed and redeposited much like during pressureless recrystallization of SiC. This is a commercial process used to strengthen SiC parts without altering their dimensions. From Figure 6.17 the sequence of events can be reconstructed. As the sample heated up, SiC from the surface started to sublime forming larger pores and an open cell structure in zone 2. When the power was cut the surface cooled and SiC re condensed on the surface leaving a dense coating in zone 1. For longer processing times the sample heated up hot enough for sublimation to occur rapidly in the entire thickness of the sample[176]. Then material

was lost to the surroundings as there was no cool region for SiC to redeposit and this lead to a thinning of the sample as seen in the 10s sample. The electrical data shows no obvious trends for voltage or current implying the arcs and sample resistance were both stable.

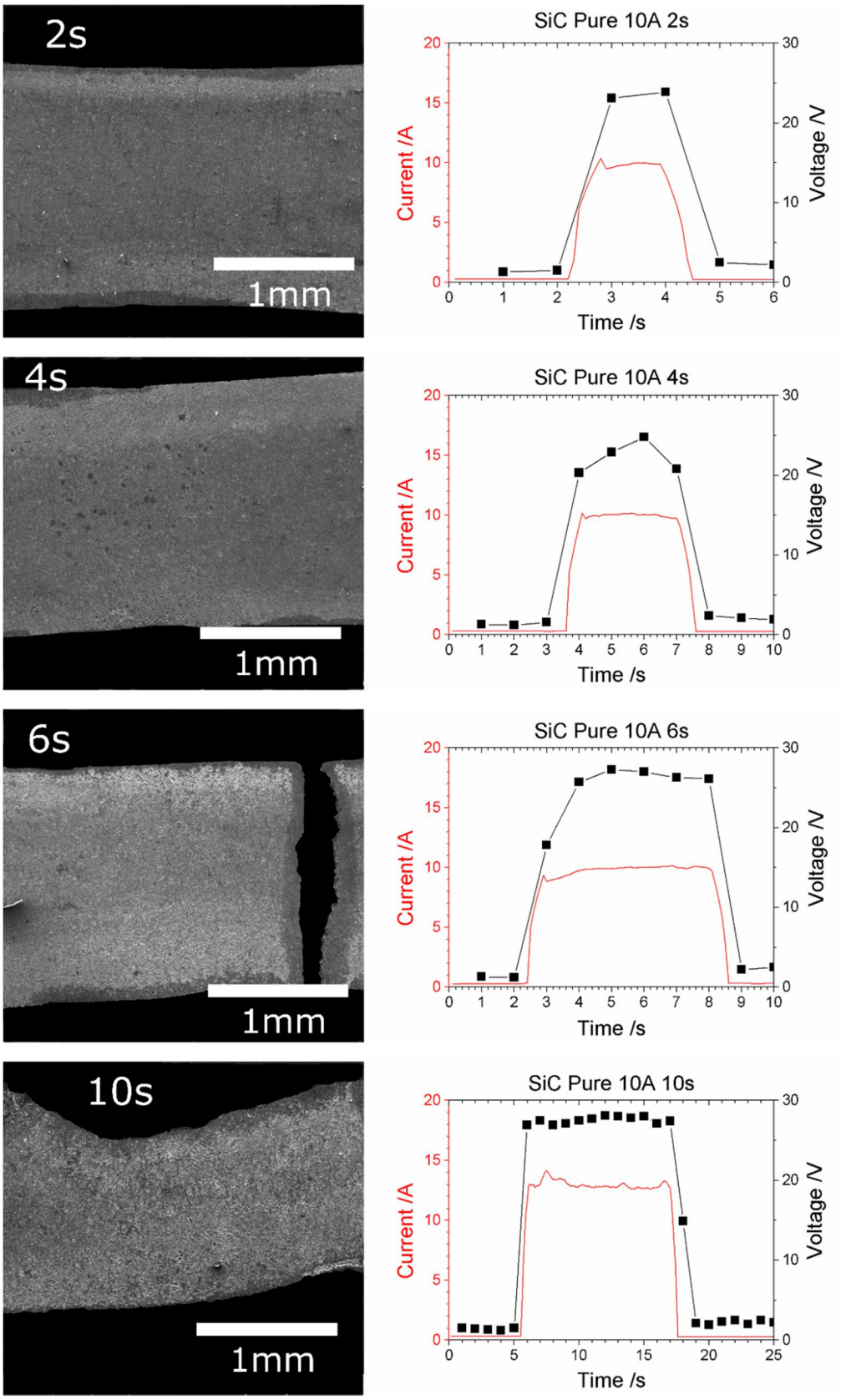

Figure 6.17 Cross section micrographs and electrical data for pure SiC at various times

6.4 Conclusion

This work demonstrates for the first time that contactless flash sintering is possible. The absence of contacts provides great versatility to the FS process. It makes it possible to achieve continuous sintering, where the sample is set in relative motion with respect to plasma electrodes. Removing the need for electrodes also removes a process step, the application and removal of electrodes. The preheating of the arcs also does away with the need for a separate preheating furnace, which further streamlines the whole flash sintering process.

The proposed methodology can be applied to flash sinter various refractory materials, within a certain range of electrical resistivity. Guidance for the selection of suitable plasma type was developed from earlier work in the field (plasma temperatures, plasma conductivities and maximum currents etc.). The most promising result was found starting from a SiC 50%wt B_4C block with initial relative density of 65%. Contactless flash sintering produced a fully dense cylindrical region with a volume of $14mm^3$ in a discharge time of 3s with a current of 6A. Due to the particulars of experimental setup, the only value that can be used in comparison with the literature is the current density. This was calculated by taking the diameter of the sintered region and the flash sintering current. The current density was $0.6A/mm^2$ for pure SiC (recrystallized microstructure), $0.3A/mm^2$ for SiC B_4C (fully dense) and $0.32A/mm^2$ for pure B_4C (nearly full density). A rough estimate of the heating rate was in the order of 14000-18000°C/min, which is even higher than those reported for flash sintering[8,182].

Unsurprisingly with such high power densities the microstructure was found to be very dependent on the discharge time.

Chapter 7. Summary and Future Work

7.1 Summary

This work has focused on understanding the effects of passing an electric current through ceramics and the resulting changes at the microstructural level. This was with the hope of finding new ways to exploit these ECE phenomena. Electrical current is passed through ceramics in various industrial process as surveyed in Chapter 2. Various ECE have been proposed as explanations for the differing behaviour in these processes. Plasma and electromigration/electrochemistry were found to be the most clear cut examples of ECEs and can drastically alter a material's processing e.g. EDM and Anodic bonding. However there are lots of processes that were not designed to exploit a particular ECE and in many of these processes the actual contribution of current is likely to be just Joule heating. To further develop the field of ECEs in ceramics it is important to be able to isolate and verify a particular ECE's contribution / existence. For electromigration / electrochemistry the prerequisite is that the material is an ionic conductor at the processing conditions. This can usually be found in literature or experimentally by impedance spectroscopy. For electrochemical changes the voltage must exceed the standard electrode potential of the reaction (which can be found in literate). The situation with plasma contributions is much more complicated and was the focus of Chapter 4.

In Chapter 4 the main value was not in proving that there is no plasma in SPS, as

there was already significant evidence of this. Instead it laid in creating more general guidelines to the conditions required for plasma ignition and stability. This was possible by drawing parallels with arcing electrical contacts, which already exists a wealth of experimental data and usable models. Plasma is an inherently complex material and is not often studied by material scientists, but it is often proposed as a possible explanation for abnormal results. This work helps to rule out some of these spurious claims. Some useful guidelines are that the breakdown of gas between particles cannot occur below 100V no matter the pressure or how close the particles are (except in truly abnormal situations). Arcing or any other plasma is very unlikely to occur below 10V, between 10-20V it is dependent on the material being processed. Glow discharge is unlikely to occur at atmospheric pressure with dc (unless a special electrode geometry or PSU is used).

Experiments were done to verify plasma formation in powder compacts as this is the case in the early stages of all sintering techniques. Due to the requirement for <10V to be applied across a contact the actual voltage required to form plasma in a powder was found to be much higher (50V). This was because there was significant voltage drop through the powder compact. Contact pressure was also found to play an important role. To apply 50V across a powder compact the current required is proportion to the resistance of the powder which is a function of contact pressure. To minimise Joule heating low compression pressure was used to give a high resistance compact.

Optical spectroscopy was also found to be an excellent tool to investigate plasma emission as it easily separates black body radiation from plasma emission.

Spectroscopy also allows characterisation of the materials constituting the arc. In this case the powder material was clearly ionized in the arc and there were signs that surface contaminates were also vaporised. Fibre optic probes also allow in situ data collection, making them an excellent tool to experimentally verify the existence of plasma in practically any experimental equipment.

As mentioned earlier electromigration/electrochemistry and plasma were identified as having the greatest potential to alter materials and so experiments were designed to exploit both of these effects to produce novel processing techniques.

In Chapter 5 electromigration was exploited to alter the oxidation rate of zirconium diboride. However, the technique is potentially applicable to a vast array of materials. The technique exploits the oxygen pumping capabilities of oxide ceramics (zirconia in this case) to pump oxygen away from the oxidizing surface. This is of particular significance for UHTCs as it offers a way to increase the operating temperature of materials in air beyond the limit of conventional oxide scales. This is vital for UHTCs as the there are no oxide scales that function as effective oxygen barriers above 2000°C. In this work diboride was heated to 1200°C to produce a thin (120μm) oxide layer to avoid shorting the PSU. This was then heated at 1400°C for 5hrs, without an applied field this resulted in a 360μm scale growing. However if 10V 100mA was applied (through platinum electrodes on the surface) during oxidation the oxide only grew to 150μm, a significant reduction. This technique has some drawbacks not least the need for platinum electrodes on the surface.

With the earlier work done on understanding plasma and the increasing academic and commercial interest in flash sintering (a possible electromigration phenomena) an attempt was made to merge these interests. This was achieved by construct a CFS setup using plasma as the electrodes. The CFS setup was constructed using two plasma electrodes (made from TIG welding torches) each with their own ac power supply. A third flash power supply was connected between the two electrodes. The arc electrodes heated the porous sample (1.8mm thick 65% dense) up to 1400°C in 5s at which point the samples became sufficiently conductive and the flash power supply was switched on. Various materials were tested but reasonable results were only found using refractory ceramics as otherwise the arcs melted/sublimed the samples. SiC, B_4C and SiC:B_4C 50:50 were all sintered using this CFS setup. However, the SiC did not sinter, but just sublimed forming recrystallized SiC, even after 10s at 10A (0.6A/mm^2). B_4C produced significant densification with the best results were seen with 4A for 2s (0.32A/mm^2). The most impressive sample was the SiC:B_4C composite, which achieved 14mm^3 of fully dense material in 3s with 6A (0.3A/mm^2). There was limited grain growth and no segregation. This was a world first for flash sintering and has the potential to create continuous sintering of ceramics.

Taken together this work shows the untapped potential for ECEs in ceramic processing to go from being an academic curiosity to an exploitable foundation for developing new and novel processing techniques.

7.2 Future Work

With the result of this work and other publications on the topic, the question of plasma in SPS is generally considered closed. However, the same technique used in this work could be used to investigate the case of plasma in other ECAS processes. Capacitor discharge is a very likely candidate for plasma formation as the high voltages and currents make the formation of plasmas much more likely. While spectroscopy can confirm the existence of plasma and even give some properties about it (temperature and composition) that alone does not give a full picture. Significant work would be needed to understand how the plasma might interact with the sintering process. In fact plasma might actually be a hindrance as it is likely to lead to inhomogeneity in the sample.

The work on reducing the rate of oxidation in zirconium diboride (Chapter 5) had some significant issues that will likely prevent this technique from being used in practice. The need for a surface electrode being the prime one, as for high temperatures platinum is the best choice. While the possibility of using HF and exotic waveforms/PSUs to overcome this was proposed, it was ultimately considered unfeasible. The effect on oxidation is just one example of how electromigration can be exploited in unexpected ways. For example electromigration could potentially be used in the field of electroceramics to modify defect structures in functional ceramics.

Flash sintering shows the most promise for development as there is clear academic interest in flash sintering (given the constant stream of publications) and

commercial interest with lucideon's pilot plant. While the experimental setup developed in Chapter 6 showed significant success, it could only process a limited amount of material in one go. There were also significant issues with material compatibility and the arc electrodes. However, these are all issues that could be improved with a more refined experimental setup. As discussed in Chapter 6.2 there are many way to produce plasma and for sintering different materials different plasma could be used. If lower current/ higher voltages were used, e.g. to sintering more resistive materials like zirconia, then glow discharge would be a better choice. It would also provide a way to achieve densification over the entire surface, but this would likely require a low pressure chamber. A simpler way to increases the utility of the CFS process would be to develop some kind of X-Y stage to move the samples through the plasma electrodes. This would allow sintering of larger parts and possibly in a continuous fashion. It would also be of academic interest to develop some way to measure the temperature of the sample during processing, but this has proven difficult with conventional flash sintering. The only techniques used successfully are from modelling or the use of in situ XRD to detect the associated lattice thermal expansion.

In summary, there are many ECEs that could be exploited to produce novel and unique processing techniques, and the groundwork to understand them has already been laid. The interest in flash sintering has massively increased the work being done to understanding at every level what happens inside a ceramic as it passes electric current. One can only hope that this will lead to new or improved ceramics processing methods.

Chapter 8. List of Publications

Publications

Saunders, T., Grasso, S. & Reece, M. J. Plasma formation during electric discharge (50V) through conductive powder compacts. *Journal of the European Ceramic Society* **35**, 871-877 (2015).

Saunders, T., Grasso, S. & Reece, M. J. Limiting oxidation of ZrB 2 by application of an electric field across its oxide scale. *Journal of Alloys and Compounds* **653**, 629-635 (2015).

Saunders, T., Grasso, S. & Reece, M. J. Ultrafast-Contactless Flash Sintering using Plasma Electrodes. *Scientific reports* **6**, 27222 (2016).

Collaborations

Viola, G. *et al.* Contribution of piezoelectric effect, electrostriction and ferroelectric/ferroelastic switching to strain-electric field response of dielectrics. *Journal of Advanced Dielectrics* **3**, 1350007 (2013).

Grasso, S. *et al.* Flash spark plasma sintering (FSPS) of pure ZrB_2. *Journal of the American Ceramic Society* **97**, 2405-2408 (2014).

Grasso, S., Saunders, T., Porwal, H. & Reece, M. Ultra-high temperature spark Plasma sintering of α-SiC. *Ceramics International* **41**, 225-230 (2015).

Grasso, S. *et al.* Ultra-Rapid Crystal Growth of Textured SiC Using Flash Spark Plasma Sintering Route. *Crystal Growth & Design* **16**, 2317-2321 (2016).

Grasso, S. *et al.* Flash Spark Plasma Sintering (FSPS) of α and β SiC. *Journal of the American Ceramic Society* (2016).

Porwal, H. *et al.* Effect of lateral size of graphene nano-sheets on the mechanical properties and machinability of alumina nano-composites. *Ceramics International* **42**, 7533-7542 (2016).

Picot, Olivier T. *et al*. Using graphene networks to build bioinspired self-monitoring ceramics. *Nature Communications* 8 (2017): 14425.

Yu, Min, *et al.* "Review of flash sintering: materials, mechanisms and modelling." *Advances in Applied Ceramics* 116.1 (2017): 24-60.

Chapter 9. References

1 Cologna, M., Rashkova, B. & Raj, R. Flash Sintering of Nanograin Zirconia in< 5 s at 850 C. *Journal of the American Ceramic Society* **93**, 3556-3559 (2010).

2 Niu, B. *et al.* Ultra-fast densification of boron carbide by flash spark plasma sintering. *Scripta Materialia* **116**, 127-130 (2016).

3 Cologna, M., Francis, J. S. & Raj, R. Field assisted and flash sintering of alumina and its relationship to conductivity and MgO-doping. *Journal of the European Ceramic Society* **31**, 2827-2837 (2011).

4 Das, D. *et al.* Solution sol–gel processing and investigation of percolation threshold in La 2/3 Ca 1/3 MnO 3: xSiO 2 nanocomposite. *Journal of Magnetism and Magnetic Materials* **238**, 178-184 (2002).

5 Jiang, T. *et al.* An improved direct current sintering technique for proton conductor–BaZr 0.1 Ce 0.7 Y 0.1 Yb 0.1 O 3: The effect of direct current on sintering process. *Journal of Power Sources* **248**, 70-76 (2014).

6 Zapata-Solvas, E., Bonilla, S., Wilshaw, P. & Todd, R. Preliminary investigation of flash sintering of SiC. *Journal of the European Ceramic Society* **33**, 2811-2816 (2013).

7 da Silva, J. G. P., Al-Qureshi, H. A., Keil, F. & Janssen, R. A dynamic bifurcation criterion for thermal runaway during the flash sintering of ceramics. *Journal of the European Ceramic Society* (2015).

8 Todd, R., Zapata-Solvas, E., Bonilla, R., Sneddon, T. & Wilshaw, P. Electrical characteristics of flash sintering: thermal runaway of Joule heating. *Journal of the European Ceramic Society* **35**, 1865-1877 (2015).

9 Todd, R. in *Proceedings of the IV Advanced Ceramics and Applications Conference.* 1-12 (Springer).

10 Yu, M., Grasso, S., Mckinnon, R., Saunders, T. & Reece, M. J. Review of flash sintering: materials, mechanisms and modelling. *Advances in Applied Ceramics* **116**, 24-60 (2017).

11 Dancer, C. Flash sintering of ceramic materials. *Materials Research Express* **3**, 102001 (2016).

12 Chaim, R. Particle Surface Softening as Universal Behaviour during Flash Sintering of Oxide Nano-Powders. *Materials* **10**, 179 (2017).

13 McLaren, C., Heffner, W., Tessarollo, R., Raj, R. & Jain, H. Electric field-induced softening of alkali silicate glasses. *Applied Physics Letters* **107**, 184101 (2015).

14 Terauds, K. *et al.* Electroluminescence and the measurement of temperature during Stage III of flash sintering experiments. *Journal of the European Ceramic Society* **35**, 3195-3199 (2015).

15 Biesuz, M. *Flash Sintering of Alumina-based Ceramics*, University of Trento, (2017).

16 Caliman, L. B., Bouchet, R., Gouvea, D., Soudant, P. & Steil, M. C. Flash sintering of ionic conductors: The need of a reversible electrochemical reaction. *Journal of the European Ceramic Society* **36**, 1253-1260 (2016).

17 Anselmi-Tamburini, U., Gennari, S., Garay, J. & Munir, Z. A. Fundamental

investigations on the spark plasma sintering/synthesis process: II. Modeling of current and temperature distributions. *Materials Science and Engineering: A* **394**, 139-148 (2005).

18 Grasso, S., Sakka, Y. & Maizza, G. Pressure effects on temperature distribution during spark plasma sintering with graphite sample. *Materials transactions* **50**, 2111-2114 (2009).

19 Hulbert, D. M. *et al.* The absence of plasma in "spark plasma sintering". *Journal of Applied Physics* **104**, 033305 (2008).

20 Yanagisawa, O., Kuramoto, H., Matsugi, K. & Komatsu, M. Observation of particle behavior in copper powder compact during pulsed electric discharge. *Materials Science and Engineering: A* **350**, 184-189 (2003).

21 Chu, M. Y., Rahaman, M. N., Jonghe, L. C. & Brook, R. J. Effect of heating rate on sintering and coarsening. *Journal of the American Ceramic Society* **74**, 1217-1225 (1991).

22 Gould, J. An examination of nugget development during spot-welding, using both experimental and analytical techniques. *Welding journal* **66**, S1-S10 (1987).

23 Walker, I. & Moss, C. Spot welder for making small electrical contacts. *Review of scientific instruments* **69**, 2747-2756 (1998).

24 Jeong, H., Cho, J., Lee, N. K. & Park, H. in *Materials science forum.* 142-145 (Trans Tech Publ).

25 Bunget, C., Salandro, W., Mears, L. & Roth, J. T. Energy-based modeling of an electrically-assisted forging process. *Trans. North Am. Manuf. Res. Inst. SME* **38**, 647-654 (2010).

26 Yao, K.-F., Wang, J., Zheng, M., Yu, P. & Zhang, H. A research on electroplastic effects in wire-drawing process of an austenitic stainless steel. *Scripta materialia* **45**, 533-539 (2001).

27 Jameson, E. C. *Electrical discharge machining*. (Society of Manufacturing Engineers, 2001).

28 Descoeudres, A., Hollenstein, C., Demellayer, R. & Wälder, G. Optical emission spectroscopy of electrical discharge machining plasma. *Journal of materials processing technology* **149**, 184-190 (2004).

29 Lee, S. H. & Li, X. Study of the surface integrity of the machined workpiece in the EDM of tungsten carbide. *Journal of materials processing technology* **139**, 315-321 (2003).

30 Johnson, R. N. & Sheldon, G. Advances in the electrospark deposition coating process. *Journal of Vacuum Science & Technology A* **4**, 2740-2746 (1986).

31 Sarathi, R., Sindhu, T. & Chakravarthy, S. Generation of nano aluminium powder through wire explosion process and its characterization. *Materials Characterization* **58**, 148-155 (2007).

32 Sindhu, T., Sarathi, R. & Chakravarthy, S. R. Understanding nanoparticle formation by a wire explosion process through experimental and modelling studies. *Nanotechnology* **19**, 025703 (2007).

33 Quigley, M., Richards, P., Swift-Hook, D. & Gick, A. Heat flow to the workpiece from a TIG welding arc. *Journal of Physics D: Applied Physics* **6**, 2250 (1973).

34 Zhu, J., Xiong, Z.-Y. & Li, X.-X. Research on the cathode cleaning area in

aluminum alloy AC TIG welding based on visual image processing. *Dianhanji/ Electric Welding Machine* **42**, 26-30 (2012).

35 Mimura, K., Lee, S.-W. & Isshiki, M. Removal of alloying elements from zirconium alloys by hydrogen plasma-arc melting. *Journal of alloys and compounds* **221**, 267-273 (1995).

36 Schmidt-Ott, K. in *Metal 04: proceedings of the international conference on metals conservation, Canberra, Australia, 4-8 October 2004.* 235-246, ill. (National Museum of Australia).

37 Palmer, R., Doan, T., Lloyd, P., Jarvis, B. & Ahmed, N. Reduction of TiO2 with hydrogen plasma. *Plasma chemistry and plasma processing* **22**, 335-350 (2002).

38 Schmidt, B. *et al.* In situ investigation of ion drift processes in glass during anodic bonding. *Sensors and Actuators A: Physical* **67**, 191-198 (1998).

39 Mantell, C. Economic Importance of the Electrochemical Industries. *Transactions of The Electrochemical Society* **62**, 15-25 (1932).

40 Mohandas, K. & Fray, D. FFC Cambridge process and removal of oxygen from metal-oxygen systems by molten salt electrolysis: an overview. *Trans. Indian Inst. Met* **57**, 579-592 (2004).

41 Wang, J. *Analytical electrochemistry*. (John Wiley & Sons, 2006).

42 Wu, J. *et al.* Diagnostic tools in PEM fuel cell research: Part I Electrochemical techniques. *International journal of hydrogen energy* **33**, 1735-1746 (2008).

43 Wroughton, D., Okress, E., Brace, P., Comenetz, G. & Kelly, J. A technique for eliminating crucibles in heating and melting of metals. *Journal of the Electrochemical Society* **99**, 205-211 (1952).

44 Hömberg, D. A mathematical model for induction hardening including mechanical effects. *Nonlinear Analysis: Real World Applications* **5**, 55-90 (2004).

45 Fujitsu, S., Ikegami, M. & Hayashi, T. Sintering of partially stabilized zirconia by microwave heating using ZnO–MnO2–Al2O3 plates in a domestic microwave oven. *Journal of the American Ceramic Society* **83**, 2085-2087 (2000).

46 Tian, Y. L. Practices of Ultra Rapid Sintering of Ceramics Using Single Mode Applicators. (DTIC Document, 1992).

47 Zhao, C., Vleugels, J., Groffils, C., Luypaert, P. & Van der Biest, O. Hybrid sintering with a tubular susceptor in a cylindrical single-mode microwave furnace. *Acta materialia* **48**, 3795-3801 (2000).

48 Chen, W., Gutmann, B. & Kappe, C. O. Characterization of Microwave-Induced Electric Discharge Phenomena in Metal–Solvent Mixtures. *ChemistryOpen* **1**, 39-48 (2012).

49 Chatterjee, A., Basak, T. & Ayappa, K. Analysis of microwave sintering of ceramics. *AIChE Journal* **44**, 2302-2311 (1998).

50 Takahashi, H. *et al.* Lead-free barium titanate ceramics with large piezoelectric constant fabricated by microwave sintering. *Japanese journal of applied physics* **45**, L30 (2006).

51 Held, J. S. & Schiffmann, R. F. Container for microwave treatment of surgical instrument with arcing prevention. (1997).

52 Takahashi, H., Numamoto, Y., Tani, J. & Tsurekawa, S. Piezoelectric properties of BaTiO3 ceramics with high performance fabricated by microwave sintering. *Japanese journal of applied physics* **45**, 7405 (2006).

53 Mortensen, A., Andrews, R. M. & Flemings, M. C. Method for producing metal matrix composites using electromagnetic body forces. (1998).

54 Becker, A. *et al.* The effect of Peltier heat during current activated densification. *Applied Physics Letters* **101**, 013113 (2012).

55 Grasso, S., Saunders, T., Porwal, H. & Reece, M. Ultra-high temperature spark plasma sintering of α-SiC. *Ceramics International* **41**, 225-230 (2015).

56 Munir, Z. A. Surface Oxides and Sintering of Metals. *Powder Metallurgy* **24**, 177-180, doi:10.1179/pom.1981.24.4.177 (1981).

57 Kawamura, G. *et al.* Production of Oxidation-Resistant Cu-Based Nanoparticles by Wire Explosion. *Scientific reports* **5** (2015).

58 Dargatz, B. *et al.* FAST/SPS sintering of nanocrystalline zinc oxide—Part I: Enhanced densification and formation of hydrogen-related defects in presence of adsorbed water. *Journal of the European Ceramic Society* **36**, 1207-1220 (2016).

59 Milazzo, G., Caroli, S. & Braun, R. D. Tables of standard electrode potentials. *Journal of The Electrochemical Society* **125**, 261C-261C (1978).

60 Choi, J. S. & Kim, H. G. Influence of stoichiometry and impurity on the sintering behaviour of barium titanate ceramics. *Journal of materials science* **27**, 1285-1290 (1992).

61 Song, X., Liu, X. & Zhang, J. Neck Formation and Self-Adjusting Mechanism of Neck Growth of Conducting Powders in Spark Plasma Sintering. *Journal of the American Ceramic Society* **89**, 494-500 (2006).

62 Lai, W. & Haile, S. M. Impedance spectroscopy as a tool for chemical and electrochemical analysis of mixed conductors: a case study of ceria. *Journal of the American Ceramic Society* **88**, 2979-2997 (2005).

63 Riess, I. Review of the limitation of the Hebb-Wagner polarization method for measuring partial conductivities in mixed ionic electronic conductors. *Solid State Ionics* **91**, 221-232 (1996).

64 Glickstein, S. Temperature measurements in a free burning arc. *Welding Journal* **55**, 222-229 (1976).

65 Leal-Quirós, E. Plasma processing of municipal solid waste. *Brazilian Journal of Physics* **34**, 1587-1593 (2004).

66 Parvulescu, V. I., Magureanu, M. & Lukes, P. *Plasma chemistry and catalysis in gases and liquids*. Chapter 1.3 (John Wiley & Sons, 2012).

67 Berzak, L., Dorfman, S. & Smith, S. Paschen's Law in Air and Noble Gases. (2006).

68 Slade, P. G. *Electrical contacts: principles and applications*. Pg. 565 (CRC Press, 2013).

69 TE Conductivity, Aplication Note on Relay Contact life, http://www.te.com/usa-en/products/relays-contactors-switches/relays/intersection/application-notes.html

70 Wang, P.-C. & Filippi, R. Electromigration threshold in copper interconnects. *Applied Physics Letters* **78**, 3598-3600 (2001).

71 Hu, Y., Lin, Y., Kao, C. & Tu, K. Electromigration failure in flip chip solder joints due to rapid dissolution of copper. *Journal of materials research* **18**, 2544-2548 (2003).

72 Tao, J., Cheung, N. W. & Hu, C. Electromigration characteristics of copper

interconnects. *IEEE Electron Device Letters* **14**, 249-251 (1993).
73 Lodding, A. MEASUREMENTS OF ISOTOPE ELECTROMIGRATION IN METALS. *Journal de Chimie Physique (France) Merged with Rev. Gen. Colloides to form J. Chim. Phys. Rev. Gen. Colloides* **60** (1963).
74 Huntington, H. & Grone, A. Current-induced marker motion in gold wires. *Journal of Physics and Chemistry of Solids* **20**, 76-87 (1961).
75 Bach, H., Baucke, F. K. & Krause, D. *Electrochemistry of glasses and glass melts, including glass electrodes*. (Springer Science & Business Media, 2013).
76 Anderson, O. & Stuart, D. Calculation of activation energy of ionic conductivity in silica glasses by classical methods. *Journal of the American Ceramic Society* **37**, 573-580 (1954).
77 Zoski, C. G. *Handbook of electrochemistry*. (Elsevier, 2006).
78 Okazaki, K., Kagawa, M. & Conrad, H. Additional results on the electroplastic effect in metals. *Scripta Metallurgica* **13**, 277-280 (1979).
79 Mai, J., Peng, L., Lin, Z. & Lai, X. Experimental study of electrical resistivity and flow stress of stainless steel 316L in electroplastic deformation. *Materials Science and Engineering: A* **528**, 3539-3544 (2011).
80 Conrad, H. Thermally activated plastic flow of metals and ceramics with an electric field or current. *Materials Science and Engineering: A* **322**, 100-107 (2002).
81 Molotskii, M. & Fleurov, V. Magnetic effects in electroplasticity of metals. *Physical Review B* **52**, 15829 (1995).
82 Conrad, H. Electroplasticity in metals and ceramics. *Materials Science and Engineering: A* **287**, 276-287 (2000).
83 Kaiser, K. L. *Electromagnetic compatibility handbook*. chapter 5-3 (CRC press, 2004).
84 Rowe, D. M. *CRC handbook of thermoelectrics*. (CRC press, 1995).
85 Trombin, F. & Raj, R. Developing processing maps for implementing flash sintering into manufacture of whiteware ceramics. *Bulletin American Ceramic Society* **93**, 348-354 (2014).
86 Zhang, Z.-H. *et al.* The sintering mechanism in spark plasma sintering–Proof of the occurrence of spark discharge. *Scripta Materialia* **81**, 56-59 (2014).
87 Chen, W., Anselmi-Tamburini, U., Garay, J., Groza, J. & Munir, Z. A. Fundamental investigations on the spark plasma sintering/synthesis process: I. Effect of dc pulsing on reactivity. *Materials Science and Engineering: A* **394**, 132-138 (2005).
88 Shen, Z., Johnsson, M., Zhao, Z. & Nygren, M. Spark plasma sintering of alumina. *Journal of the American Ceramic Society* **85**, 1921-1927 (2002).
89 Wang, S., Chen, L., Hirai, T. & Kang, Y. Microstructure inhomogeneity in Al2O3 sintered bodies formed during the plasma-activated sintering process. *Journal of materials science letters* **18**, 1119-1121 (1999).
90 Mundy, J. Electrical resistivity-temperature scale of tungsten. *Philosophical Magazine A* **46**, 345-349 (1982).
91 Rahman, M., Wang, C. C., Chen, W., Akbar, S. A. & Mroz, C. Electrical resistivity of titanium diboride and zirconium diboride. *Journal of the American Ceramic Society* **78**, 1380-1382 (1995).
92 Caliman, L. B., Bichaud, E., Soudant, P., Gouvea, D. & Steil, M. C. A simple flash

sintering setup under applied mechanical stress and controlled atmosphere. *MethodsX* **2**, 392-398, doi:http://dx.doi.org/10.1016/j.mex.2015.10.004 (2015).

93 Raizer, Y. P., Kisin, V. I. & Allen, J. E. *Gas discharge physics*. Vol. 1 (Springer-Verlag Berlin, 1991).

94 Van de Sanden, M., Schram, P., Peeters, A., Van der Mullen, J. & Kroesen, G. Thermodynamic generalization of the Saha equation for a two-temperature plasma. *Physical Review A* **40**, 5273 (1989).

95 Winge, R., Peterson, V. & Fassel, V. A. Inductively coupled plasma-atomic emission spectroscopy: prominent lines. *Applied Spectroscopy* **33**, 206-219 (1979).

96 Bengtson, A. Quantitative depth profile analysis by glow discharge. *Spectrochimica Acta Part B: Atomic Spectroscopy* **49**, 411-429 (1994).

97 Striganov, A. R. & Sventitskii, N. *Tables of spectral lines of neutral and ionized atoms*. (IFI/Plenum New York, 1968).

98 Vol. Ver. 2.0 (National Institute of Standards and Technology, 1999).

99 Wiese, W., Smith, M. & Glennon, B. ATOMIC TRANSITION PROBABILITIES. VOLUME 1. HYDROGEN THROUGH NEON. (DTIC Document, 1966).

100 Kurucz R L , B. B. (Cambridge, Mass.: Smithsonian Astrophysical Observatory, 1995).

101 Keyvan, S., Rossow, R. & Romero, C. Blackbody-based calibration for temperature calculations in the visible and near-IR spectral ranges using a spectrometer. *Fuel* **85**, 796-802 (2006).

102 Park, J. & Mackay, S. *Practical data acquisition for instrumentation and control systems*. (Newnes, 2003).

103 Jerri, A. J. The Shannon sampling theorem—Its various extensions and applications: A tutorial review. *Proceedings of the IEEE* **65**, 1565-1596 (1977).

104 Altan, T., Lilly, B. & Yen, Y. Manufacturing of dies and molds. *CIRP Annals-Manufacturing Technology* **50**, 404-422 (2001).

105 Bellosi, A., Monteverde, F. & Sciti, D. Fast Densification of Ultra-High-Temperature Ceramics by Spark Plasma Sintering. *International journal of applied ceramic technology* **3**, 32-40 (2006).

106 Tokita, M. in *Materials Science Forum.* 83-88 (Trans Tech Publ).

107 Demuynck, M., Erauw, J.-P., Van der Biest, O., Delannay, F. & Cambier, F. Densification of alumina by SPS and HP: A comparative study. *Journal of the European Ceramic Society* **32**, 1957-1964 (2012).

108 Siemiaszko, D., Jóźwiak, S., Czarnecki, M. & Bojar, Z. Influence of temperature during pressure-assisted induction sintering (PAIS) on structure and properties of the Fe40Al intermetallic phase. *Intermetallics* **41**, 16-21 (2013).

109 LaLonde, A. D., Ikeda, T. & Snyder, G. J. Rapid consolidation of powdered materials by induction hot pressing. *Review of Scientific Instruments* **82**, 025104 (2011).

110 Shongwe, M. B. *et al.* A comparative study of spark plasma sintering and hybrid spark plasma sintering of 93W–4.9Ni–2.1Fe heavy alloy. *International Journal of Refractory Metals and Hard Materials* **55**, 16-23, doi:http://dx.doi.org/10.1016/j.ijrmhm.2015.11.001 (2016).

111 Nguyen-Kuok, S., Malakhov, Y. & Korotkich, I. Calculation of diffusion, thermal

diffusion, thermal conductivity and electrical conductivity for argon plasma.
112 Montes, J. M., Cuevas, F. G., Cintas, J. & Urban, P. Electrical conductivity of metal powders under pressure. *Appl. Phys. A* **105**, 935-947, doi:10.1007/s00339-011-6515-9 (2011).
113 Tokita, M. in *Proceeding of NEDO International Symposium on Functionally Graded Materials.* 22 (Japan).
114 Chaim, R. Densification mechanisms in spark plasma sintering of nanocrystalline ceramics. *Materials Science and Engineering: A* **443**, 25-32 (2007).
115 Tokita, M. *Recent Advanced Spark Plasma Sintering (SPS) Technology , Systems and Applications in Japan* (The 1st Russia-Japan SPS Workshop Moscow, Russia 2013).
116 Demirskyi, D., Borodianska, H., Grasso, S., Sakka, Y. & Vasylkiv, O. Microstructure evolution during field-assisted sintering of zirconia spheres. *Scripta Materialia* **65**, 683-686 (2011).
117 Hulbert, D. M., Anders, A., Andersson, J., Lavernia, E. J. & Mukherjee, A. K. A discussion on the absence of plasma in spark plasma sintering. *Scripta Materialia* **60**, 835-838 (2009).
118 Grasso, S., Sakka, Y. & Maizza, G. Electric current activated/assisted sintering (ECAS): a review of patents 1906–2008. *Science and Technology of Advanced Materials* **10**, 053001, doi:10.1088/1468-6996/10/5/053001 (2009).
119 Yurlova, M. *et al.* Electric pulse consolidation: an alternative to spark plasma sintering. *Journal of Materials Science* **49**, 952-985 (2014).
120 Kiyoshi, I. Method of electrically sintering discrete bodies. United States patent (1967).
121 Hara, M. & Akazaki, M. A method for prediction of gaseous discharge threshold voltage in the presence of a conducting particle. *Journal of Electrostatics* **2**, 223-239 (1977).
122 Decker, R. & Eve, D. Wandering of the column of a dc arc used in spectrographic analysis. *Spectrochimica Acta Part B: Atomic Spectroscopy* **25**, 411-417 (1970).
123 Inoue, K. Method of electrically sintering discrete bodies. (1967).
124 Natsu, W., Ojima, S., Kobayashi, T. & Kunieda, M. Temperature distribution measurement in EDM arc plasma using spectroscopy. *JSME International Journal Series C* **47**, 384-390 (2004).
125 Wagatsuma, K. & Hirokawa, K. Effect of oxygen addition to an argon glow-discharge plasma source in atomic emission spectrometry. *Analytica chimica acta* **306**, 193-200 (1995).
126 Kim, S. W., Kang, S. J. L. & Chen, I. W. Ionomigration of Pores and Gas Bubbles in Yttria-Stabilized Cubic Zirconia. *Journal of the American Ceramic Society* **96**, 1090-1098 (2013).
127 JHA, S. K., TERAUDS, K., LEBRUN, J.-M. & RAJ, R. Beyond flash sintering in 3 mol% yttria stabilized zirconia. *Journal of the Ceramic Society of Japan* **124**, 283-288 (2016).
128 Yuan, D. & Kröger, F. Stabilized zirconia as an oxygen pump. *Journal of The Electrochemical Society* **116**, 594-600 (1969).
129 Kitahara, T. Oxygen concentration detecting system using oxygen sensor including oxygen ion pump. (1986).

130 Heuer, A. H. & Lou, V. L. Volatility Diagrams for Silica, Silicon Nitride, and Silicon Carbide and Their Application to High-Temperature Decomposition and Oxidation. *Journal of the American Ceramic Society* **73**, 2789-2803 (1990).

131 Popova, I., Zhukov, V. & Yates, J. Electrostatic Field Enhancement of Al(111) Oxidation. *Physical Review Letters* **89**, doi:10.1103/PhysRevLett.89.276101 (2002).

132 Lawless, G. W. & Lombard, C. A. The Effect of a Static Electric Field on the Oxidation of Certain Metals. (DTIC Document, 1966).

133 Jorgensen, P. J. Effect of an electric field on silicon oxidation. *The Journal of Chemical Physics* **37**, 874-877 (1962).

134 Hunt, G. & Ritchie, I. The effect of an applied electric field on the oxidation of aluminum in the temperature range 50–400° C. *Oxidation of Metals* **2**, 361-371 (1970).

135 Parkansky, N. *et al.* The effect of an electric field on the high temperature oxidation of copper in air. *Surface and Coatings Technology* **120**, 668-671 (1999).

136 Ko, C. & Ramanathan, S. Electric field induced phase transitions and dynamic tuning of the properties of oxide structures. (2011).

137 Rashkovan, A., Sher, E. & Kalman, H. Experimental optimization of an electric blower by corona wind. *Applied thermal engineering* **22**, 1587-1599 (2002).

138 Ranke, W. & Jacobi, K. Electron stimulated oxidation of GaAs, studied by quantitative auger electron spectroscopy. *Surface Science* **47**, 525-542 (1975).

139 Kitahara, T. Oxygen concentration detecting system using oxygen sensor including oxygen ion pump. (1986).

140 Eddy, D. S. Physical principles of the zirconia exhaust gas sensor. *Vehicular Technology, IEEE Transactions on* **23**, 125-128 (1974).

141 Esposito, V. *et al.* Electrical properties of YSZ/NiO composites prepared by a liquid mixture technique. *Journal of the European Ceramic Society* **25**, 2637-2641 (2005).

142 Feighery, A. & Irvine, J. Effect of alumina additions upon electrical properties of 8 mol.% yttria-stabilised zirconia. *Solid State Ionics* **121**, 209-216 (1999).

143 Gibson, I., Dransfield, G. & Irvine, J. Influence of yttria concentration upon electrical properties and susceptibility to ageing of yttria-stabilised zirconias. *Journal of the European Ceramic Society* **18**, 661-667 (1998).

144 Guo, X. & Waser, R. Electrical properties of the grain boundaries of oxygen ion conductors: acceptor-doped zirconia and ceria. *Progress in Materials Science* **51**, 151-210 (2006).

145 Ikeda, S., Sakurai, O., Uematsu, K., Mizutani, N. & Kato, M. Electrical conductivity of yttria-stabilized zirconia single crystals. *Journal of materials science* **20**, 4593-4600 (1985).

146 Ji, Y., Kilner, J. & Carolan, M. Electrical properties and oxygen diffusion in yttria-stabilised zirconia (YSZ)–La 0.8 Sr 0.2 MnO 3±δ (LSM) composites. *Solid State Ionics* **176**, 937-943 (2005).

147 Jiang, S., Schulze, W. A., Amarakoon, V. R. & Stangle, G. C. Electrical properties of ultrafine-grained yttria-stabilized zirconia ceramics. *Journal of materials research* **12**, 2374-2380 (1997).

148 Aldebert, P. & TRAVERSE, J. P. Structure and ionic mobility of zirconia at high temperature. *Journal of the American Ceramic Society* **68**, 34-40 (1985).

149 Iwase, M., Ichise, E., Takeuchi, M. & Yamasaki, T. Measurements of the parameter, P, for the determinations of mixed ionic and n-type electronic conduction in commercial zirconia electrolytes. *Trans. Japan Inst. Metals* **25**, 43-52 (1984).

150 Karlsdottir, S. N., Halloran, J. W. & Grundy, A. N. Zirconia transport by liquid convection during oxidation of zirconium diboride–silicon carbide. *Journal of the American Ceramic Society* **91**, 272-277 (2008).

151 Parthasarathy, T., Rapp, R., Opeka, M. & Kerans, R. A model for the oxidation of ZrB_2, HfB_2 and TiB_2. *Acta Materialia* **55**, 5999-6010 (2007).

152 Abdelkader, A., Daher, A., Abdelkareem, R. A. & El-Kashif, E. Preparation of zirconium metal by the electrochemical reduction of zirconium oxide. *Metallurgical and Materials Transactions B* **38**, 35-44 (2007).

153 Laguna-Bercero, M. A., Campana, R., Larrea, A., Kilner, J. A. & Orera, V. M. Electrolyte degradation in anode supported microtubular yttria stabilized zirconia-based solid oxide steam electrolysis cells at high voltages of operation. *Journal of Power Sources* **196**, 8942-8947, doi:http://dx.doi.org/10.1016/j.jpowsour.2011.01.015 (2011).

154 Heitjans, P. & Kärger, J. *Diffusion in condensed matter: methods, materials, models*. (Springer Science & Business Media, 2006).

155 Noirault, S., Célérier, S., Joubert, O., Caldes, M. T. & Piffard, Y. Incorporation of Water and Fast Proton Conduction in the Inherently Oxygen-Deficient Compound La26O27□(BO3) 8. *Advanced Materials* **19**, 867-870 (2007).

156 Levy, M., Fouletier, J. & Kleitz, M. Model for the electrical conductivity of reduced stabilized zirconia. *Journal of the Electrochemical Society* **135**, 1584-1589 (1988).

157 Cologna, M., Rashkova, B. & Raj, R. Flash sintering of nanograin zirconia in <5 s at 850°C. *Journal of the American Ceramic Society* **93**, 3556-3559 (2010).

158 Karakuscu, A. *et al.* Defect Structure of Flash-Sintered Strontium Titanate. *Journal of the American Ceramic Society* **95**, 2531-2536 (2012).

159 Muccillo, R. & Muccillo, E. Electric field-assisted flash sintering of tin dioxide. *Journal of the European Ceramic Society* **34**, 915-923 (2014).

160 Prette, A. L., Cologna, M., Sglavo, V. & Raj, R. Flash-sintering of Co 2 MnO 4 spinel for solid oxide fuel cell applications. *Journal of Power Sources* **196**, 2061-2065 (2011).

161 Yoshida, H., Sakka, Y., Yamamoto, T., Lebrun, J.-M. & Raj, R. Densification behaviour and microstructural development in undoped yttria prepared by flash-sintering. *Journal of the European Ceramic Society* **34**, 991-1000 (2014).

162 Park, J. & Chen, I. W. In Situ Thermometry Measuring Temperature Flashes Exceeding 1,700° C in 8 mol% Y2O3-Stablized Zirconia Under Constant-Voltage Heating. *Journal of the American Ceramic Society* **96**, 697-700 (2013).

163 Marinel, S., Savary, E. & Gomina, M. Sintering of CuO and ZnO in a single mode microwave cavity with shrinkage control. *Journal of Microwave Power and ElectromagneticEnergy* **44**, 57 (2010).

164 Bykov, Y. V. *et al.* Flash Microwave Sintering of Transparent Yb:(LaY) 2O3

Ceramics. *Journal of the American Ceramic Society* (2015).

165 Janney, M. A., Calhoun, C. L. & Kimrey, H. D. Microwave sintering of solid oxide fuel cell materials: I, Zirconia-8 mol% Yttria. *Journal of the American Ceramic Society* **75**, 341-346 (1992).

166 Bonizzoni, G. & Vassallo, E. Plasma physics and technology; industrial applications. *Vacuum* **64**, 327-336 (2002).

167 Shahidi, S., Ghoranneviss, M. & Moazzenchi, B. in *RMUTP 4th International Conference: Textiles & Fashion.*

168 Roth, J. R. *Industrial plasma engineering volume 1: principles*. (Taylor and Francis, 1995).

169 Roth, J. R. *Industrial Plasma Engineering: Volume 2-Applications to Nonthermal Plasma Processing*. Vol. 2 (CRC Press, 2001).

170 Yugeswaran, S. & Selvarajan, V. Electron number density measurement on a DC argon plasma jet by stark broadening of Ar I spectral line. *Vacuum* **81**, 347-352 (2006).

171 Vervisch, P., Cheron, B. & Lhuissier, J. Spectroscopic analysis of a TIG arc plasma. *Journal of Physics D: Applied Physics* **23**, 1058 (1990).

172 Gick, A., Quigley, M. & Richards, P. The use of electrostatic probes to measure the temperature profiles of welding arcs. *Journal of Physics D: Applied Physics* **6**, 1941 (1973).

173 Secrist, D. Phase Equilibria in the System Boron Carbide-Silicon Carbide. *Journal of the American Ceramic Society* **47**, 127-130 (1964).

174 Goto, T., Ito, E., Mukaida, M. & Hirai, T. Microstructure and Seebeck Coefficient of SiC-B4C Eutectic Ceramics. *Journal of the Japan Society of Powder and Powder Metallurgy* **41**, 1304-1307 (1994).

175 Korniyenko, K. in *Refractory metal systems* 499-534 (Springer, 2009).

176 Lilov, S. Study of the equilibrium processes in the gas phase during silicon carbide sublimation. *Materials Science and Engineering: B* **21**, 65-69 (1993).

177 Lankau, V., Martin, H.-P., Hempel-Weber, R., Oeschler, N. & Michaelis, A. Preparation and Thermoelectric Characterization of SiC-B4C Composites. *Journal of electronic materials* **39**, 1809-1813 (2010).

178 Wurst, J. & Nelson, J. Lineal Intercept Technique for Measuring Grain Size in Two-Phase Polycrystalline Ceramics. *Journal of the American Ceramic Society* **55**, 109-109 (1972).

179 Gunjishima, I., Akashi, T. & Goto, T. Characterization of Directionally Solidified B4C-SiC Composites Prepared by a Floating Zone Method. *Materials transactions* **43**, 2309-2315 (2002).

180 Gomi, T., Fukushima, N. & Matsushita, J. High temperature electrical conductivity of B~ 4C, SiC and SiB~ 6 sintered bodies. *JOURNAL OF ADVANCED SCIENCE* **13**, 15-16 (2001).

181 Grasso, S. *et al.* Flash Spark Plasma Sintering (FSPS) of α and β SiC. *Journal of the American Ceramic Society* (2016).

182 Grasso, S. *et al.* Modeling of the temperature distribution of flash sintered zirconia. *Journal of the Ceramic Society of Japan* **119**, 144-146 (2011).